

ABSTRACT

Title of Document: SYNTHESIS OF ZEOLITE@MOF
NANOPOROUS COMPOSITES AS
BIFUNCTIONAL CATALYSTS

Guanghai Zhu, Master of Science, 2014

Directed By: Professor, Dr. Dongxia Liu, Department of
Chemical and Biomolecular Engineering
And
Professor, Dr. Kyu Yong Choi, Department of
Chemical and Biomolecular Engineering

As nanoporous materials, zeolite and metal organic framework (MOF) share common characteristics of high surface areas and uniform micropores and differ in thermal/mechanical stability and structural flexibility. The integration of MOF and zeolite into composite particles is expected to produce useful hybrid nanoporous materials where inorganic zeolite and organic MOF components impart the advantages of high thermal, mechanical and structural stability of zeolites and specific functionality and high flexibility of MOFs. This thesis work addresses the synthesis of zeolite@MOF composites and the exploration of their applications as bifunctional catalysts in one-pot cascade reaction. Zeolite@MOF core-shell composites have been synthesized by solvothermal growth of MOFs on the surface of ZSM-5 particles. The acidity from framework Al-O(H)-Si sites in ZSM-5 and basicity from amine groups in

MOFs obtained by pre-/post-synthetic modification endow zeolite@MOF composites bifunctionality in two-step cascade catalytic reactions.

SYNTHESIS OF ZEOLITE@MOF NANOPOROUS COMPOSITES AS
BIFUNCTIONAL CATALYSTS

By

Guanghai Zhu

Thesis submitted to the Faculty of the Graduate School of the
University of Maryland, College Park, in partial fulfillment
of the requirements for the degree of
Master of Science
2014

Advisory Committee:
Professor Dongxia Liu, Chair
Professor Kyu Yong Choi
Professor Michael R. Zachariah

© Copyright by
Guanghai Zhu
2014

Dedication

This work is dedicated to my parents, Honghua Zhu and Xuerong Geng, who have supported and encouraged me during my graduate study. Without them I cannot finish this Master's degree. This work is also dedicated to my fiancée, Xueting Wang, for everything she have done including doing nothing but missing me 4000 miles away.

Acknowledgements

I want to give my thanks to my advisor, Dr. Dongxia Liu, for her guidance and instructions during my graduate study and research in her group. She worked diligently to help me with my research project and writing this thesis. I also thank her for her sound recommendation in my PhD applications which gave me the chance to pursue a higher education. I also want to thank my co-advisor Dr. Kyu Yong Choi, for his wise advice and encouragement during writing of the thesis.

Thank you Dr. Dongxia Liu, Dr. Kyu Yong Choi, and Dr. Michael Zachariah for agreeing to serve on my committee.

I would like to thank my labmates for their guidance and assistance during my 1 year stay in Dr. Liu's lab. I want to thank Laleh Emdadi for her expertise in zeolite synthesis and her assistance in using scanning and transmission electron microscopy. I want to thank Yiqing Wu for sharing his catalyst characterization knowledge. I want to thank Baoyu Liu for sharing his material simulation knowledge.

I would like to thank Dr. Dongxia Liu, Christina Fontanos, Su Cheun Oh, Fudong Han and Xueting Wang for their help in reading and editing this thesis.

At last, I want to thank all my fellow graduate students and friends for making my stay here meaningful and memorable.

Table of Contents

Dedication.....	ii
Acknowledgements.....	iii
Table of Contents.....	iv
List of Tables.....	vii
List of Figures.....	viii
Chapter 1: Introduction.....	1
1.1 Background on Nanoporous Materials.....	1
1.2 Zeolite Materials.....	1
1.2.1 Zeolite Structure and Nomenclature.....	2
1.2.2 Synthesis of zeolites.....	5
1.2.3 Applications of zeolites.....	7
1.3 MOF Nanoporous Materials.....	9
1.3.1 MOF structures.....	10
1.3.2 Synthesis of MOFs.....	11
1.3.3 Functionalization of MOFs.....	13
1.3.4 Application of MOF Materials.....	14
1.3.5 MOF-based Core-Shell Composites.....	15
1.4 Motivation and Thesis Outlines.....	17
Chapter 2: Synthesis and Postsynthetic Modification of ZSM-5@UiO-66 Core-Shell Particles as Bifunctional Catalysts.....	19
2.1 Introduction.....	19

2.2 Experimental	22
2.2.1 Materials	22
2.2.2 Synthesis of ZSM-5	22
2.2.3 Synthesis of UiO-66 and ZSM-5@UiO-66	23
2.2.4 Incorporation of amine ($-NH_2$) groups into ZSM-5@UiO-66	23
2.2.5 Product characterizations	24
2.2.6 Catalytic reaction over ZSM-5@UiO-66 composite	25
2.3 Results and Discussion	27
2.4 Conclusions.....	53
Chapter 3: Synthesis and Presynthetic Modification of ZSM-5@UiO-66 Core-Shell	
Particles as Bifunctional Catalysts.....	55
3.1 Introduction.....	55
3.2 Experimental Part.....	56
3.2.1 Materials	56
3.2.2 Synthesis of UiO-66-NH ₂ and ZSM-5@UiO-66-NH ₂	56
3.2.3 Activation of the catalyst	57
3.2.4 Product characterizations	57
3.2.5 Catalytic reaction test over ZSM-5@UiO-66-NH ₂ composite.....	58
3.3 Results and Discussion	58
3.4 Conclusions.....	67
Chapter 4: Synthesis of ZSM-5@MIL-101 Core-Shell Particles as Bifunctional	
Catalysts.....	68
4.1 Introduction.....	68

4.2 Experimental	68
4.2.1 Materials	68
4.2.2 Synthesis of MIL-101 and ZSM-5@MIL-101	69
4.2.3 Incorporation of amine ($-NH_2$) groups into ZSM-5@MIL-101 composite	69
4.2.4 Acid Exchange Activation	70
4.2.5 Product characterizations	70
4.2.6 Catalytic reaction test over ZSM-5@MIL-101 composite	71
4.3 Results and Discussion	71
4.4 Conclusions.....	75
Chapter 5: Conclusions and Future Work.....	77
5.1 Conclusions.....	77
5.2 Future Work	78
5.2.1 Mechanism investigation on growth of MOFs on zeolite surface	78
5.2.2 Optimization the functionalization process of zeolite@MOF composites	78
5.2.3 Shape selectivity of zeolite@MOF composites in other applications	79
References.....	80

List of Tables

- Table 1-1.** Chemical sources and their functions in zeolite synthesis.
- Table 1-2.** Commercial processes using zeolite catalysts.
- Table 1-3.** List of most studied MOF structures and their properties.
- Table 1-4.** Recent studies on MOF-based core-shell composites and their applications.
- Table 2-1.** Textural properties of UiO-66, ZSM-5, ZSM-5@UiO-66, ED-ZSM-5@UiO-66, and HCl- ED-ZSM-5@UiO-66, derived from N₂ and Ar isotherms.
- Table 2-2.** Catalytic Reaction Results Summary.

List of Figures

Figure 1-1. Primary building units, secondary building units, and three dimensional structures of zeolites.

Figure 1-2. The secondary units (SBUs) recognized in zeolite frameworks. (a) Single four rings (S4R), (b) single six rings (S6R), (c) single eight rings (S8R), (d) double four rings (D4R), (e) single six rings (D6R), (f) four five rings, (g) pentasil unit, and (h) sodalite unit, respectively.

Figure 1-3. Zeolite framework types: (A) FAU, (B) MOR, (C) MFI, (D) SOD, and (E) LTA, respectively.

Figure 1-4. Active acid sites in zeolite framework. The bridging hydroxyl group in the structure is Brønsted acid site.

Figure 1-5. Transition state shape selectivity of 1,2,4-trimethylbenzene production from m-xylene.

Figure 1-6. Organic linkers commonly used in building MOF structures.

Figure 2-1. Calibration curves of benzaldehyde dimethyl acetal, malononitrile, benzaldehyde and benzylidene malononitrile.

Figure 2-2. SEM images of (A) ZSM-5 zeolite, (B) UiO-66 MOF, and TEM images of (C) ZSM-5, (D), (E) and (F) ZSM-5@UiO-66.

Figure 2-3. XRD patterns of (a) ZSM-5, (b) UiO-66, (c) ZSM-5@UiO-66, and (d) ED-ZSM-5@UiO-66.

Figure 2-4. EDX spectra of as-synthesized (A) ZSM-5 zeolite and (B) ZSM-5@UiO-66 core-shell composite.

Figure 2-5. N₂ adsorption-desorption isotherms of UiO-66, ZSM-5, ZSM-5@UiO-66, ED-ZSM-5@UiO-66, and HCl-ED-ZSM-5@UiO-66, respectively.

Figure 2-6. Ar adsorption-desorption isotherms (A), and the corresponding pore size distributions (B) derived from Ar sorption (NLDFT on the adsorption branch on the basis of spherical/cylindrical pore model) and (C) NLDFT on the adsorption branch on the basis of cylindrical pore model, of as-synthesized UiO-66, ZSM-5, ZSM-5@UiO-66, ED-ZSM-5@UiO-66, and HCl-ED-ZSM-5@UiO-66, respectively.

Figure 2-7. FTIR spectra of UiO-66, ZSM-5, ZSM-5@UiO-66, ED-ZSM-5@UiO-66, and HCl-ED-ZSM-5@UiO-66, respectively.

Figure 2-8. TGA curves of ZSM-5, UiO-66, ZSM-5@UiO-66 and HCl-ED-ZSM-5@UiO-66, respectively.

Figure 2-9. SEM images of (A) (B) ZSM-5 and ZSM-5@UiO-66 with SAR= ∞ , (C) (D) ZSM-5 and ZSM-5@UiO-66 with SAR=100, (E) (F) ZSM-5 and ZSM-5@UiO-66 with SAR=40.

Figure 2-10. Catalytic reaction results of as-synthesized ZSM-5@UiO-66 composite evacuated at 423 K. Molar fraction of benzaldehyde dimethyl acetal, benzaldehyde and benzylidene malononitrile versus reaction time.

Figure 2-11. Catalytic reaction results of ED-ZSM-5@UiO-66 composite treated with 1 M NH₄NO₃ water solution, evacuated at 343 K. Molar fraction of benzaldehyde dimethyl acetal, benzaldehyde and benzylidene malononitrile versus reaction time.

Figure 2-12. Catalytic reaction results of ED-ZSM-5@UiO-66 composite treated with HCl ethanol solution, evacuated at (A) 343 K, (B) 423 K, (C) 473 K.

Figure 2-13. A comparison of benzaldehyde dimethyl acetal conversion, benzaldehyde yield, benzylidene malononitrile yield and selectivity, rate constant of the composite treated with HCl ethanol solution and evacuated at 343 K, 423 K and 473 K.

Figure 2-14. Catalytic reaction results of HCl-ED-ZSM-5@UiO-66 composite. Molar fraction of benzaldehyde dimethyl acetal, benzaldehyde and benzylidene malononitrile versus reaction time.

Figure 2-15. Catalytic reaction results of (A) ZSM-5, (B) ED-ZSM-5, (C) HCl-ED-ZSM-5. Molar fraction of benzaldehyde dimethyl acetal, benzaldehyde and benzylidene malononitrile versus reaction time.

Figure 2-16. Catalytic reaction results of HCl-ED-UiO-66. Molar fraction of benzaldehyde dimethyl acetal, benzaldehyde and benzylidene malononitrile versus reaction time.

Figure 3-1. SEM images of (A) ZSM-5 zeolite, (B) (C) UiO-66 MOF, and (D) ZSM-5@UiO-66-NH₂. TEM images of (E) (F) ZSM-5@UiO-66.

Figure 3-2. XRD patterns of (a) ZSM-5, (b) UiO-66-NH₂ and (c) ZSM-5@UiO-66-NH₂, respectively.

Figure 3-3. EDX spectra of as-synthesized (A) ZSM-5 zeolite and (B) ZSM-5@UiO-66-NH₂ core-shell composite.

Figure 3-4. N₂ adsorption-desorption isotherms of UiO-66-NH₂, ZSM-5, and ZSM-5@UiO-66-NH₂, respectively.

Figure 3-5. FTIR spectra of UiO-66-NH₂, ZSM-5 and ZSM-5@UiO-66-NH₂, respectively.

Figure 3-6. Catalytic reaction results of as-synthesized ZSM-5@UiO-66-NH₂ and acid-exchanged ZSM-5@UiO-66-NH₂. Molar fraction of benzaldehyde dimethyl acetal, benzaldehyde and benzylidene malononitrile versus reaction time.

Figure 4-1. SEM images of (A) commercial ZSM-5 zeolite, (B) MIL-101 MOF, and (C) ZSM-5@MIL-101.

Figure 4-2. XRD patterns of (a) ZSM-5, (b) MIL-101 and (c) ZSM-5@MIL-101, respectively.

Figure 4-3. N₂ adsorption-desorption isotherms of MIL-101, ZSM-5, ZSM-5@MIL-101, and ED-ZSM-5@MIL-101, respectively.

Figure 4-4. Catalytic reaction results of ZSM-5@MIL-101. Molar fraction of benzaldehyde dimethyl acetal, benzaldehyde and benzylidene malononitrile versus reaction time.

Chapter 1: Introduction

1.1 Background on Nanoporous Materials

Nanoporous materials are comprised of organic, inorganic, or organic-inorganic hybrid frameworks that support regular porous structures. The pore size in nanoporous materials is generally smaller than 100 nm. According to the International Union of Pure and Applied Chemistry (IUPAC),[1] the nanoporous materials can be categorized into three classes: microporous materials of 0.2 – 2 nm in pore size, mesoporous materials of 2 – 50 nm in pore size, and macroporous materials of 50 – 1000 nm in pore size. High specific surface area, large pore volume and uniform pore size are characteristics of nanoporous materials, which endow them superior performances in adsorption, separation and catalysis applications in comparison with their solid counterparts.[2, 3] Zeolites and metal organic frameworks (MOFs) are two important examples of nanoporous materials, being intensively studied for many applications.[4-7]

1.2 Zeolite Materials

Zeolites are microporous aluminosilicates whose basic units are TO_4 tetrahedrons (T: Tetrahedrally coordinated atoms, e.g. $[SiO_4]$ or $[AlO_4]^-$).[8] The discovery and use of zeolite can be tracked back to 1756 by Swedish mineralogist Cronstedt.[9] Since then, the natural zeolites have been discovered and known for adsorption and ion-exchange applications. In 1980's, the development of petroleum industry inspired an explosion on synthetic zeolites.[10] In the last couple of decades, numerous publications and patents have reported advances in new synthetic approaches

to produce zeolites with new structures and applications of zeolite membranes in separations.[11] Today, zeolite science is active in engineering hierarchical zeolites with desirable meso- and microporous topologies for bulky molecules involved separation or catalysis applications.[12, 13] Synthesis of ultra-thin such as unit-cell thick zeolites is an emerging area with promising applications as thin membranes for desirable separations.[14]

1.2.1 Zeolite Structure and Nomenclature

The basic TO_4 tetrahedrons in zeolite are called primary building units, which are connected alternatively by sharing oxygen atoms as bridges to form secondary building units such as rings or other complex blocks, as shown in Figure 1-1. The secondary building unit may contain four, five, six, or more atoms in each ring, as illustrated in Figure 1-2. Each apex stands for a tetrahedron and the lines between apexes are oxygen bridges. The assembly of the secondary building units generates three dimensional zeolite structures. The connectivity (topology) of the tetrahedral atoms in three dimensional zeolites defines the zeolite framework type and determines the size and shape of the pores and the channel systems in zeolites. Each framework topology is assigned a three capital letter code by the Structure Commission of the International Zeolite Association (IZA).[15] A collection of nomenclature for zeolites is also available on the IZA's website (<http://www.iza-synthesis.org/>).

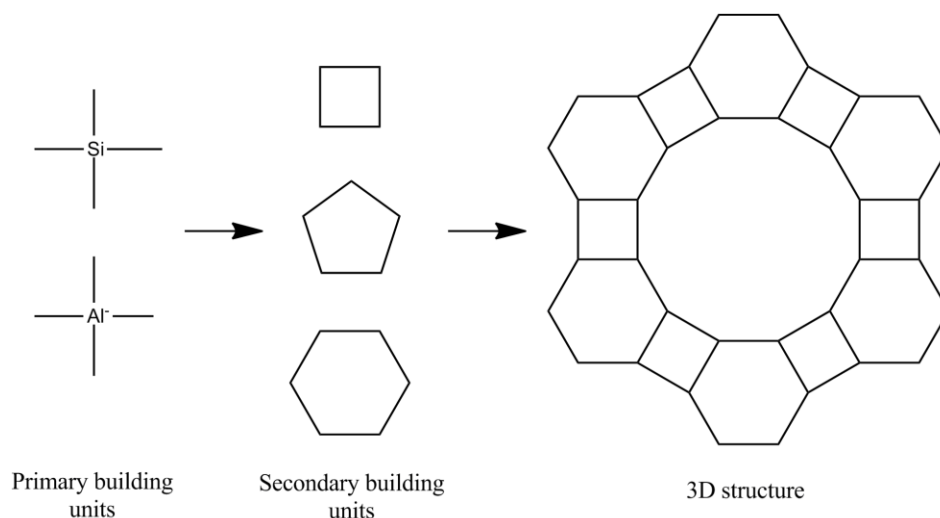


Figure 1-1. Primary building units, secondary building units, and three dimensional structures of zeolites.

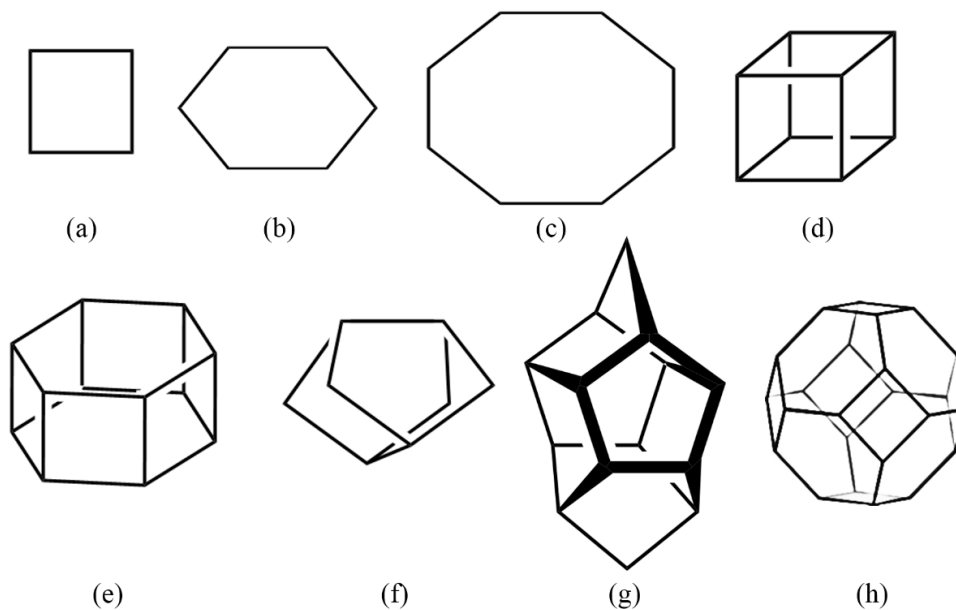


Figure 1-2. The secondary units (SBUs) recognized in zeolite frameworks. (a) Single four rings (S4R), (b) single six rings (S6R), (c) single eight rings (S8R), (d) double four rings (D4R), (e) double six rings (D6R), (f) four five rings, (g) pentasil unit, and (h) sodalite unit, respectively.[16]

According to IZA publications, there are around 206 zeolite framework types.[15] The most commonly studied zeolite framework types are FAU (**Faujasite**), MOR (**Mordenite**), MFI (ZSM-5(**FIVE**)), SOD (**Sodalite**) and LTA (**Linde Type A**)

zeolites. Below is a brief description for topological structures of these five zeolites. Figure 1-3 demonstrates the corresponding cage and/or channel structures of these zeolites.

FAU-type zeolite (Figure 1-3 (A)) has SOD cages joined by double 6 rings in the same way as diamond. This creates a 12-membered ring and a 3-dimensional channel system. FAU belongs to large-pore zeolites, widely used as catalysts for fluid catalytic cracking of heavy compounds in petroleum refinery.[17, 18] MOR-type zeolite (Figure 1-3 (B)) is built on 5-ring units. Four 5-rings are interconnected by oxygen bridges. Mirror images of the 5-ring chains are connected to form sheets. The sheets are connected to one another to form adjacent 12- and 8-membered ring one dimensional channels along the z-axis. MFI (example: Zeolite Socony Mobil-5 (ZSM-5)) type is constructed by pentasil units (see Figure 1-2 (g)). Several pentasil units are linked together by oxygen bridges to form pentasil chains, which are interconnected by oxygen bridges to form corrugated sheets with 10-ring holes. A stack of sheets are connected by oxygen bridges to form a structure with straight and zig-zag 10-membered ring channels parallel and perpendicular to the sheets (Figure 1-3 (C)). The latter zig-zag channels in the x-direction link the straight channels to form a 3-dimensional 10-membered ring channel system. The pore opening is slightly smaller than the 12-membered ring in FAU, which is classified as medium pore zeolites.[19, 20] SOD (example: sodalite) type zeolite has a body-centered cubic arrangement of sodalite units (Figure 1-3 (D)). It has small pore openings of the 6-membered ring windows, which limit the application capacity of sodalite cavities inside. It is an important material as a host of advanced materials.[21] LTA (example: Linde Type A)

type is a structure in which SOD cages are connected by double 4-ring units in a cubic arrangement (Figure 1-3 (E)). This creates an 8-membered ring in the center of 4 sodalite cages, giving a larger pore opening than sodalite. Zeolite A is used as desiccant and ion-exchanger in laundry detergents.[22]

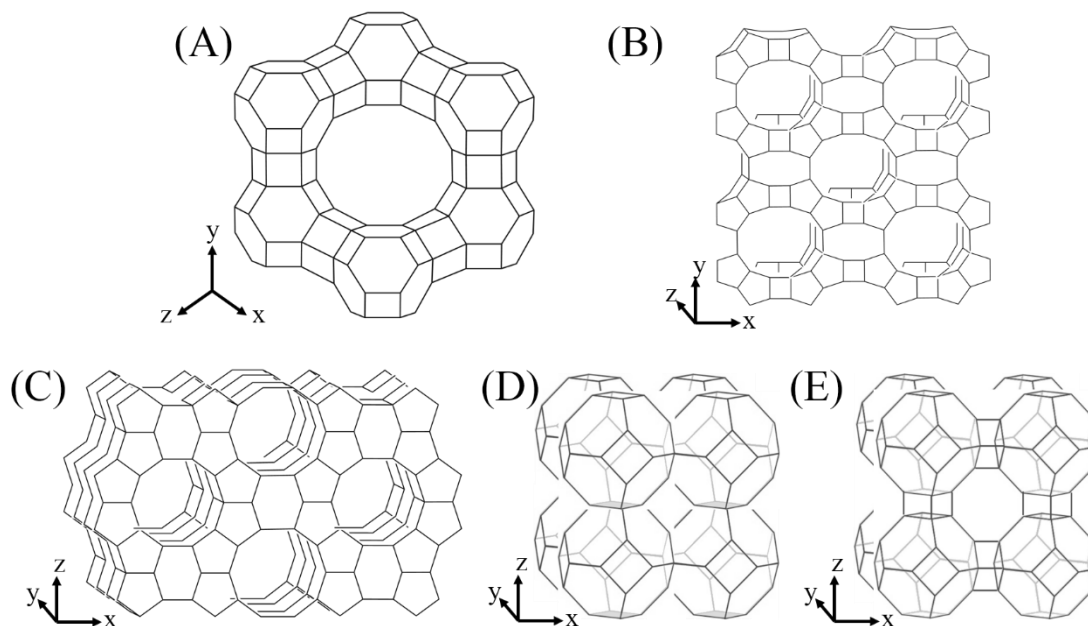
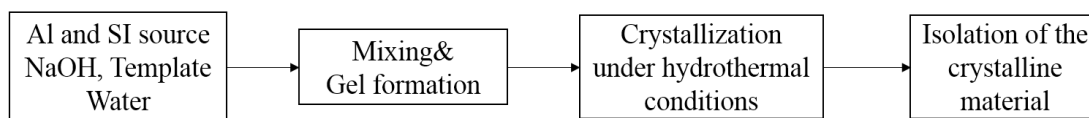


Figure 1-3. Zeolite framework types: (A) FAU, (B) MOR, (C) MFI, (D) SOD, and (E) LTA, respectively.[15]

1.2.2 Synthesis of zeolites

Natural zeolites are formed under volcanic conditions with extremely long reaction times.[23] The early work in synthesizing zeolites mimicked the high temperature and salt concentrations found in nature. Since 1946, many zeolite types without a natural counterpart have been synthesized.[24] Hydrothermal synthesis is the conventional method used for generating zeolite materials. The general synthetic procedure is illustrated in the flow chart of Scheme 1-1. The first two steps in the scheme can be summarized as the preparation of the zeolite synthetic gel, which is the

most time-consuming step in the whole process. The composition of the synthetic gel determines the zeolite structure to be produced. Crystallization is the third step in the process, which is usually carried out in an autoclave that is held in a preheated oven for a period of time ranging from a few minutes to weeks. The temperature and duration of crystallization affects the size and morphology of the zeolite. The isolation of zeolite can be done by centrifugation or flocculation, which is the last step in the process.



Scheme 1-1. General procedure for synthesis of zeolite.

The chemical sources and their functions in the synthesis of zeolites are listed in Table 1-1. Inorganic silicon sources include soluble silicates and silica sols that are made from fumed silica. Organic silicon sources such as tetraethyl orthosilicate (TEOS) and silicic acid are also widely used in the synthesis. It has been reported that different silicon sources influence the ageing time for gelation of the zeolite synthetic precursors.[25] Sodium aluminate, aluminum hydroxide ($\text{Al}(\text{OH})_3$), aluminum alkoxide and aluminum sulfate etc. are commonly used as aluminum sources in the zeolite synthesis. The optimal pH range for zeolite synthesis is 11-13[26], which can be modulated by the addition of OH^- guest molecules. Organic templates are used extensively as structure directing agents (SDAs) for certain types of zeolite structures. To avoid the toxicity and high cost of SDAs, template-free syntheses of zeolites are drawing a lot of research interest in commercial production of zeolite materials.[27, 28]

Table 1-1. Chemical sources and their functions in zeolite synthesis.

Sources	Functions
SiO ₂	Primary building units
AlO ₂ ⁻	Origin of framework charge
OH ⁻	Mineralizer
Alkali cation, template	Counterion of AlO ₂ ⁻
Water	Solvent

Hydrothermal crystallization is the conventional method used in the synthesis of zeolites. The required synthesis temperature and pressure depends on the zeolite type. Most commercial zeolites are synthesized at 363-373 K, but some dense zeolites need higher crystallization temperatures (up to 623 K). The ageing time is important in that a certain induction period is needed at ambient temperature before the crystallization take place. It has to be noted that different reaction times will sometimes result in different zeolite structures. This is because all zeolites are metastable species and they will convert to denser structures over time. Aside from the conventional hydrothermal method, microwave-mediated synthesis has been applied to the synthesis and modification of zeolites.[29] In microwave-assisted synthesis, the heating comes from the interactions between polar molecules and the electromagnetic field. Rapid crystallization of zeolite is achieved in microwave-assisted synthesis in comparison with hydrothermal synthesis as a result of high rates of temperature rise and different heating mechanisms.[30]

1.2.3 Applications of zeolites

The periodic channel systems and crystalline structure makes zeolites physically and chemically stable compounds that can be widely used in gas storage, separation and heterogeneous catalysis. For the gas storage applications, the large void

volume in the zeolite framework offers the storage capacities. When water molecules are removed from the framework, zeolites can take in other molecules. The adsorption and storage of hydrocarbons in zeolites has been studied intensively.[31-33] Zeolites possess a wide variety of internal channels and cavities accessed through oxygen windows which have sizes similar to the dimensions of common organic and inorganic molecules. This unique textural property endows zeolites with capabilities to separate mixtures of molecules with different sizes. For example, FAU and ZSM-5 are widely used in separating C8 aromatics and alkane isomers.[34, 35] The extensive internal surface, variable pore sizes and ion-exchange properties make zeolites good candidates as catalysts for many catalytic reactions in industry. For example, zeolite has been used as acid catalysts petroleum refining processes, including catalytic cracking, hydrocracking, isomerization, alkylation and oligomerization.[23]

The zeolite acidity in H⁺-form zeolites originates from framework Al species, as shown in Figure 1-4 (A).[36] The unique pore systems in zeolites only allow them to admit certain sized molecules to enter or reside in the framework, and thus offer zeolite unique shape selectivity in catalysis. One example of zeolite shape selectivity is the production of 1,2,4-trimethylbenzene from m-xylene. The transition state shown in Figure 1-4(B) in the upper channel cannot fit in the zeolite channel. This prevents the production of 1,3,5-trimethylbenzene and offers high selectivity for the 1,2,4-trimethylbenzene molecules.

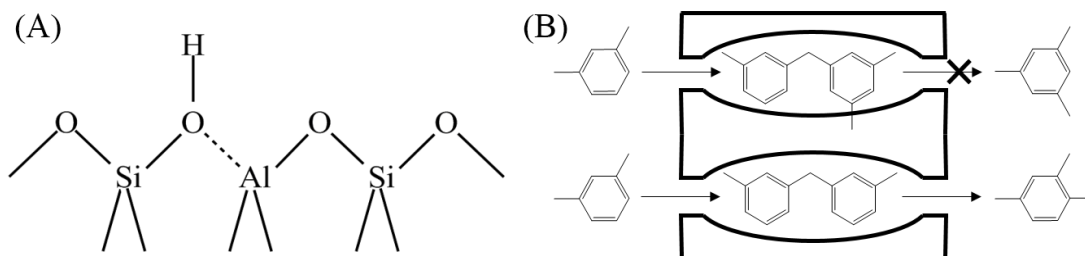


Figure 1-4. (A) Active acid sites in zeolite framework. The bridging hydroxyl group in the structure is Brønsted acid site. (B) Transition state shape selectivity of 1,2,4-trimethylbenzene production from m-xylene. (Reproduced from Reference [23])

1.3 MOF Nanoporous Materials

Metal organic frameworks (MOFs) are a group of emerging nanoporous materials containing inorganic building bricks and organic linkers.[37, 38] This new class of nanoporous materials was first discovered by Bernard Hoskins and Richard Robson in 1989.[39] They proposed a prototype in which tetrahedral or octahedral arrays of valences are linked by rod-like molecular linkers, similar to the modern concept of MOF. The large size of cavities and opening windows were considered intriguing features of this new kind of material. These structures also drew interest from many other curious researchers in the past years.[40-45] Omar Yaghi is one of them who made the most impressive progress and popularized the name “metal organic frameworks”.[46-49] Yaghi and his coworkers developed thermally stable MOF structures capable of reversible guest molecule subtraction with permanent micropore systems.[49] This was a big breakthrough for MOFs towards various potential applications. Ever since the first several proof-of-concept practical MOF structures were discovered, a lot of thermal/chemical stable MOFs has been developed with high pore volume and surface area.[50]

1.3.1 MOF structures

It has been established that the structure of MOFs is constructed from metal-containing units (SBUs) that act as lattice nodes and are held in place by multidentate organic linkers. Because a range of SBUs and organic linkers can be built into MOFs, a wide structural diversity and highly designable pore sizes and shapes in MOFs is expected.[38, 51] A collection of common linker structures are shown in Figure 1-6. Some of the most studied MOF structures and their topological and structural properties are summarized in Table 1-3.

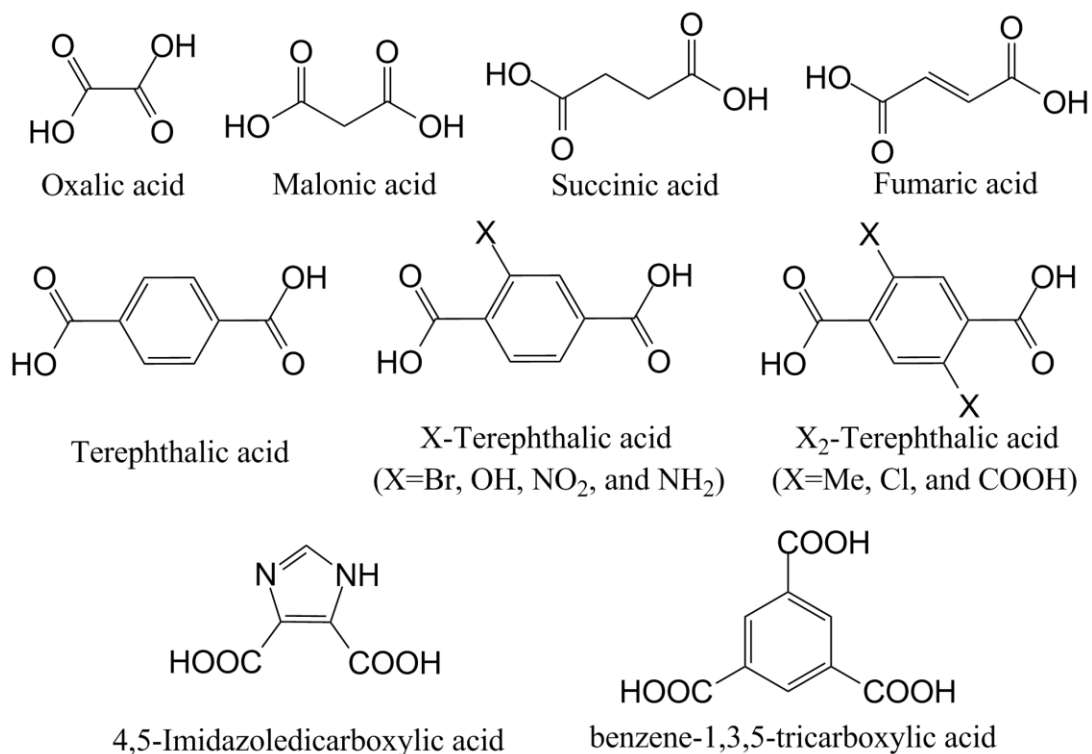


Figure 1-6. Organic linkers commonly used in building MOF structures.

Table 1-3. List of most studied MOF structures and their properties.

Nomenclature	Chemical Formula	Topological Properties	Structural Properties
MOF-5[52]	$Zn_4O(BDC)_3$	ZnO_4 tetrahedra joined by benzene dicarboxylate linkers to give a cubic framework with interconnected pores of 8 Å aperture width and 12 Å pore diameter.	Exchangeable properties of guest molecules while maintaining its morphology and crystallinity.
HKUST-1[53]	$Cu_3(TMA)_2(H_2O)_3$	Cu(II) paddlewheel dimers linked by trimesate trianions with 10 Å pore size.	The water ligands in the structure can be removed. It rehydrates when exposed to moisture. The metal ion in the cluster can be exchanged with oxophilic transition metals with higher stability.
ZIFs[54, 55]	$Zn(im)_2$	Composed of tetrahedrally-coordinated transition metal ions (e.g. Fe, Co, Cu, Zn) connected by organic imidazole linkers.	More than 100 topologies of ZIFs have been discovered[55]. The most studied ZIF-8, with a sodalite topology[56], has applications in CO ₂ capture and separation[57] and also in MOF composites.
MIL-101[58, 59]	$Cr_3F(H_2O)_2O[(O_2C-C_6H_4-CO_2)_3]$	Linked by chromium trimers and terephthalate. The pore space is constructed from two cages with diameters of 2.9 and 3.4 nm which are connected with windows with diameters of 1.2 and 1.45 nm.	Thermally stable up to 773 K with high surface area (~6000 m ² g ⁻¹).
UiO-66[60]	$Zr_3O_2(OH)_2(O_2C-C_6H_4-CO_2)_3$	Linked by zirconium trimers and terephthalate, leading to a 3D arrangement of micropores in which each centric octahedral cage (free diameter: 11 Å) is connected to eight corner tetrahedral cages (free diameter 8 Å) through triangular windows (6 Å).	Thermally stable up to 813 K; Both metal clusters and organic linkers can be functionalized easily.

1.3.2 Synthesis of MOFs

Since the discovery of MOF structures, research emphasis has been placed on synthesis of new MOF structures and better crystallinity/morphology control of existing MOFs. Until now, a number of conventional[61, 62] and novel synthesis methods have been developed. A description of these synthesis routes is listed below:

(i) Conventional synthesis methods: Conventional synthesis methods usually refer to syntheses carried out using electric heating of the synthesis devices. Based on the temperature used in the synthesis, these synthesis methods are sub-classified into solvothermal synthesis and nonsolvothermal synthesis methods. Solvothermal synthesis requires closed vessels such as autoclaves to hold the MOF precursors at the temperatures higher than the solvent boiling point. Nonsolvothermal synthesis, on the contrary, is conducted at temperatures lower than or at the boiling point of the solvent. A precipitation reaction followed by recrystallization is common in nonsolvothermal synthesis.[39] ZIF-8[63] and HKUST-1[64], for example, are commonly synthesized at low temperatures using nonsolvothermal method.

(ii) Novel synthesis methods: Novel synthesis methods use unconventional energy sources to produce MOFs, such as electrochemical energy,[65] microwave-assisted heating,[66] mechanochemical energy,[67] and sonochemical energy.[68] Electrochemical synthesis of MOF was developed by BASF[65] in the path of commercializing MOF products. Their initial purpose was to exclude anions by using metal electrodes as metal sources. This method has been proved to be a potential candidate for industrial continuous synthesis of MOFs.[69, 70] Microwave-assisted synthesis is most widely used among the novel methods.[71] Like described in microwave synthesis of zeolites, this method allows for a faster crystallization rate and production of smaller MOF crystals.[66, 72] Mechanical force can also induce chemical reactions.[73] For example, stoichiometric amounts of metal salt and organic linkers can be mixed by liquid-assisted grinding or ion-assisted grinding to produce MOF crystals. This method shows a promising path in which no external heating or

solvent is needed, and reduces the washing and activation labor after the synthesis. In sonochemical synthesis, ultrasound is applied to induce high temperature and pressure inside the system through the cavitation process. Chemical reactions can take place within the cavity, at the interface, or in the bulk media. Early works demonstrated MOF nanocrystals can be obtained by room temperature fast synthesis assisted by ultrasound.[68, 74]

1.3.3 Functionalization of MOFs

The diversity of MOF structures creates a variety of functionalities and potential applications for the as-synthesized MOFs. Additionally, the components in MOFs, either metal clusters or organic linkers, can be further modified to bring in new functionalities. The methods for functionalization of MOFs include presynthetic modification, postsynthetic modification (PSM) and postsynthetic deprotection (PSD), respectively.

The presynthetic modification requires the introduction of functional groups to the building blocks (most commonly functionalized linkers) prior to the synthesis. In this method, the synthetic conditions developed for the original MOFs may become inefficient because of the changes in chemical properties of linkers.[52, 75] Therefore, only a limited number of functional groups can be introduced into MOF frameworks.

The postsynthetic modification of MOFs, however, circumvents problems in the presynthetic modification of MOFs. PSMs are heterogeneous processes in which the modifications are directly performed on the MOF frameworks via covalent PSM or dative PSM, on the basis of chemical bond type formed or broken in the process. This functionalization method has been widely reported by the work in Cohen's group.[76-

79] A concern in this method is that the framework remains unimpaired during the process.

PSD is a variant of PSM in which a protected functional group is introduced before the solvothermal reaction without interfering with the solvothermal conditions. Afterwards, the protecting groups are removed either in situ[80] or after synthesis[81] to recover the functional groups.

1.3.4 Application of MOF Materials

As nanoporous materials, MOFs break the limitation of the small pore sizes of zeolites. They can be used for a number of potential applications, including gas separation, storage, and heterogeneous catalysis.[6, 7, 38, 62, 82-87] Below is a brief description for each type of applications.

(i) Gas storage: The gas storage capability of MOFs originates from the large void volume in the framework. The first example in MOF storage showed a comparable CH₄ adsorption capacity to that of zeolite and activated carbon.[88] To date, the highest CH₄ uptake reported is 189 mg g⁻¹ in Porous Coordination Network-14 (PCN-14) at 35 bar and 290 K.[89]

MOFs are also good storage materials for H₂ at 77 K and moderate pressure (<100 bar) conditions,[62] however, the cryogenic and high pressure systems are usually not feasible for practical applications. To improve H₂ loading capability of MOFs at low pressure, kinetic trapping mechanism can be used by creating modulated interactions and distances between MOF framework and adsorbate molecules entering the framework.[90] On the other hand, Pt particles loaded to the MOF framework will

lead to H₂ spillover effect,[91] which will improve H₂ diffusion and make it possible to adsorb H₂ at room temperature.

(ii) Gas separation: MOFs have regulated and uniform pore systems and thus can be used in separation applications. For this application, MOFs are usually mixed with a substrate to improve permeability and stability of the MOF materials. For example, ZIF-8/Matrimid was prepared by a solution-blending approach and the as-prepared membranes enhanced the transport of CO₂ gas from CO₂/CH₄ gas mixtures.[92] Silica@MOF core-shell composite spheres were fabricated by the seeded growth method and the application of silica@MOF composite spheres as stationary phases for chromatographic separation.[93]

(iii) Catalysis: MOFs as catalysts can be synthesized or functionalized with active sites including unsaturated metal sites or functional groups on organic linkers. Synthesis of MOFs containing unsaturated metal sites requires the introduction of labile guest molecules that can be removed in the activation stage. MOFs with metal active sites have been used in catalytic reactions such as hydrogenation/isomerization,[94, 95] cyanosilylation,[96] oxidation,[97, 98] photocatalysis,[99] etc. Organic functional groups are brought into the framework by either presynthetic modification or postsynthetic modification. MOFs with functional groups as active sites have been reported in Knoevenagel condensation,[100, 101] and also in transesterification,[102] polymerization[103] and aldol reactions.[104]

1.3.5 MOF-based Core-Shell Composites

In addition to tailoring frameworks for potential broad applications, synthesis of MOF-based composites is another approach to improve the functionalities and

applications of MOFs. Generally, the composites are formed by physical or chemical mixing of MOFs with inorganic or organic materials, which allows easy modification of MOFs for practical subjects. The materials selected possess properties that are complementary with MOFs, resulting in combined merits coming from MOFs (high surface area, tunable pore size and functionality) and functional materials (mechanical, electrical, magnetic and catalytic properties). Up to now, MOF composites have been built successfully with metal,[105] oxides (metal oxides, silica),[106, 107] polymers,[84] carbons (CNTs, graphene)[108] and semiconductors,[109] etc. Table 1-4 lists the recent studies on MOF-based core-shell composites.

Table 1-4. Recent studies on MOF-based core-shell composites and their applications.

Core-shell composite	Synthesis method	Applications	Example materials
Metal nanoparticles (MNPs)@MOF	Grow MOFs around pre-synthesized MNPs. Surface modification to the MNPs is essential in some cases to facilitate MOF growth on the surface of MNPs	Hydrogen storage,[110] heterogeneous catalysis[111] and sensing[112]	Au/Ag/Pt NPs@ZIF-8.[113]
Metal oxide nanoparticles @MOF	Metal oxide NPs surface are decorated with analogs of MOF building blocks (functional groups with amine or carboxylic acid) to facilitate MOF growth.	Magnetism[114]	Fe ₂ O ₃ NP@DUT-4/DUT-5/HKUST-1 [114]
Silica@MOF	Grow MOF on surface decorated SiO ₂ .	Drug delivery[115]	SiO ₂ @In(IPA) _m [116]
Polymer@MOF	Grow MOF on surface-decorated polymer particles	Catalysis, separations, gas storage	Polystyrene@ZIF-8[117]
Quantum dots (QDs)@MOF	The modification of QD surfaces can promote MOF formation around QDs	photostability, fluorescent properties and quantum effects[118]	CdTe@ZIF-8.[113]
Carbon@MOF	Grow MOF on graphene and CNTs.	Hydrogen storage[108]	CNT@MOF-5[108]

1.4 Motivation and Thesis Outlines

Zeolites are traditional crystalline microporous aluminosilicates, while MOFs are an emerging class of nanoporous materials. The combination of zeolites and MOFs should be a very promising platform for advancing these two materials for various applications considering the well-developed catalytic applications of zeolites and the intriguing potential of MOFs. The synthesis of zeolite/MOF composites, however, has not been reported in literature. This thesis work aimed to explore the approaches to synthesize the composite materials and their applications as catalysts in cascade reactions.

The integration of MOF and zeolite into composite materials especially core-shell composites is the main objective of this thesis. Moreover, presynthetic and postsynthetic modification has been carried out to make the composites catalytic bifunctionality in two-step cascade reactions. Chapter 2 of this thesis reports the synthesis of ZSM-5@UiO-66, an example of zeolite/MOF core-shell composite, by sequential hydrothermal synthesis of ZSM-5 core and solvothermal growth of UiO-66 on the zeolite support. The as-synthesized composite was modified by PSM to acquire acid-base bifunctionality for two step cascade reactions. Chapter 3 discusses the synthesis of ZSM-5@UiO-66 with 2-aminobenzene-1,4-dicarboxylic acid (NH₂-BDC) linkers. By using the NH₂-BDC linkers, amine groups were incorporated into the catalyst in MOF crystallization step. The bifunctionality in the ZSM-5@UiO-66-NH₂ synthesized by this approach was confirmed by the two-step cascade reactions used in Chapter 2. Chapter 4 summarizes the work on the synthesis of ZSM5@MIL-101 nanoporous composites. The replacement of UIO-66 with MIL-101 in the composites

indicates that the synthetic methodology developed in this thesis is applicable to produce other types of zeolite@MOF composites. Chapter 5 summarizes the conclusions of this thesis work with proposed future research as extensions of this work.

Chapter 2: Synthesis and Postsynthetic Modification of ZSM-5@UiO-66 Core-Shell Particles as Bifunctional Catalysts

2.1 Introduction

Metal-organic frameworks (MOFs) are an emerging class of crystalline microporous materials. The uniform micropores and high surface areas enable them a number of potential applications, including separation, storage, and heterogeneous catalysis.[6, 7, 38, 62] The structure of MOFs is constructed by metal ions or clusters that act as lattice nodes and are held in place by multidentate organic ligands. Since a range of metal clusters and organic ligands can be built into MOFs, a wide structural diversity and highly designable pore sizes and shapes in MOFs are expected, which endow MOFs with tunable cavity architectures and properties.[37] Furthermore, the primary framework of MOFs can be functionalized through pre- or post-synthetic modification of metal clusters and/or organic ligands, and thus offers the possibility for fine-tuning their pore dimensions and local environment inside the micropores.[79] The great tunability in structures and functional properties of MOFs allows potential implementation of MOFs into technical materials for practical applications.

In addition to tailoring the structure of MOFs, synthesis of MOF-based composites is another approach to advance their functionalities for practical applications.[119] MOF-based composites are generally formed by physical or chemical mixing of MOFs with inorganic and/or organic substrates that allows an easy modification of MOFs for practical applications. Recently, MOF-based composite membranes and spherical solids have been prepared for direct uses in gas or liquid

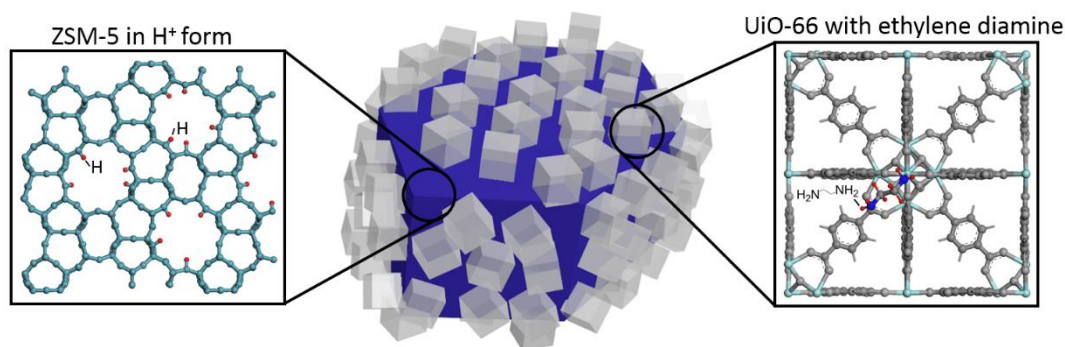
separations and as catalysts in heterogeneous catalytic reactions. For example ZIF-8/Matrimid were prepared by a solution blending approach and the as-prepared membranes have been found to enhance the transport of CO₂ gas from the CO₂/CH₄ gas mixtures;[92] Uniform coating of Cr-MIL-101 inside the macropores of a cylindrical cordierite monolith was achieved by the secondary growth technique and the composite was used as stable catalyst in liquid-phase oxidation reactions;[120] Silica@MOF core-shell composite spheres were fabricated by the seeded growth method and they were used as stationary phases for chromatographic separation to overcome the problems such as low column efficiency, high column back pressure, and undesirable peak shapes caused by the direct packing of MOF particles of irregular shapes.[93] These studies illustrate the recent research efforts in advancing MOF-based composites into technical materials for practical applications.

In this study, we report the synthesis of zeolite@MOF core-shell structured composites by solvothermal growth of MOF on the surface of zeolite support and demonstrate an application of this material as a bifunctional acid-base catalyst in two-step cascade reactions. Zeolites are crystalline microporous aluminosilicates, widely used as heterogeneous catalysts, adsorbents, and ion-exchange materials in petrochemical and fine chemical industries.[8, 121-123] As porous materials, zeolite and MOF share common characteristics of high surface areas and uniform micropores but they differ in thermal/mechanical stability and structural flexibility.[124] In this context, the zeolite@MOF composites are expected to be a novel and useful porous system where inorganic zeolite and organic MOF components impart the advantages of higher thermal, mechanical and structural stability of zeolites and specific

functionality and high flexibility of MOFs for a variety of applications. To our knowledge, however, the integration of MOF and zeolite into core-shell structured composites has not been reported in literature.

In this chapter, the synthesis of ZSM-5@UiO-66 core-shell structured composites and demonstration of this material as a bifunctional acid-base catalyst in two-step cascade reactions is reported. ZSM-5 is a medium pore zeolite with a pore system consisting of two types of intersecting straight and zig-zag 10 member ring channels, which is widely studied as membrane materials in xylene separation and catalysts in petroleum refinery.[125-127]

UiO-66 is Zr-containing MOF composed of hexameric Zr_6O_32 units linked by benzenedicarboxylate (BDC) linkers and has excellent stabilities not typically found in common porous MOFs.[60] The ZSM-5@UiO-66 composite is a promising chemical and thermal stable material with a wide range of applications. A schematic illustration of the functional composite is shown in Scheme 2-1.



Scheme 2-1. Schematic illustration of the functional composite with acid and base catalytic sites in zeolite and MOF framework, respectively.

2.2 Experimental

2.2.1 Materials

Tetrapropylammonium hydroxide (TPAOH, 40% in aqueous solution), tetraethylorthosilicate (TEOS, 98%), aluminum isopropoxide (99.99%), $ZrCl_4$ (99.9%) and 1,4-benzene-dicarboxylate (BDC, 98%) were purchased from Alfa Aesar. NaOH (97%), ethylene diamine (ED, 99.5%) and malononitrile (99%) were purchased from Sigma-Aldrich. Dimethylformamide (DMF, 99.8%) and anhydrous toluene (99.5%) were purchased from BDH. Hydrochloric acid (36.5%-38.0%) was purchased from JT Baker. Acetonitrile (99.9%) was purchased from Fisher. Benzaldehyde dimethyl acetal (98%) was purchased from SAFC. All chemicals were used as received without further treatment. Deionized (DI) water was used in all purpose.

2.2.2 Synthesis of ZSM-5

Zeolite ZSM-5 was hydrothermally synthesized by using the recipe with a composition of $100SiO_2:0.5Al_2O_3:1NaOH:36TPAOH:4000H_2O$. Typically, 0.0111 g NaOH and 5.075 g TPAOH solution were added to 20 g DI water. Subsequently, 0.0564 g aluminum isopropoxide and 5.78 g TEOS were added to the solution. The as-prepared mixture was stirred vigorously at room temperature for 8 h, followed by 5 days in tumbling Teflon-lined steel autoclaves at 423 K. The product was collected by centrifugation and washed repeatedly with DI water to reduce pH to ~ 9 . Afterwards, the product was dried at 343 K and calcined at 873 K under flowing air (150 mL min^{-1}) for 6 h. The as-synthesized ZSM-5 was ion exchanged three times using 1 mol L^{-1} aqueous NH_4NO_3 solution at 353 K for 2 h, and subsequently, collected by

centrifugation, washed with DI water for three times, and dried at 343 K overnight. The zeolite sample in its NH_4^+ -form was treated in flowing air (150 mL min^{-1}) by increasing the temperature from ambient to 823 K at 1.5 K s^{-1} and holding for 4 h to thermally decompose to NH_3 and H^+ .

2.2.3 Synthesis of UiO-66 and ZSM-5@UiO-66

The synthesis of UiO-66 particles was carried out as follows: 0.106 g ZrCl_4 and 0.068 g BDC were dissolved in 24.9 g DMF in sequence. The solution was transferred to a Teflon-lined stainless steel autoclave and allowed to react at 393 K for 24 h. The product was collected by centrifugation and washed by dispersing in DMF for 12 h under rigorous magnetic stirring. The DMF washing and centrifugation steps were repeated three times. Afterwards, the sample was dispersed in methanol solvent for 12 h followed by centrifugation in order to remove the DMF solvent. This step was repeated two times. Finally, the sample was dried in a vacuum oven at 423 K overnight. The synthesis of ZSM-5@UiO-66 core-shell composite was performed with the same procedure as described above except that 0.15 g ZSM-5 particles were added to the UiO-66 synthetic solution prior to the solvothermal crystallization of MOF particles.

2.2.4 Incorporation of amine ($-\text{NH}_2$) groups into ZSM-5@UiO-66

The incorporation of amine groups into the composite was performed in a 150 mL flask equipped with a reflux condenser and heated in a temperature controlled oil bath under atmospheric pressure and magnetic stirring (500 rpm) conditions. Firstly, 150 μL ethylene diamine and 90 mL anhydrous toluene were added into the flask. 1.5g ZSM-5@UiO-66 composite particles were then added to the ethylene diamine/toluene

solution. After the suspension was refluxed at 385 K for 12 h, the ZSM-5@UiO-66 particles were collected by centrifugation and washed by dispersing in absolute ethanol. The ethanol washing and centrifugation steps were repeated three times. Finally, the particles were dried in convective oven at 343 K overnight. The as-obtained sample was denoted as ED-ZSM-5@UiO-66.

The intrinsic acid sites in zeolite micropores were deactivated during the synthesis and incorporation of amine groups. Several solution exchange methods followed by intermediate temperature treatment were tested to optimize the catalytic activity. The ED-ZSM-5@UiO-66 was soaked in exchange solution in order to extract free ethylene diamine trapped in zeolite micropores. The exchange solutions include NH_4NO_3 water solution, NH_4NO_3 ethanol solution, and HCl ethanol solution (with different concentrations). The general exchange procedure is described as follows. The exchange was performed in a 50 mL flask equipped with a reflux condenser and heated in a temperature controlled oil bath under atmospheric pressure and magnetic stirring. 0.1 g ED-ZSM-5@UiO-66 was added to 20 mL exchange solution. The mixture was refluxed at 363 K 3 times for a total of 6 h. The exchanged particles were washed with water and ethanol repeatedly. The sample was then dried at 423K in vacuum oven. The sample was denoted as NH_4NO_3 -ED-ZSM-5@UiO-66 or HCl-ED-ZSM-5@UiO-66 after this step.

2.2.5 Product characterizations

The crystalline phase of the samples was determined by X-Ray powder diffraction (XRD) using Bruker D8 Advance Lynx Powder Diffractometer. The integration time was 0.3 hours and the step size was 0.032 degrees/second. The

morphology and elemental analysis of the samples were obtained by a scanning electron microscope (SEM, Hitachi SU-70) equipped with an energy dispersive X-ray (EDX) spectrometer. Transmission electron microscopy (TEM) images were recorded on a JEM 2100 LaB6 microscope at an accelerating voltage of 200 KV. Nitrogen (N₂) and Argon (Ar) adsorption-desorption measurements were carried out at 77 K and 87 K on an Autosorb-iQ analyzer (Quantachrome Instruments), respectively. Prior to the N₂ and Ar measurements, samples were outgassed at 423 K overnight. The FT-IR spectrum was recorded with a spectrometer (Nicolet Magna-IR 560) in the range of 4000 - 400 cm⁻¹. Each sample was measured with 128 scans at an effective resolution of 4 cm⁻¹. The thermogravimetric analysis (TGA) was conducted using a thermogravimetric analyzer (TGA 2950, TA Instruments) under a mixed air and N₂ flow (100 mL min⁻¹, 60% air and 40% N₂) with a heating rate of 5 K min⁻¹ from 298 K to 1073 K.

2.2.6 Catalytic reaction over ZSM-5@UiO-66 composite

The liquid phase catalytic conversion of benzylidene malononitrile from malononitrile and benzaldehyde dimethyl acetal (Scheme 2-2) was carried out in a three-necked flask equipped with a reflux condenser and heated in a temperature controlled oil bath under atmospheric pressure and magnetic stirring (0.5" stirring bar and 500 rpm stirring speed) conditions. In a typical experiment, 20 mL acetonitrile, 0.0866 g malononitrile (1.31 mmol), 7.5 μ L DI water, and 0.05 g catalyst (NH₄NO₃-ED-ZSM-5@UiO-66 or HCl-ED-ZSM-5@UiO-66) were added into the flask in sequence. After bubbled the mixture with flowing helium for 0.5 h, the flask was immersed in the oil bath preheated at 353 K. The reaction mixture was maintained for

0.5 h at the required reaction temperature and stirring conditions and then 0.2045 mL of benzaldehyde dimethyl acetal (1.36 mmol) was added. This moment of addition was taken as the initial reaction time. Liquid samples were withdrawn at regular intervals and analyzed by the gas chromatograph (Agilent 7890A) equipped with a methylsiloxane capillary column (HP-1, 50.0 m x 320 μm x 0.52 μm) connected to a flame ionization detector (FID). The influence of external mass transfer limitations on the reaction rates was ruled out by running the reactions at a high enough stirring speed (500 rpm), showing a further increase in the stirring speed did not enhance the reaction rate. The reactant mixture without addition of zeolite catalysts showed no conversion under the investigated reaction conditions.

The GC calibration curves of all the reactants (benzaldehyde dimethyl acetal, malononitrile) and products (benzaldehyde, benzylidene malononitrile) in the cascade reactions were obtained by the external calibration method. The maximum concentration of the chemicals in the catalytic reaction was 0.068 mol L⁻¹. The standard samples were prepared with concentrations of 0.015 mol L⁻¹, 0.030 mol L⁻¹, 0.045 mol L⁻¹, 0.060 mol L⁻¹ and 0.075 mol L⁻¹. The calibration curves are shown in Figure 2-1. All curves show a linear response of peak area vs. concentration with R² larger than 0.9996.

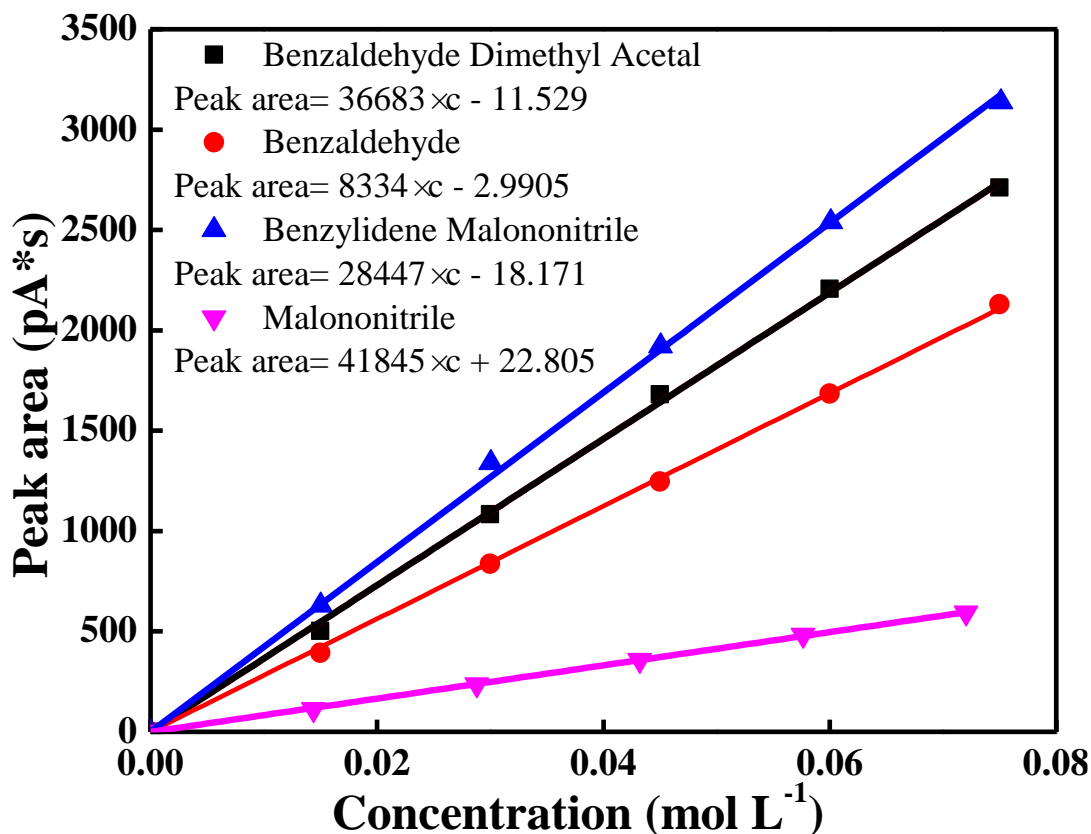


Figure 2-1. Calibration curves of benzaldehyde dimethyl acetal, malononitrile, benzaldehyde and benzylidene malononitrile.

2.3 Results and Discussion

The morphologies of ZSM-5, UiO-66, and ZSM-5@UiO-66 composite samples were observed with scanning electron microscope (SEM) and transmission electron microscope (TEM), and the representative images are shown in Figure 2-2. The ZSM-5 zeolite (Figure 2-2(A)) consists of short cylindrical particles with well crystallized smooth surfaces. The average width the particles is 250 nm and thickness is 180 nm. The UiO-66 (Figure 2-2(B)) contains aggregated cubic particle with an average size of ~ 100 nm. ZSM-5@UiO-66 composite (Figure 2-2(D)-(F)) contains bulk ZSM-5 cores and sparse UiO-66 particles on the ZSM-5 surface, showing the formation of core-shell zeolite@MOF composite clearly. In particular, Figure 2-2 (E) shows the side view of

the cylinder shape ZSM-5 and Figure 2-2 (F) shows the top view of the cylinder shape ZSM-5. The similarity between the lattice parameters of ZSM-5 ($a = 20.090 \text{ \AA}$, $b = 19.738 \text{ \AA}$, $c = 13.142 \text{ \AA}$, $\alpha = \beta = \gamma = 90^\circ$) and UiO-66 ($a = b = c = 20.700 \text{ \AA}$, $\alpha = \beta = \gamma = 90^\circ$) might lead to an epitaxial growth of UiO-66 from ZSM-5 crystal surface[60, 128]. Nanosized zeolite seeds have been reported to promote fast growth of MOF crystals[129]. Extra experiments using ZSM-5 cores with different size and silica-alumina ratio were investigated and presented at the last of this section.

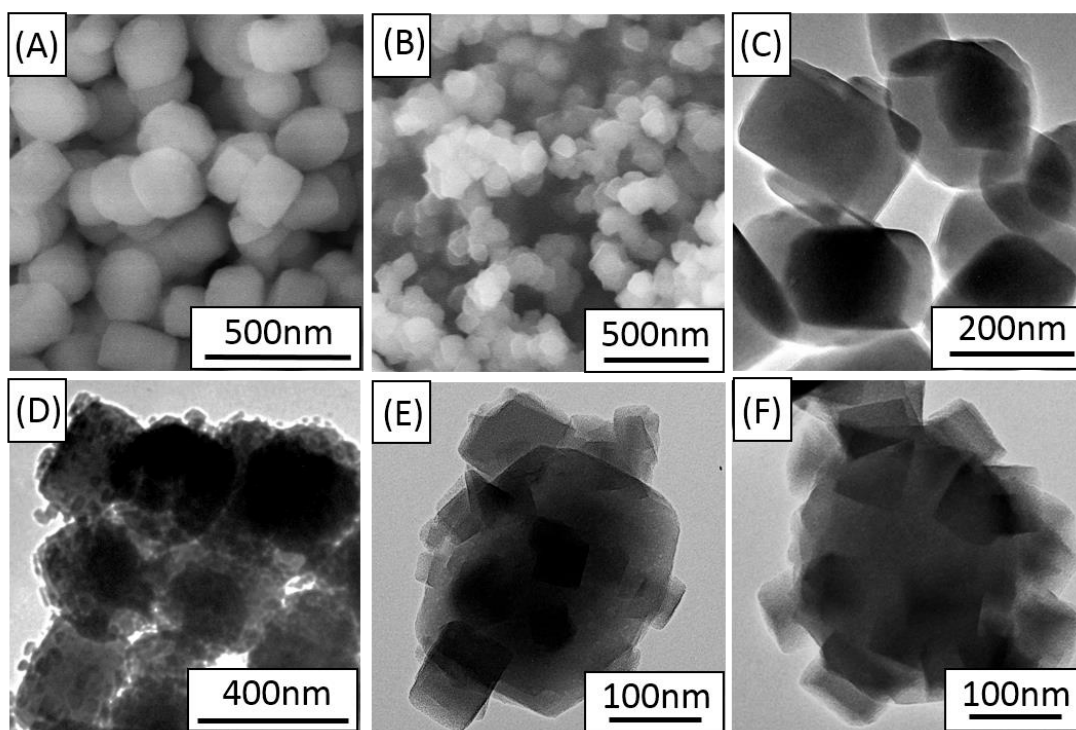


Figure 2-2. SEM images of (A) ZSM-5 zeolite, (B) UiO-66 MOF, and TEM images of (C) ZSM-5, (D), (E) and (F) ZSM-5@UiO-66.

In order to confirm the composition and crystallinity of the particles, powder X-ray diffraction (XRD) and energy-dispersive X-ray (EDX) spectroscopy were employed. Figure 2-3 shows the XRD patterns of the synthesized ZSM-5, UiO-66, ZSM-5@UiO-66 and ED-ZSM-5@UiO-66 particles, respectively. Both ZSM-5 (a) and

UiO-66 (b) are highly crystallized, resembling the characteristic of a crystalline ZSM-5 and UiO-66 reported in literature[60, 125]. The ZSM-5@UiO-66 (c) composite consists of diffraction peaks from both UiO-66 and ZSM-5, indicating the presence of both phases in the composite materials. In addition, the absence of new diffraction peaks or broadening of characteristic peaks of ZSM-5 or UiO-66 indicates no other structure formation and deterioration of the crystalline phases in the synthesis conditions. In addition, all of the crystalline phases were well preserved after the addition of ethylene diamine (ED).

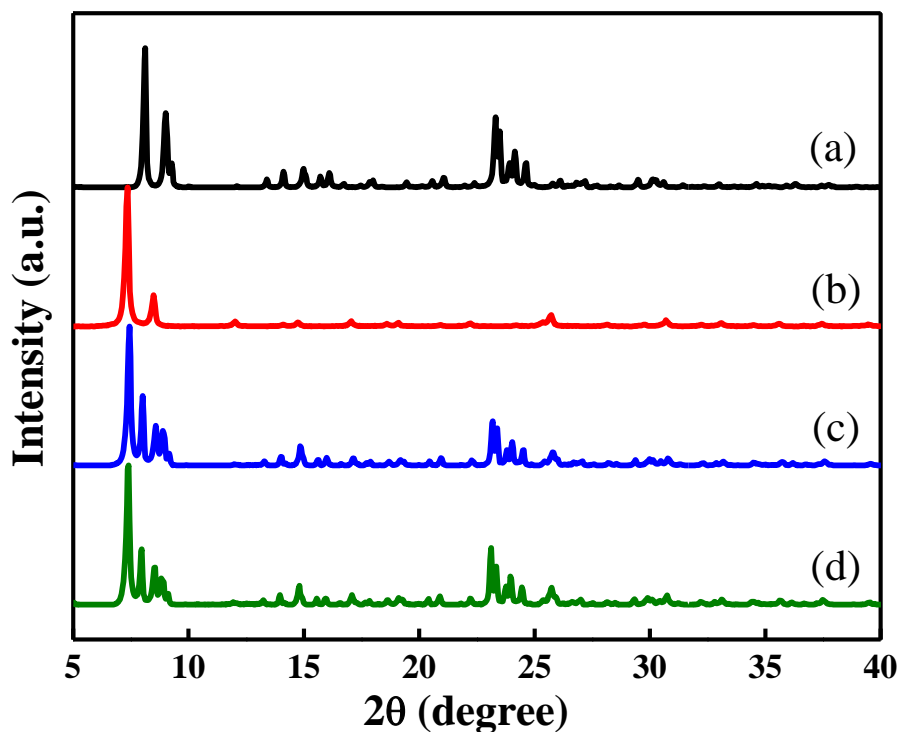


Figure 2-3. XRD patterns of (a) ZSM-5, (b) UiO-66, (c) ZSM-5@UiO-66, and (d) ED-ZSM-5@UiO-66.

The elemental compositions of the ZSM-5 solid core and ZSM-5@UiO-66 core-shell particle were verified with EDX spectroscopy, as shown in Figure 2-4, to distinguish the core-shell structure from a physical mixture of ZSM-5 and UiO-66. The

EDX spectrum (A) is of the ZSM-5 solid core particles. The ZSM-5 construction element Si, Al and O are shown in the figure with $K\alpha$ characteristic X-ray energy of 1.739 KeV, 1.486 KeV and 0.525 KeV, indicating the presence of zeolite particles. The EDX spectrum (B) is of the core-shell particles and is comprised of Si, Al, O and Zr peaks, indicating the presence of zeolite and MOF structures. The primary construction element of UiO-66 Zr is shown with $L\alpha$ characteristic X-ray energy of 2.042 KeV. The C peaks in both figures are from the carbon tape used for sample preparation in SEM characterization. The peaks at 0 come from the X-ray beam of the instrument. The EDX was done during the SEM and was performed on isolated particles, thus confirms the successful growth of UiO-66 onto ZSM-5 and the preservation of the crystallinity of both materials.

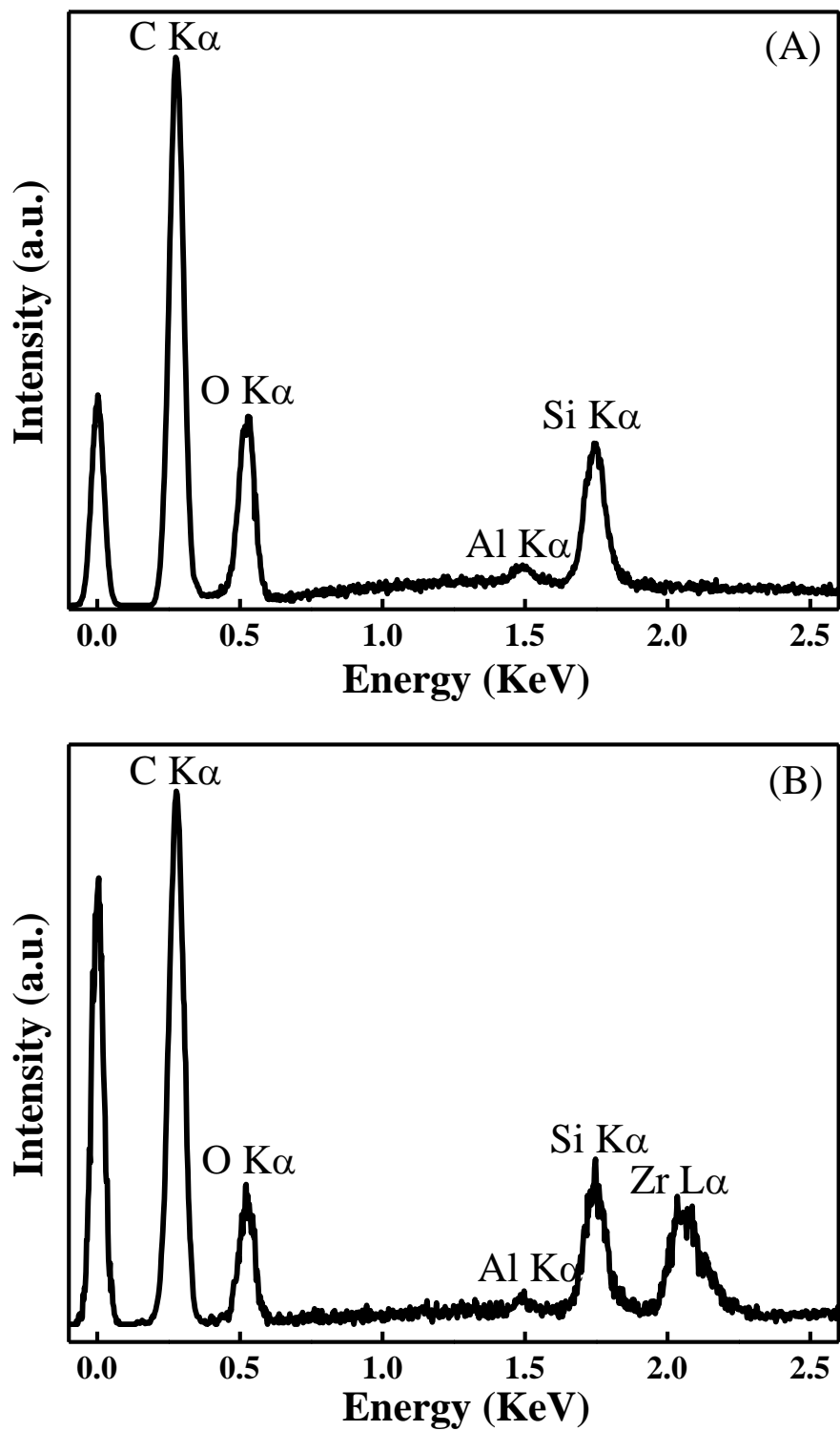


Figure 2-4. EDX spectra of as-synthesized (A) ZSM-5 zeolite and (B) ZSM-5@UiO-66 core-shell composite.

N₂ and Ar adsorption/desorption isotherms were used to characterize the textural properties of the samples. In particular, N₂ adsorption-desorption isotherms (Figure 2-5) were carried out to determine the surface area and total pore volume of the samples. The surface area was calculated using the multipoint BET method. The total pore volume was calculated using the NLDFIT method on the adsorption branch. The textural parameters of the synthesized samples extracted from N₂ and Ar adsorption/desorption measurements are summarized in Table 2-1. The surface area of UiO-66 was comparable to the value reported in literature. The ZSM-5 showed a slightly surface area than the normal microporous ZSM-5 due to its smaller particle size. The surface area and total pore volume of core-shell structure shows a combination of ZSM-5 and UiO-66, revealing the accessibility of the micropores of both materials. The surface area and total pore volume decreased upon addition of ED because ED occupied the micropores of the sample. The surface area and total pore volume resumed after the sample was washed with HCl solution.

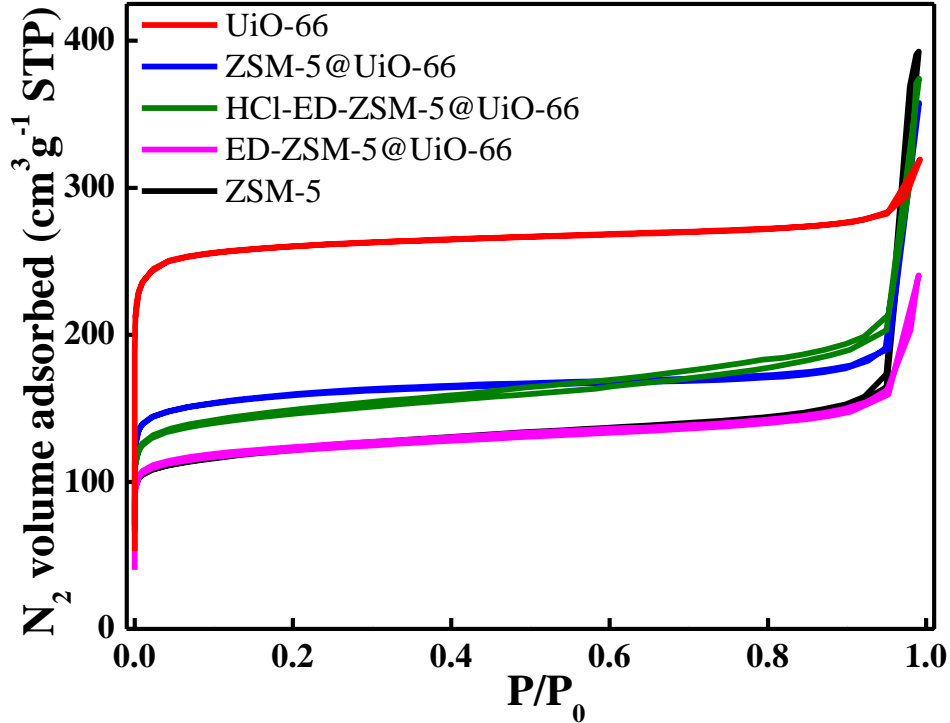


Figure 2-5. N₂ adsorption-desorption isotherms of UiO-66, ZSM-5, ZSM-5@UiO-66, ED-ZSM-5@UiO-66, and HCl-ED-ZSM-5@UiO-66, respectively.

Table 2-1. Textural properties of UiO-66, ZSM-5, ZSM-5@UiO-66, ED-ZSM-5@UiO-66, and HCl-ED-ZSM-5@UiO-66, derived from N₂ and Ar isotherms.

Samples	S_{micro}^a [m ² g ⁻¹]	S_{ext}^a [m ² g ⁻¹]	V_{micro}^a [cm ³ g ⁻¹]	V_{total}^b [cm ³ g ⁻¹]	S_{BET}^c [m ² g ⁻¹]
UiO-66	1002	47	0.38	0.43	1048
ZSM-5	390	76	0.15	0.25	466
ZSM-5@UiO-66	570	51	0.22	0.29	621
ED-ZSM-5@UiO-66	403	68	0.16	0.25	471
HCl- ED-ZSM-5@UiO-66	466	98	0.19	0.31	564
Samples	S_{micro}^d [m ² g ⁻¹]	S_{ext}^d [m ² g ⁻¹]	V_{micro}^d [cm ³ g ⁻¹]	V_{total}^e [cm ³ g ⁻¹]	S_{BET}^f [m ² g ⁻¹]
UiO-66	837	42	0.30	0.35	879
ZSM-5	458	28	0.17	0.22	486
ZSM-5@UiO-66	513	41	0.19	0.25	554
ED-ZSM-5@UiO-66	410	47	0.15	0.22	456
HCl-ED-ZSM-5@UiO-66	475	60	0.17	0.27	536

^a Determined from *t*-plot method applied to the N₂ isotherm. ^b Total pore volume calculated at P/P₀=0.95 applied to the N₂ isotherm. ^c Determined from multi-point BET method applied to the N₂ isotherm. ^d Determined from *t*-plot method applied to the Ar isotherm. ^e Total pore volume calculated at P/P₀=0.95 applied to the Ar isotherm. ^f Determined from multi-point BET method applied to the Ar isotherm.

Ar adsorption-desorption measurements were conducted to examine the porosity features of the composite samples. In Figure 2-6 (A), the Ar isotherms show similar behavior with N₂ isotherms. The pore size distributions of the materials were derived from the Ar adsorption-desorption isotherms using the non-local density functional theory (NLDFT) method on the adsorption branches assuming spherical/cylindrical pores are shown in Figure 2-6 (B). The pore sizes of UiO-66 are 7.2 Å and 9.6 Å, respectively, smaller than the ones corresponding to the tetrahedral cages (8 Å) and octahedral cages (11 Å). The spherical/cylindrical pore model was also used to calculate the pore size of pure ZSM-5, resulting in larger pore size (7.3 Å) than its theoretical value of 5.4-5.6 Å. The isotherm of as-synthesized ZSM-5@UiO-66 shown in Figure 2-6 (B) illustrating the combination of the two pore systems inherited from ZSM-5 and UiO-66, suggesting no intergrowth of the two materials.

NLDFT pore size analysis in Figure 2-6(B) shows that ZSM-5 has a micropore size of 7.1 Å, larger than the typical micropore size (5.4-5.6 Å) of ZSM-5. The analysis was derived from the adsorption branch of Ar isotherms on the basis of spherical/cylindrical pore model. To verify the influences of pore model selected in the analysis on the micropore sizes of ZSM-5 and UiO-66 materials, the Ar adsorption branches were further analyzed on the basis of a cylindrical pore model, and the resultant pore size distributions are shown in Figure 2-6(C). ZSM-5 has a typical pore size of ~ 5.2 Å, while UiO-66 has a micropore size of ~ 6.1 Å and ~ 5.0 Å (a shoulder next to the peak), corresponding to its tetrahedral cages and octahedral cages, respectively. These results also demonstrate that ZSM-5@UiO-66-NH₂ and ZSM-5@UiO-66 are comprised of dual micropore systems.

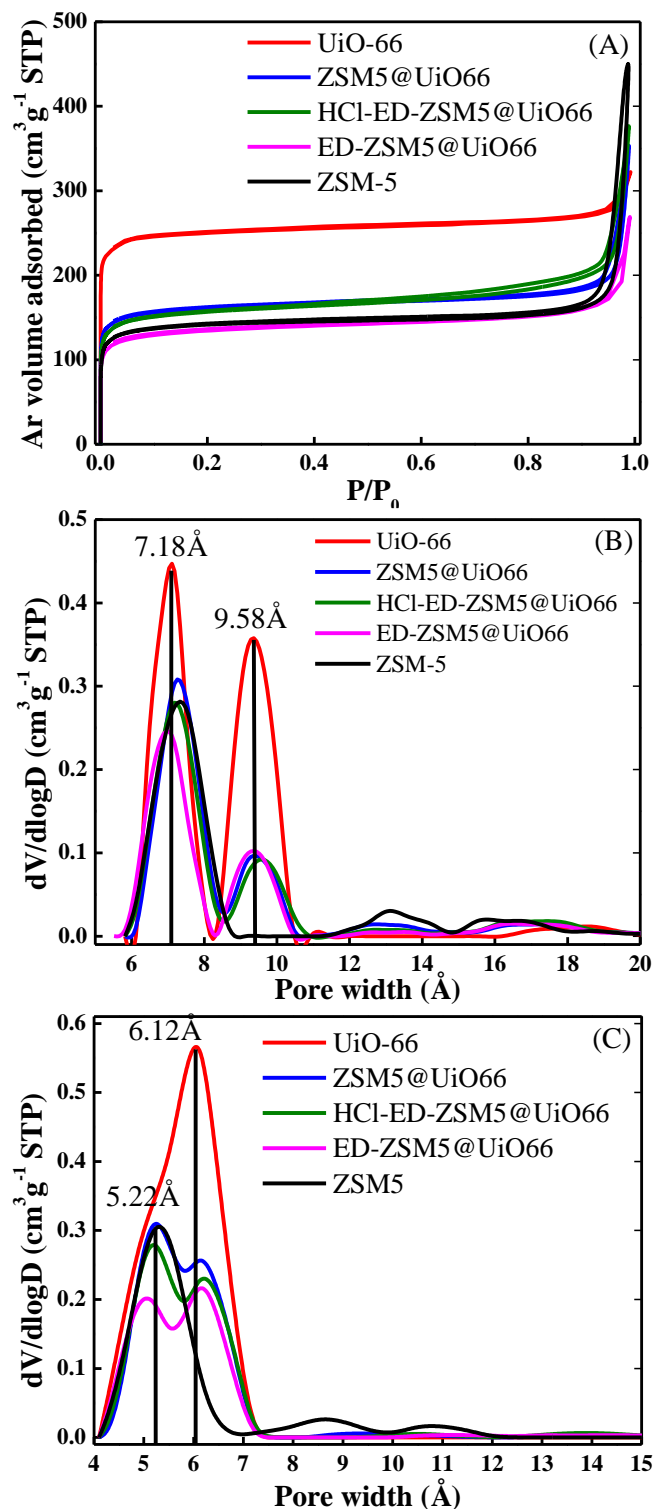


Figure 2-6. Ar adsorption-desorption isotherms (A), and the corresponding pore size distributions (B) derived from Ar sorption (NLDFT on the adsorption branch on the basis of spherical/cylindrical pore model) and (C) NLDFT on the adsorption branch on the basis of cylindrical pore model, of as-synthesized UiO-66, ZSM-5, ZSM-5@UiO-66, ED-ZSM-5@UiO-66, and HCl-ED-ZSM-5@UiO-66, respectively.

Infrared spectroscopy was applied to characterize the amine group grafting. The absorption bands centered around 1390, 1506, and 1583 cm^{-1} correspond to the O-C-O symmetric stretching ($\nu_{s,\text{O-C-O}}$), C-C ring symmetric stretch ($\nu_{s,\text{C-C}}$), and O-C-O asymmetric stretching ($\nu_{as,\text{O-C-O}}$) vibrational modes, respectively, of the organic BDC linkers in UiO-66[130]. The absorption band centered at 1087 cm^{-1} is attributed to the asymmetric stretching vibration of T-O-T (T: Si or Al) ($\nu_{as,\text{T-O-T}}$) in the framework of the ZSM-5 zeolite[131]. The appearance of these absorption bands, for example, 1087 cm^{-1} and 1390 cm^{-1} , in ZSM-5@UiO-66 and HCl-ED-ZSM-5@UiO-66 suggests the coexistence of ZSM-5 and UiO-66 in the composite. The presence of amine groups in HCl-ED-ZSM-5@UiO-66 is revealed by the asymmetric ($\nu_{as,\text{C-H}} = 3016 \text{ cm}^{-1}$) and symmetric ($\nu_{s,\text{C-H}} = 2947 \text{ cm}^{-1}$) stretching vibrations of C-H and asymmetric stretching ($\nu_{as,\text{N-H}} = 3460 \text{ cm}^{-1}$) of bonded $-\text{NH}_2$, respectively[132].

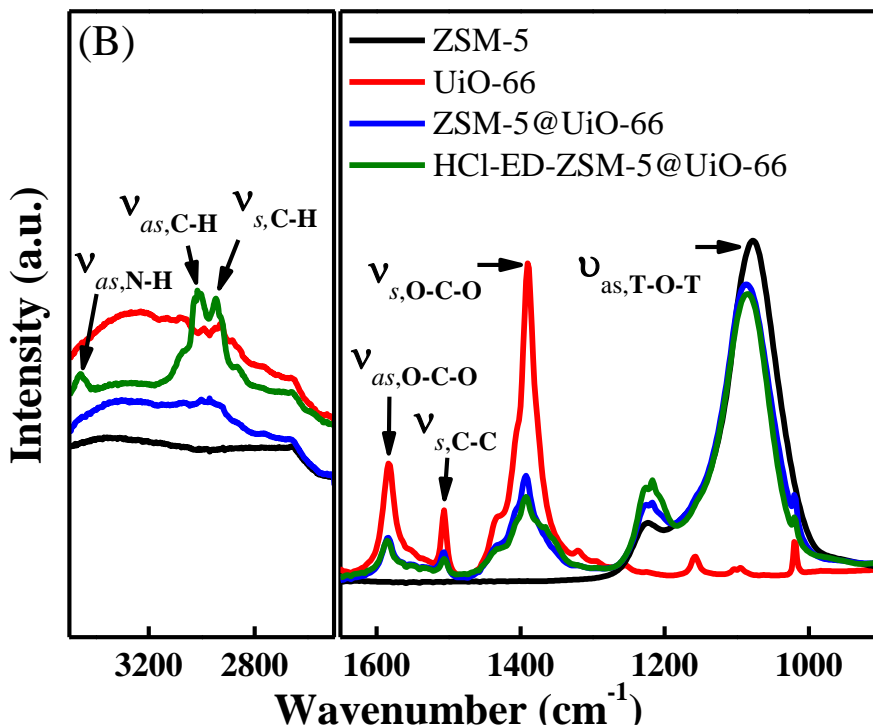


Figure 2-7. FTIR spectra of UiO-66, ZSM-5, ZSM-5@UiO-66, ED-ZSM-5@UiO-66, and HCl-ED-ZSM-5@UiO-66, respectively.

Thermogravimetric analysis (TGA) was performed to study the thermal stability and the mass fractions of UiO-66 and ZSM-5 in the composite materials. Figure 2-8 shows the TGA curves of ZSM-5, UiO-66, ZSM-5@UiO-66 and HCl-ED-ZSM-5@UiO-66, respectively. The weight loss in the proton-form ZSM-5 is 3.3 wt%, due to desorption of moisture adsorbed in the zeolite. UiO-66 shows the weight loss in two stages with increasing temperature. The first stage of weight loss happened below 650 K, which resulted from the moisture desorption from the UiO-66 sample. The second stage of weight loss stayed between 690 K and 800 K, which is mainly due to the decomposition of organic component in the sample. Clearly, UiO-66 is stable at temperature below ~ 650 K in air. The trend of ZSM-5@UiO-66 and HCl-ED-ZSM-5@UiO-66 are similar to UiO-66 with a total weight loss of 23.5 wt%. The composition of UiO-66 and ZSM-5 in the composite particles therefore can be estimated from these TGA curves. The calculation shows that the composite consists of 41.4 wt% UiO-66.

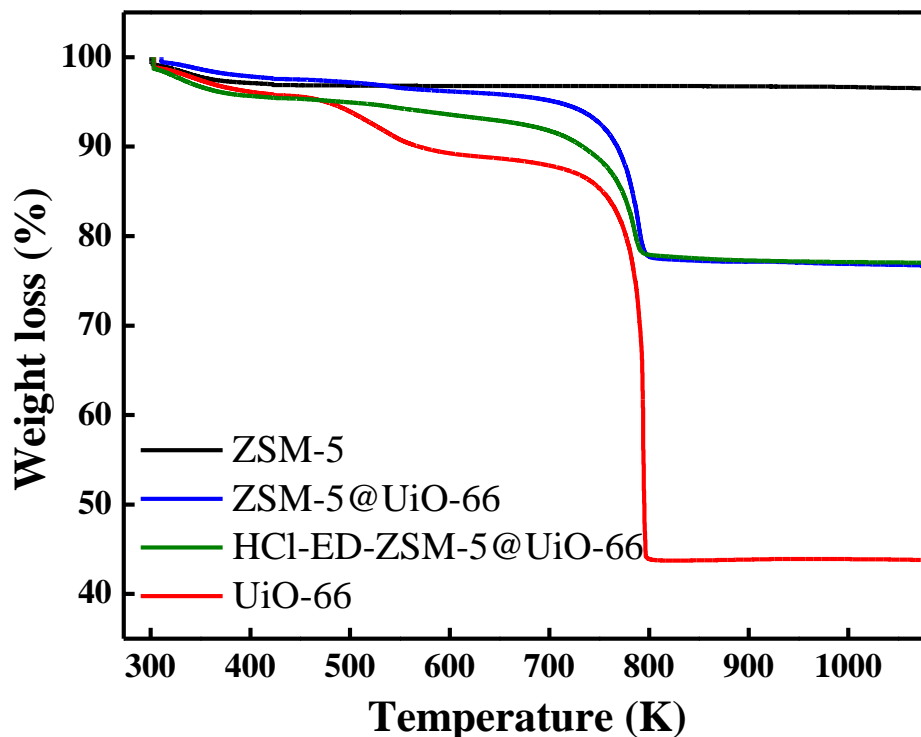


Figure 2-8. TGA curves of ZSM-5, UiO-66, ZSM-5@UiO-66 and HCl-ED-ZSM-5@UiO-66, respectively.

During the synthesis of ZSM-5@UiO-66 composite using ZSM-5 cores with different silica-alumina ratio (SAR), it was found that ZSM-5 cores with lower SAR tend to promote the growth of MOF on the surface of ZSM-5. Figure 2-9 shows the SEM images of ZSM-5@UiO-66 with ZSM-5 SAR of ∞ , 100 and 40, and their bare ZSM-5 core counterparts, respectively.

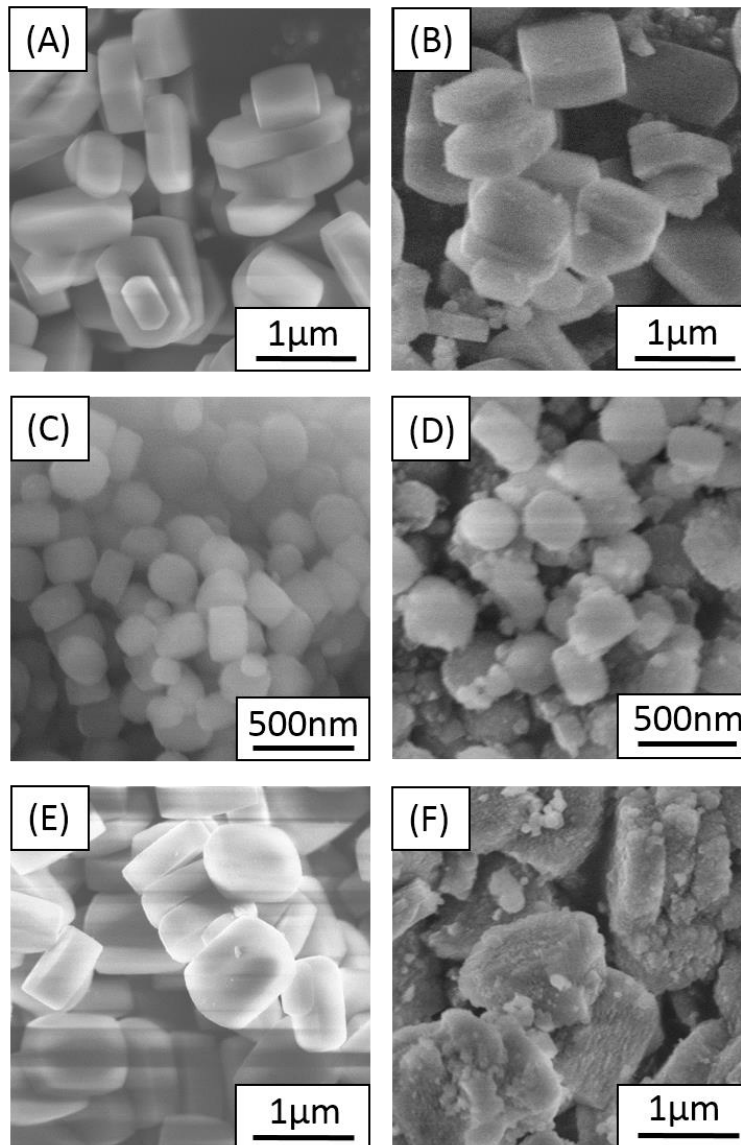
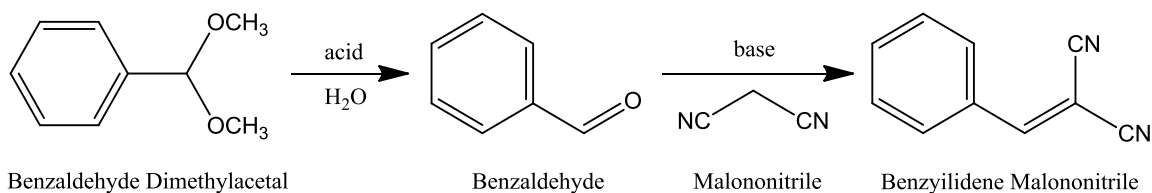


Figure 2-9. SEM images of (A) (B) ZSM-5 and ZSM-5@UiO-66 with SAR= ∞ , (C) (D) ZSM-5 and ZSM-5@UiO-66 with SAR=100, (E) (F) ZSM-5 and ZSM-5@UiO-66 with SAR=40.

Figure 2-9 (A) and (B) show the growth of UiO-66 around ZSM-5 with a SAR of ∞ . Compared to the original ZSM-5 core in (A), there is no growth of MOF species on the surface of the zeolite particles. When the aluminum content in the zeolite framework increases, as shown in Figure 2-9 (C) and (D), they form discrete UiO-66 particles surrounding the zeolite cores. If the aluminum content further increases, a

complete shell of UiO-66 is formed around the zeolite cores, as shown in Figure 2-9 (E) and (F). This UiO-66 growth trend shows that the affinity of UiO-66 to ZSM-5 increases with the increase of aluminum content in the ZSM-5 framework. This should be caused by the increasing hydrophilicity of the zeolite framework with more Al inside. These results suggest the direction for making zeolite@MOF composite in two guidelines: the lattice parameters of the two materials should be similar and the affinity between zeolite and MOF should be enhanced.

The catalytic activity of the composite porous materials was studied in a two-step tandem reaction process that requires both acid and basic sites. The cascade reaction studied involved an acetal hydrolysis followed by a Knoevenagel condensation. More specifically, benzaldehyde dimethyl acetal was hydrolyzed to produce benzaldehyde which reacts with malononitrile to give benzylidene malononitrile (see Scheme 2-2). The first reaction step requires acid sites which are supplied by the ZSM-5 core, while the condensation step involves the basic sites which are provided by the amine groups in the MOF shell.



Scheme 2-2. One-pot acetal hydrolysis-Knoevenagel condensation cascade reaction.

Several activation procedures were adopted to resume the acid catalytic activity of the composite. The conventional activation method for pure zeolite using ammonium

nitrate water solution was initially tried. The ammonium nitrate in ethanol was also used as the exchange medium. HCl in ethanol solution is adopted as a stronger exchange medium. The reaction results as well as control experiments of pure ZSM-5 and UiO-66 are listed in Table 2-2 and will be discussed in detail later. The yield is calculated by dividing the amount of the obtained product by the theoretical yield. The reaction rate is calculated assuming a first-order reaction for benzaldehyde dimethyl acetal.

Table 2-2. Catalytic Reaction Results Summary

Catalyst	Exchange Solution ^a	Evacuate Temperature (K)	Weight of Catalyst (mg)	Conversion of Benzaldehyde Dimethyl Acetal (%) ^b	Yield of Benzaldehyde (%) ^b	Yield of Benzylidene Malononitrile (%) ^b	Rate Constant (h ⁻¹ gcat ⁻¹)
ED-UiO-66	HCl/Ethanol	423	50.1	9.5	4.2	5.2	0.08
ZSM-5		423	52.0	87.8	81.7	6.1	7.47
ED-ZSM-5		423	50.0	0	0	0	0
ED-ZSM-5	HCl/Ethanol	423	51.0	74	74	0	6.59
ZSM-5@UiO-66		423	49.9	82.8	78.3	4.5	3.97
ED-ZSM-5@UiO-66		423	52.7	0	0	0	0
ED-ZSM-5@UiO-66	NH ₄ NO ₃ /H ₂ O	343	29.3	16.5	2.5	14	0.28
ED-ZSM-5@UiO-66	NH ₄ NO ₃ /Ethanol	343	44.7	0	0	0	0
ED-ZSM-5@UiO-66	HCl/Ethanol	343	31.7	11.2	0.8	10.4	1.47
ED-ZSM-5@UiO-66	HCl/Ethanol	423	49.7	23	1.5	21.5	1.25
ED-ZSM-5@UiO-66	HCl/Ethanol	473	50.7	28	21	7	1.01
ED-ZSM-5@UiO-66	HCl/Ethanol	423	201.0	89.6	14.8	74.8	0.74

^a The sample is in as-synthesized form if no exchange solution is mentioned. ^b The results were calculated based on GC data after 24h of reaction

The as-synthesized core-shell composite were dried at 423 K and tested in the catalytic reaction. The molar fraction of each component versus reaction time is shown in Figure 2-10. The reaction result showed that only the first reaction took place. The trace amount of final product benzylidene malononitrile may come from the equilibrium conversion of benzaldehyde.

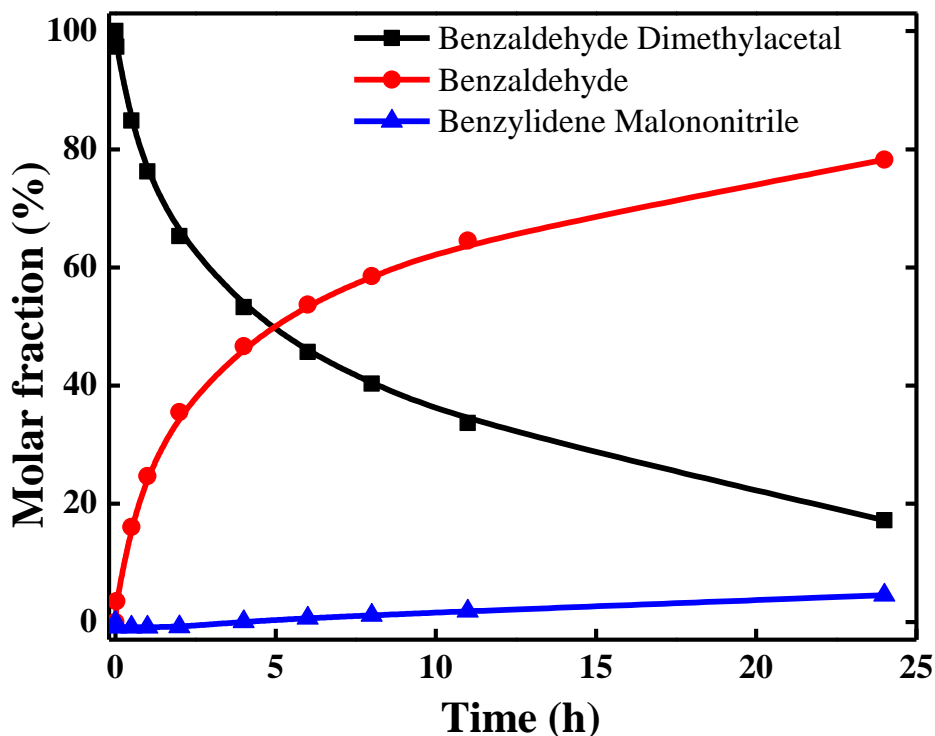


Figure 2-10. Catalytic reaction results of as-synthesized ZSM-5@UiO-66 composite evacuated at 423 K. Molar fraction of benzaldehyde dimethyl acetal, benzaldehyde and benzylidene malononitrile versus reaction time.

The composite material after incorporation of amine groups (ED-ZSM-5@UiO-66) was dried at the same temperature (423 K) and tested in the catalytic reaction. No first or second step product was detected in the reaction period of 24h. This result is consistent with the assumption that ethylene diamine blocked the acid sites in ZSM-5 micropores.

NH_4NO_3 ethanol solution and NH_4NO_3 water solution was adopted as the exchange solution for ED-ZSM-5@UiO-66. Both of the exchanged samples were dried in vacuum oven at 343 K overnight before reaction. The sample exchanged with 1 M NH_4NO_3 water solution showed activity for both products. The molar fraction of each component vs time is plotted in Figure 2-11. The conversion of benzaldehyde dimethyl acetal reached 16.5 % after 24 hours of reaction, while the selectivity of benzylidene malononitrile was 84.8 %. The rate constant was relatively low and the reaction did not reach equilibrium after 24h of reaction. The sample exchanged with NH_4NO_3 ethanol solution showed no activity because NH_4NO_3 has very low solubility in ethanol. Higher concentration of NH_4NO_3 can be obtained in DMF. However, neither of the organic NH_4NO_3 solutions can activate the composite.

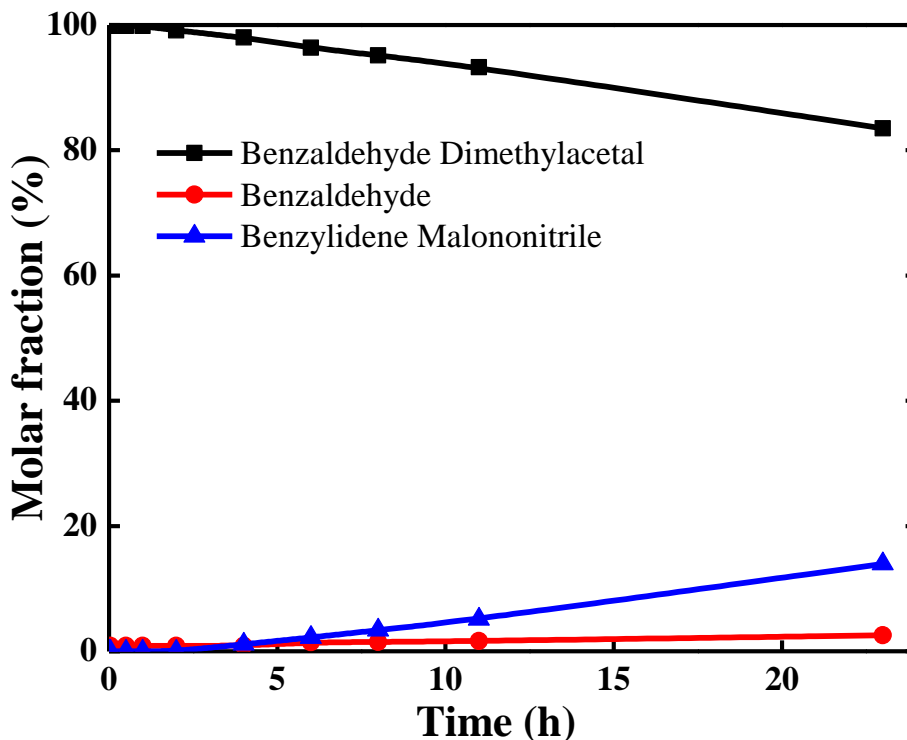


Figure 2-11. Catalytic reaction results of ED-ZSM-5@UiO-66 composite treated with 1 mol L^{-1} NH_4NO_3 water solution, evacuated at 343 K. Molar fraction of benzaldehyde dimethyl acetal, benzaldehyde and benzylidene malononitrile versus reaction time.

HCl ethanol solution was then adopted as the exchange medium. The equilibrium concentration of benzaldehyde dimethyl acetal using HCl treated sample as catalyst is relatively low compared to that using NH_4NO_3 water solution treated sample as catalyst, however, the higher reaction rate makes this activation method more promising.

A series of experiments with different evacuation temperature (343 K, 423 K, and 473 K) is carried out to optimize the equilibrium concentration of benzylidene malononitrile. The molar fraction of each component versus reaction time is shown in Figure 2-12. Figure 2-12 (A) shows the reaction result of the composite at an evacuation temperature of 343 K. The reaction reached equilibrium after 6 hours of reaction. The increase in evacuation temperature to 423 K enhanced the activity as well as the stability of the catalyst. The equilibrium concentration for benzylidene malononitrile was almost two fold of the 343 K treated sample. However, when the evacuation temperature was further raised to 473 K, the reaction showed a quite different trend. The benzaldehyde dimethyl acetal conversion increased while the selectivity for the final products dropped dramatically: the intermediate product has a higher selectivity over the final product, which is not preferable. This could be caused by the decomposition of ethylene diamine at high temperature, leading to the loss of basic catalytic activity.

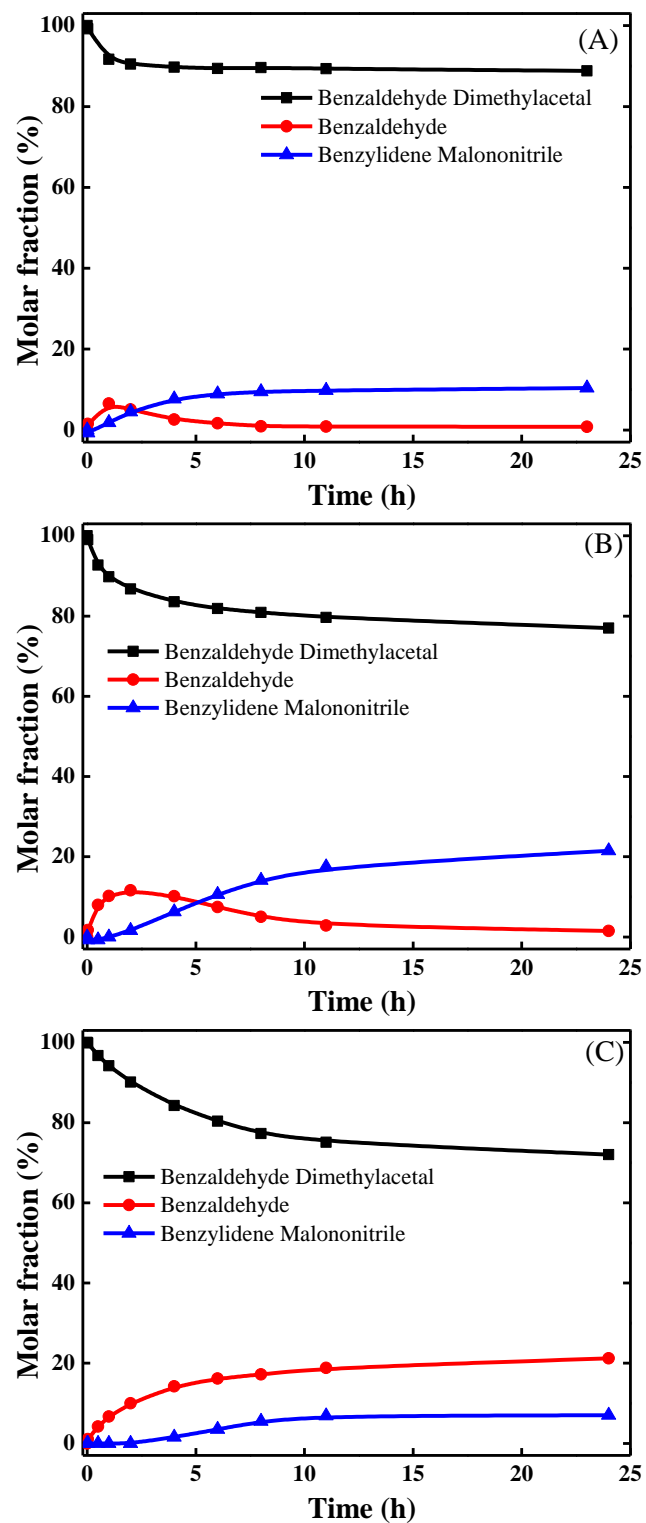


Figure 2-12. Catalytic reaction results of ED-ZSM-5@UiO-66 composite treated with HCl ethanol solution, evacuated at (A) 343 K, (B) 423 K, (C) 473 K.

The conversion of benzaldehyde dimethyl acetal, yield of benzaldehyde, yield and selectivity of benzylidene malononitrile and rate constant of the three reactions are compared in Figure 2-13. The conversion of benzaldehyde dimethyl acetal increased with the evacuation temperature, which is caused by the thermal activation of ZSM-5. The similarity of reaction trends between 343 K and 423 K treated samples suggests that the reaction in this temperature range was controlled by the first step reaction.

The reaction rate constant of each catalysts is calculated using the following equation assuming a first-order reaction,

$$kt = \ln \frac{1}{1-x}$$

where x is the conversion of benzaldehyde dimethyl acetal, k is the apparent rate constant normalized to catalyst mass, t is the reaction time.

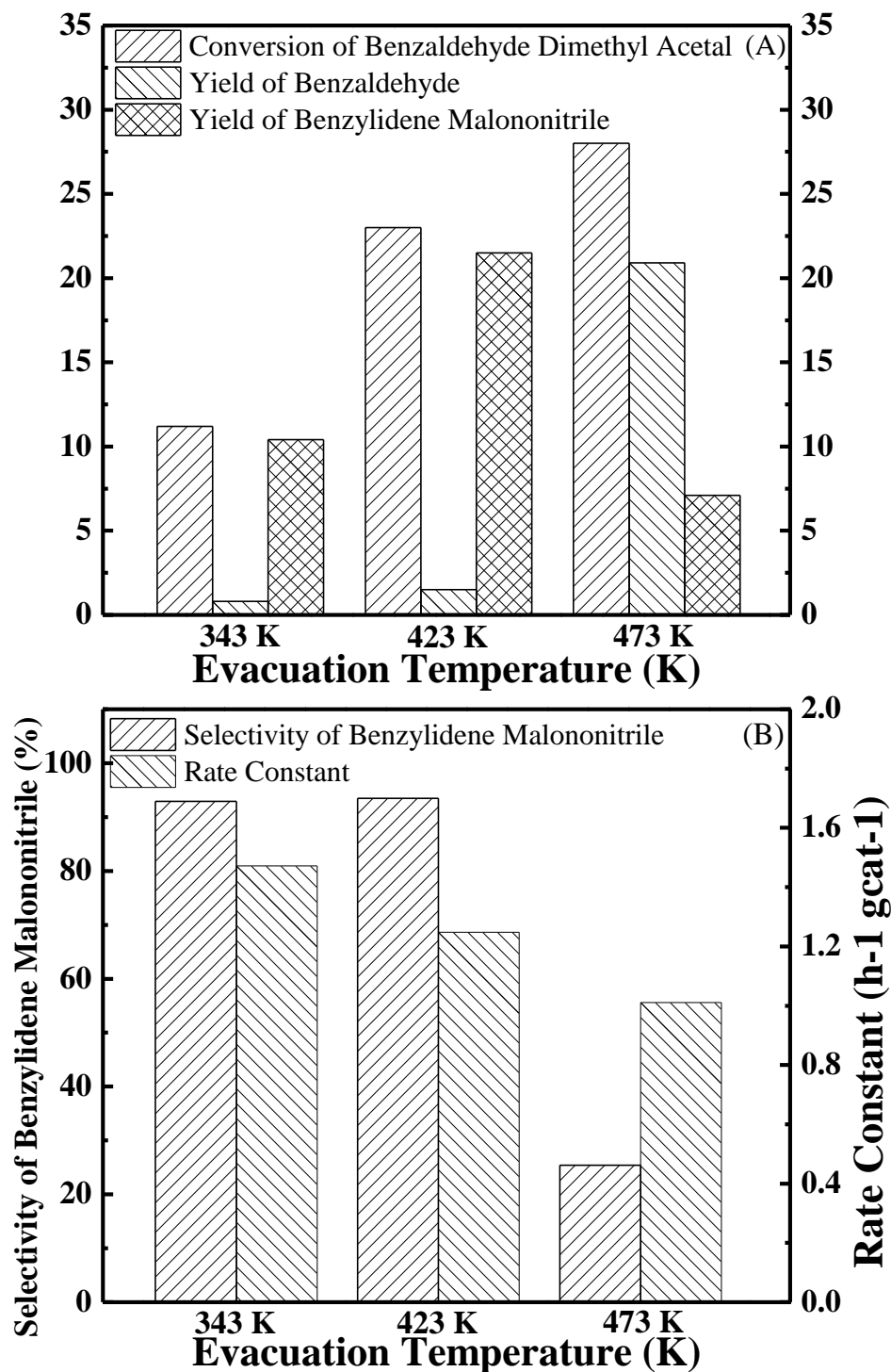


Figure 2-13. A comparison of benzaldehyde dimethyl acetal conversion, benzaldehyde yield, benzylidene malononitrile yield and selectivity, rate constant of the composite treated with HCl ethanol solution and evacuated at 343 K, 423 K and 473 K.

The sample treated with HCl ethanol solution and evacuated at 423 K showed the best catalytic performance and therefore, was tested again in the catalytic reaction using a larger amount. The results (Figure 2-14 (A)) showed that the tandem reaction was again successfully performed, with the yield of benzylidene malononitrile reached 80% and selectivity reached 88.9 %. The amount of catalyst used in this test was four times higher than the original trial (see Table 2-2). The conversion of benzaldehyde dimethyl acetal also showed four-fold increase. The selectivity of the final product was slightly lower and the rate constant remained the same.

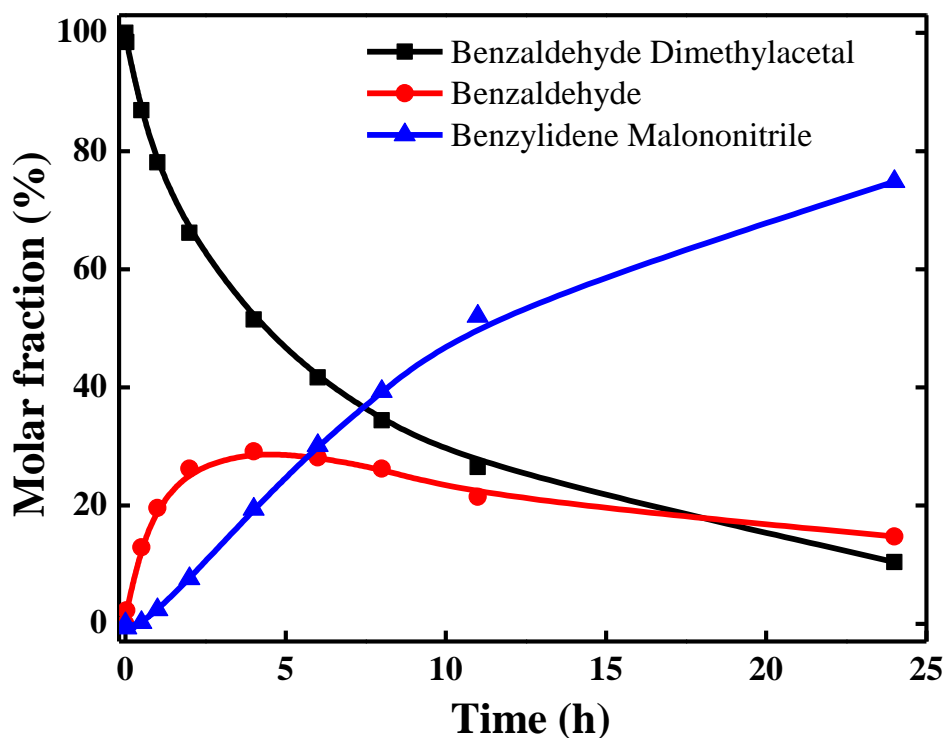
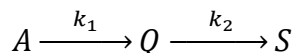


Figure 2-14 (A). Catalytic reaction results of HCl-ED-ZSM-5@UiO-66 composite. Molar fraction of benzaldehyde dimethyl acetal, benzaldehyde and benzylidene malononitrile versus reaction time.

The kinetics of this cascade reaction over scaled up HCl-ED-ZSM-5@UiO-66 composite is studied assuming a first-order cascade reaction model:



$$r_A = k_1 C_A$$

$$r_Q = k_1 C_A - k_2 C_Q$$

$$r_S = k_2 C_Q$$

Here A stands for benzaldehyde dimethyl acetal, Q stands for benzaldehyde and S stands for benzylidene malononitrile respectively. Integration gives:

$$C_A = C_{A0} e^{-k_1 t}$$

$$C_Q = \frac{k_1 C_{A0}}{k_2 - k_1} (e^{-k_1 t} - e^{-k_2 t})$$

$$C_S = C_{A0} - C_A - C_Q$$

The experimental data (solid line) in Figure 2-14 (A) and the simulated reaction trend (dash line) are compared in Figure 2-14 (B). The reaction rate constants for first and second step are $0.74 \text{ h}^{-1} \text{ gcat}^{-1}$ and $1.05 \text{ h}^{-1} \text{ gcat}^{-1}$, respectively.

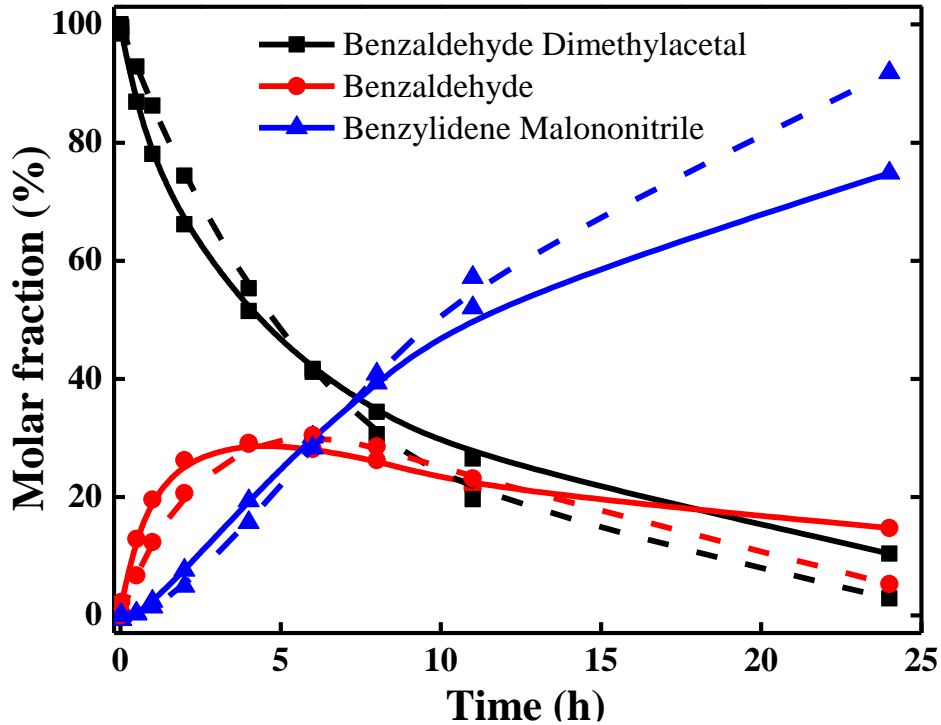


Figure 2-14 (B). Comparison of experiment and simulation results of catalytic reaction results of HCl-ED-ZSM-5@UiO-66 composite.

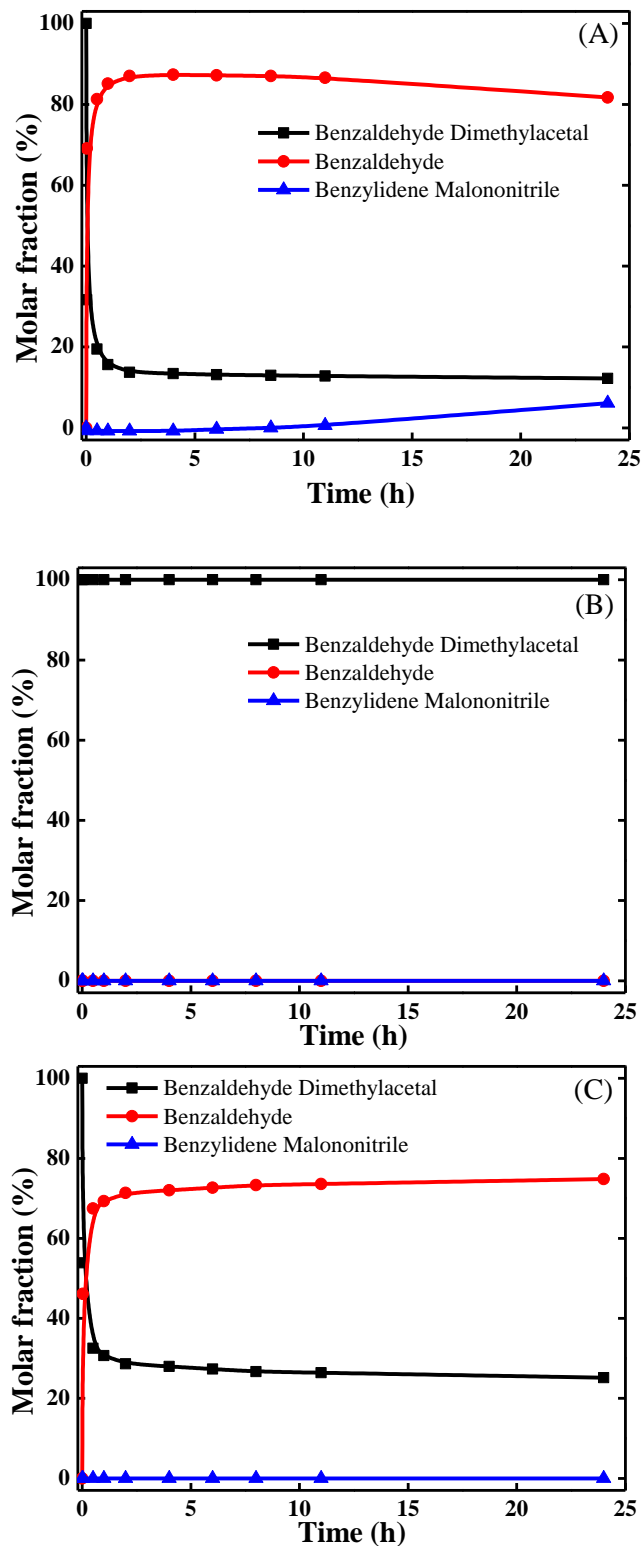


Figure 2-15. Catalytic reaction results of (A) ZSM-5, (B) ED-ZSM-5, (C) HCl-ED-ZSM-5. Molar fraction of benzaldehyde dimethyl acetal, benzaldehyde and benzylidene malononitrile versus reaction time.

The control catalytic reaction experiments were carried out on both of the raw materials. As-synthesized ZSM-5, ED-ZSM-5 and HCl-ED-ZSM-5 were tested in the catalytic reaction. The reaction results are shown in Figure 2-15 with the molar fraction of each component versus reaction time.

As shown in Figure 2-15 (A), the pure ZSM-5 showed a good catalytic activity for the first step reaction. Figure 2-15 (B) shows the reaction result of ZSM-5 after soaking in ethylene diamine solution as the catalyst. There was no trace for the first step reaction because the active sites in ZSM-5 were all blocked by ethylene diamine and could not be removed by simply heating up to 423 K. The catalytic activity resumed after the sample was treated with HCl ethanol solution. This set of control experiment on ZSM-5 was consistent with the N₂ and Ar adsorption-desorption results that the ethylene diamine occupied the micropores of ZSM-5 and was washed out by HCl ethanol solution.

The rate constants of the reactions catalyzed by ZSM-5 are 7.47 h⁻¹ gcat⁻¹ for ZSM-5 and 6.59 h⁻¹ gcat⁻¹ for HCl-ED-ZSM-5. The rate constant decreased to 3.97 h⁻¹ gcat⁻¹ in the as-synthesized ZSM-5@UiO-66 as a result of diffusion resistance of the UiO-66 shell.

The control experiment on UiO-66 was carried out using HCl-ED-UiO-66 (UiO-66 soaked in ethylene diamine solution and exchanged in HCL ethanol solution). The basic catalytic activity of UiO-66 has been confirmed by testing pure ZSM-5 (Figure 2-15 (A) and (C)). The reaction result of HCl-ED-UiO-66 is shown in Figure 2-16. There was an almost negligible conversion of benzaldehyde dimethyl acetal to

benzaldehyde and benzylidene malononitrile. This result showed that UiO-66 does not contribute to the first step reaction.

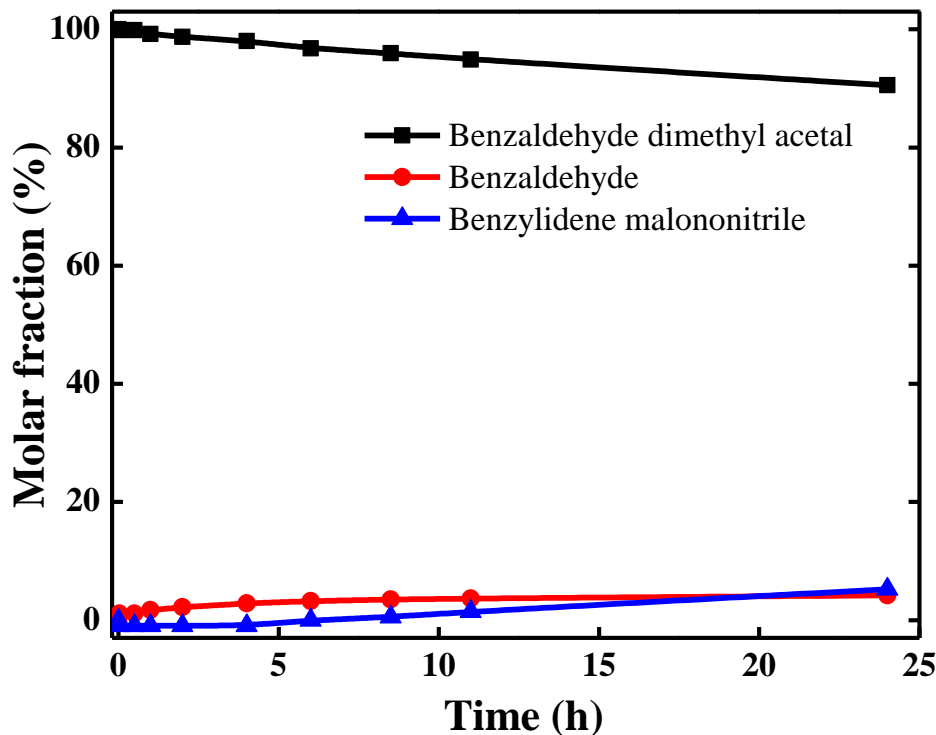


Figure 2-16. Catalytic reaction results of HCl-ED-UiO-66. Molar fraction of benzaldehyde dimethyl acetal, benzaldehyde and benzylidene malononitrile versus reaction time.

The result of control experiments on ZSM-5 and UiO-66 confirms that the hydrolysis of the acetal is catalyzed by the Brønsted acid sites in ZSM-5 and the Knoevenagel condensation reaction is catalyzed by the basic sites in UiO-66.

2.4 Conclusions

In conclusion, ZSM-5@UiO-66 core-shell composite particles were synthesized by solvothermal growth of UiO-66 shell on the surface of ZSM-5 particles that were pre-synthesized via hydrothermal crystallization. The morphologies of ZSM-5, UiO-66, and ZSM-5@UiO-66 composite were observed by SEM and TEM, which show the formation of core-shell zeolite@MOF composite. The crystallinity of the

samples was confirmed by XRD and the composition was confirmed by EDX. Textural properties of the samples were extracted from N₂ and Ar adsorption-desorption isotherms, which show the pore systems in the combined nanoporous materials. The content of the UiO-66 shell in the composite was calculated by N₂ adsorption-desorption isotherms and TGA data.

Post-synthetic modification with ethylene diamine in the UiO-66 framework incorporated amine groups into the composite. The acidity in ZSM-5 generated by aluminum in the tetrahedral site of the zeolite framework and basicity in UiO-66 originated from the amine groups enabled ZSM-5@UiO-66 composite acid-base bifunctionality for catalytic cascade reactions. The synthesis of benzylidene malononitrile from malononitrile and benzaldehyde dimethyl acetal, a process involving the hydrolysis of the acetal catalyzed by the Brønsted acid sites in zeolite followed by a Knoevenagel condensation reaction catalyzed by the basic sites in MOF confirmed the bifunctional activity of the ZSM-5@UiO-66 composite. The bifunctionality was supported by FTIR and textural properties as complementary evidences.

Chapter 3: Synthesis and Presynthetic Modification of ZSM-

5@UiO-66 Core-Shell Particles as Bifunctional Catalysts

3.1 Introduction

The functionalization of ZSM-5@UiO-66 into acid-base catalysts was successfully achieved by postsynthetic modification of metal sites using ED in Chapter 2. The synthetic procedure, however, involves multiple complicated steps, especially the incorporation of ED onto metal sites while avoiding the deactivation of acid sites in zeolite. In this chapter, we aimed to develop a simple alternative approach to introduce -NH_2 group into the composite catalysts. Synthesis of functional MOFs with organic ligands comprised of functional groups has been investigated in literature.[79] In this chapter, presynthetic modification was applied to UiO-66 in order to simplify the experimental and activation procedures.

Particularly, the original linker benzene-1,4-dicarboxylic acid (BDC) for UiO-66 was replaced by 2-aminobenzene-1,4-dicarboxylic acid (NH_2 -BDC) in the synthesis solution. The core-shell composite ZSM-5@UiO-66- NH_2 was synthesized using a similar procedure as that of ZSM-5@UiO-66 reported in Chapter 1. This synthesis yielded UiO-66- NH_2 with amine groups on the organic linkers in the MOF framework without any post-synthetic modifications. The as-synthesized composite was tested in the cascade catalytic reactions of benzaldehyde dimethyl acetal and malononitrile to benzylidene malononitrile, whose reaction scheme has been discussed in Chapter 2.

3.2 Experimental Part

3.2.1 Materials

Tetrapropylammonium hydroxide (TPAOH, 40% in aqueous solution), tetraethylorthosilicate (TEOS, 98%), aluminum isopropoxide (99.99%) and $ZrCl_4$ (99.9%) were purchased from Alfa Aesar. NaOH (97%), malononitrile (99%) and 2-aminebenzene-1,4-dicarboxylic acid (NH_2 -BDC, 99%) were purchased from Sigma-Aldrich. Dimethylformamide (DMF, 99.8%) was purchased from BDH. Hydrochloric acid (36.5%-38.0%) was purchased from JT Baker. Acetonitrile (99.9%) was purchased from Fisher. Benzaldehyde dimethyl acetal (98%) was purchased from SAFC. All chemicals were used as received without further treatment. Deionized (DI) water was used in all purpose. The zeolite core particles was synthesized as reported in section 2.2.2 in Chapter 2 of this thesis.

3.2.2 Synthesis of $UiO-66-NH_2$ and $ZSM-5@UiO-66-NH_2$

A typical procedure for synthesis of $ZSM-5@UiO-66-NH_2$ is shown as follows: 0.04 g $ZrCl_4$, and 0.031 g NH_2 -BDC were dissolved in 18.96 g DMF. 0.0125 mL DI water was then added to the mixture. The solution was transferred to a Teflon-lined steel autoclave and allowed to react at 393 K for 24 h. The product was collected by centrifugation and followed by a two-step washing procedure in order to remove the unreacted residues encapsulated in the micropores of the material. The first step involved stirring exchange with DMF for 3 times. In the second step, the high boiling point solvent DMF was exchanged with methanol for 2 times. After washing, the sample was dried at 343 K. The synthesis of $ZSM-5@UiO-66-NH_2$ core-shell

structured composite was carried out using the same procedure as that of UiO-66-NH₂ particles except that 0.284 g ZSM-5 particles was added to the synthesis solution and stirred for 1 h to get a stable colloid in the beginning of the synthesis.

3.2.3 Activation of the catalyst

The as-synthesized ZSM-5@UiO-66-NH₂ composite was tested in the catalytic reaction without any treatment. Meanwhile, the composite was acid-exchanged and tested in the catalytic reaction for comparison. The acid exchange was performed in a 50mL flask equipped with a reflux condenser and heated in a temperature controlled oil bath under atmospheric pressure and magnetic stirring. 0.1 g ZSM-5@UiO-66-NH₂ was added to 20 mL 0.1 mol L⁻¹ HCl ethanol solution. The mixture was refluxed at 363 K 3 times for a total of 6 h. The acid exchanged sample was washed with water and ethanol repeatedly and then dried at 473K in vacuum oven. The sample was denoted as HCl-ZSM-5@UiO-66-NH₂ after this step.

3.2.4 Product characterizations

The crystalline phase of catalyst samples was determined by X-Ray powder diffraction (XRD) using Bruker D8 Advance Lynx Powder Diffractometer. The integration time was 0.3 hours and the step size was 0.032 degrees/second. The morphology and elemental analysis of the samples were obtained by a scanning electron microscope (SEM, Hitachi SU-70) equipped with an energy dispersive X-ray (EDX) spectrometer. Transmission electron microscope (TEM) images were recorded on a JEM 2100 LaB6 microscope at an accelerating voltage of 200KV. N₂ adsorption-desorption measurements were carried out at 77 K and on an Autosorb-iQ analyzer

(Quantachrome Instruments), respectively. Prior to the N₂ and Ar measurements, samples were outgas at 423 K overnight. The FT-IR spectrum was recorded with a spectrometer (Nicolet Magna-IR 560) in the range of 4000 - 400 cm⁻¹. Each sample was measured with 128 scans at an effective resolution of 4 cm⁻¹.

3.2.5 Catalytic reaction test over ZSM-5@UiO-66-NH₂ composite

The liquid phase catalytic conversion of benzylidene malononitrile from malononitrile and benzaldehyde dimethyl acetal (Scheme 2-2) was performed in a three-necked flask equipped with a reflux condenser and heated in a temperature controlled oil bath under atmospheric pressure and magnetic stirring (0.5" stirring bar and 500 rpm stirring speed) conditions. In a typical experiment, 20 mL acetonitrile, 0.0866 g malononitrile, 7.5 μL DI water, and 0.05 g catalyst were added into the flask in sequence. After bubbled the mixture with flowing helium for 0.5 h, the flask was immersed in the oil bath preheated at 353 K. The reaction mixture was maintained for 0.5 h at the required reaction temperature and stirring conditions and then 0.2045 mL of benzaldehyde dimethyl acetal (1.36 mmol) was added. This moment of the addition was taken as the initial reaction time. Liquid samples were withdrawn at regular intervals and analyzed by the gas chromatograph (Agilent 7890A) equipped with a methyl-siloxane capillary column (HP-1, 50.0 m x 320 μm x 0.52 μm) connected to a flame ionization detector (FID).

3.3 Results and Discussion

The morphologies of ZSM-5, UiO-66-NH₂, and ZSM-5@UiO-66-NH₂ composite samples were observed with SEM and TEM, and the representative images

are shown in Figure 3-1. The ZSM-5 zeolite (Figure 3-1 (A)) consists of short cylindrical particles with an average width of 250 nm and thickness of 180 nm and well crystallized smooth surfaces. The UiO-66-NH₂ (Figure 3-1 (B) and (C)) consists of hexagonal polyhedrons with an average size of 350 nm. ZSM-5@UiO-66-NH₂ composite (Figure 3-1 (D)-(F)) contains bulk ZSM-5 cores and sparse UiO-66-NH₂ particles on the ZSM-5 surface, showing the formation of core-shell zeolite@MOF composite clearly.

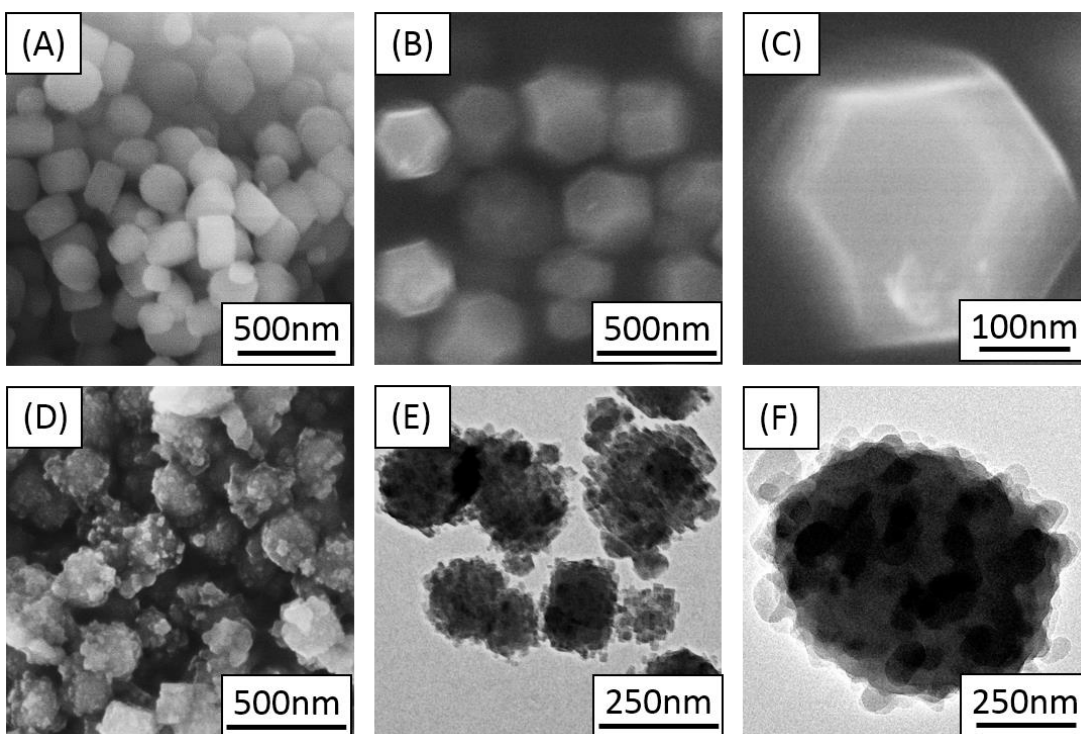


Figure 3-1. SEM images of (A) ZSM-5 zeolite, (B) (C) UiO-66 MOF, and (D) ZSM-5@UiO-66-NH₂. TEM images of (E) (F) ZSM-5@UiO-66-NH₂.

Powder X-ray diffraction (XRD) and energy-dispersive X-ray (EDX) spectroscopy were employed to confirm the composition and crystallinity of the particles. Figure 3-2 shows the XRD patterns of ZSM-5, UiO-66-NH₂ and ZSM-5@UiO-66-NH₂ particles, respectively. Both ZSM-5 and UiO-66-NH₂ are highly

crystallized. UiO-66-NH₂ shows the same diffraction peaks as UiO-66, suggesting that they have isoreticular structures. The ZSM-5@UiO-66-NH₂ composite consists of diffraction peaks from both UiO-66-NH₂ and ZSM-5, suggesting the presence of both phases in the composite material. In addition, the absence of new diffraction peaks or broadening of characteristic peaks of ZSM-5 or UiO-66-NH₂ indicates no other structure forms and deterioration of the crystalline phases in the synthesis conditions.

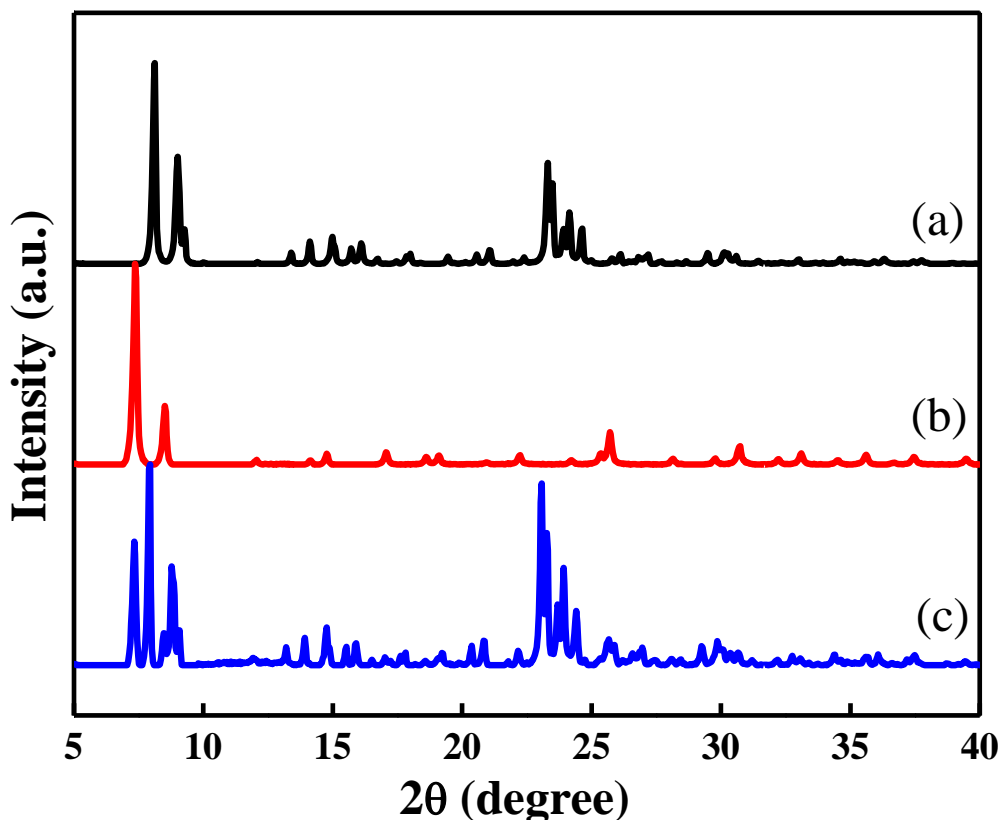


Figure 3-2. XRD patterns of (a) ZSM-5, (b) UiO-66-NH₂ and (c) ZSM-5@UiO-66-NH₂, respectively.

The elemental compositions of the ZSM-5 solid core and ZSM-5@UiO-66-NH₂ composite were verified with EDX spectroscopy (Figure 3-3), to distinguish the core-shell structure from a physical mixture of ZSM-5 and UiO-66-NH₂. Si, Al and O can be observed in the EDX spectrum of the ZSM-5 solid core particle with K α

characteristic X-ray energy of 1.739 KeV, 1.486 KeV and 0.525 KeV, respectively. The EDX spectrum (B) of the core-shell particles is comprised of Si, Al, O, N and Zr peaks, showing the presence of zeolite and MOF building elements. The primary construction element Zr of UiO-66-NH₂ is shown with L α characteristic X-ray energy of 2.042 KeV. The small peak between the C and O peaks could be attributed to N K α characteristic X-ray energy of 0.392 KeV. The C peaks in both figures are from the carbon tape used for sample preparation in the SEM characterization. The EDX was done during the SEM test and was performed on isolated particles, thus confirming the successful growth of UiO-66-NH₂ onto ZSM-5.

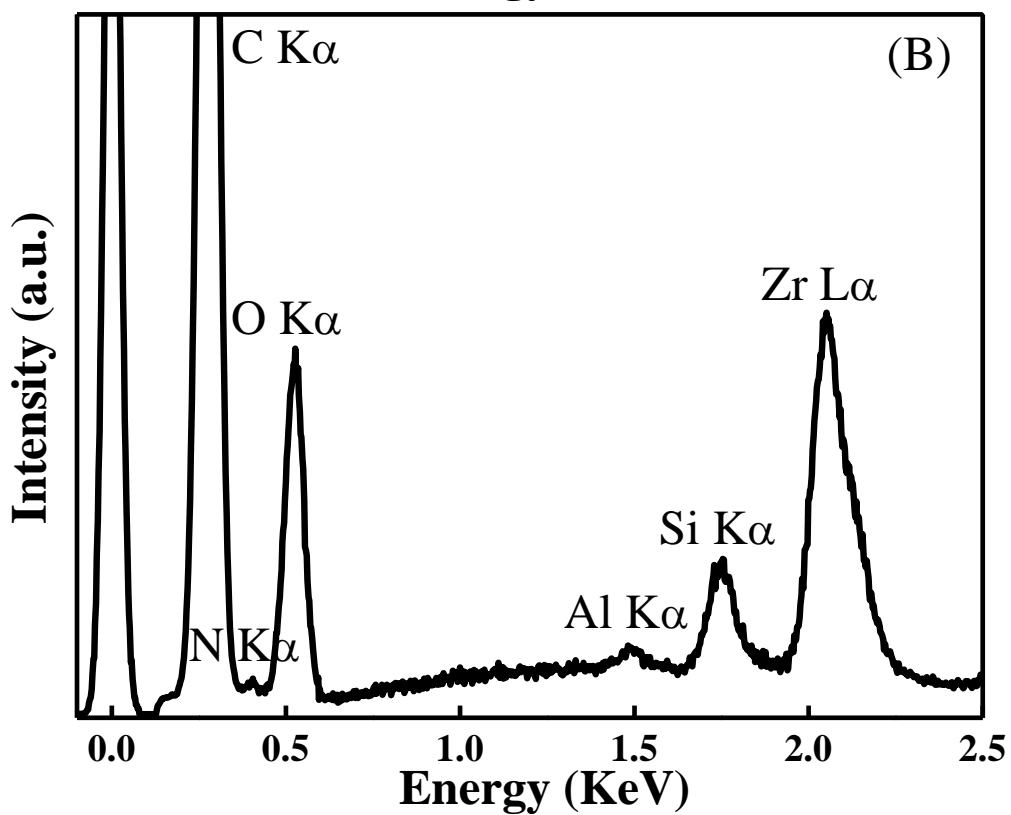
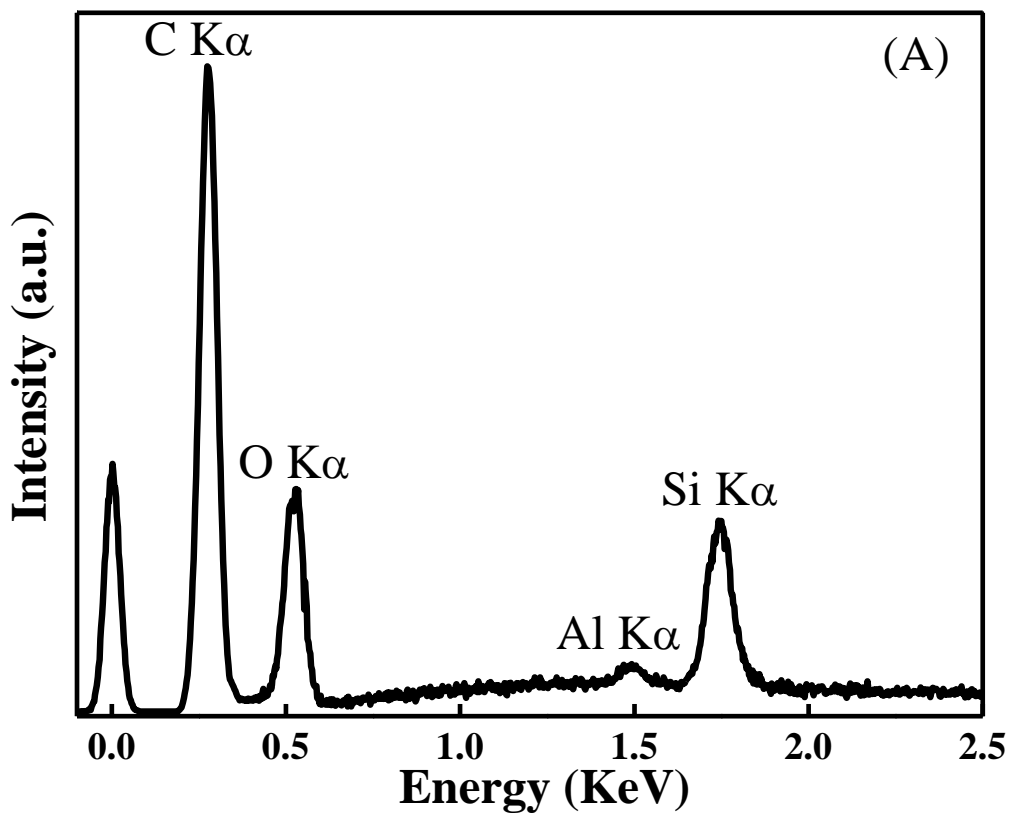


Figure 3-3. EDX spectra of as-synthesized (A) ZSM-5 zeolite and (B) ZSM-5@UiO-66-NH₂ core-shell composite.

N₂ adsorption-desorption isotherms were used to characterize the textural properties (surface area and total pore volume) of the samples as summarized Figure 3-4. The surface areas of UiO-66-NH₂, ZSM-5 and ZSM-5@UiO-66-NH₂ calculated by the multipoint BET method were 967 m²/g, 466 m²/g and 474 m²/g, respectively. The total pore volume of aforementioned samples calculated at P/P₀=0.95 were 0.44 mL/g, 0.25 mL/g and 0.28mL/g, respectively. The surface area and pore volume of UiO-66-NH₂ were smaller than that of UiO-66 because the amine groups on the linkers occupy a portion of the micropore volume. Moreover, these results show that the surface area and total pore volume of the core-shell composite are combinations of ZSM-5 and UiO-66, revealing the accessibility of the micropores of both materials.

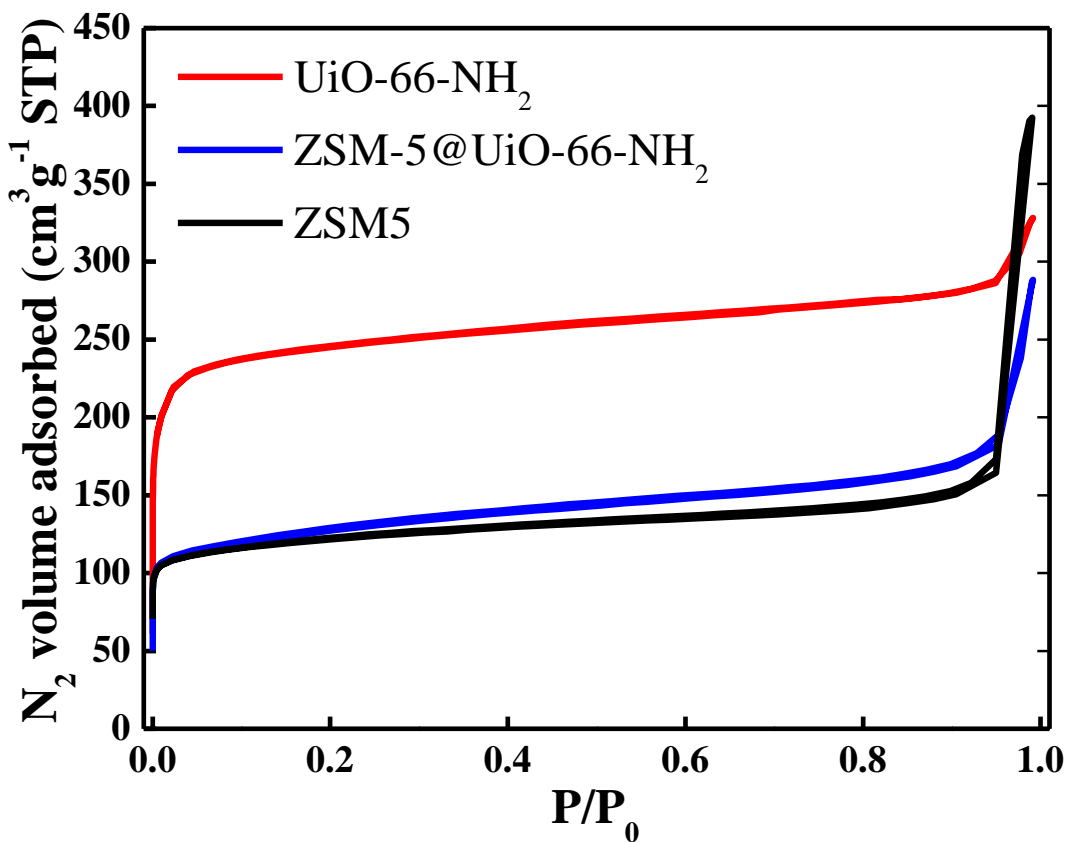


Figure 3-4. N₂ adsorption-desorption isotherms of UiO-66-NH₂, ZSM-5, and ZSM-5@UiO-66-NH₂, respectively.

Infrared spectroscopy was applied to characterize amine groups in the MOF framework. The adsorption bands centered around 3390 and 3490 cm^{-1} showed in Figure 3-5 correspond to the primary amine N-H stretching ($\nu_{s, \text{N-H}}$) vibrational modes in the organic linkers in UiO-66. The weak absorption band centered at 1573 cm^{-1} stands for the N-H bending ($\nu_{b, \text{N-H}}$) vibration mode and the absorption bands centered around 1160 cm^{-1} could attribute to the C-N stretching ($\nu_{s, \text{C-N}}$) vibration mode. The appearance of absorption bands at 1082 cm^{-1} and 1380 cm^{-1} in ZSM-5@UiO-66-NH₂ suggests the co-existence of ZSM-5 and UiO-66 in the composite, consistent with the XRD analysis.

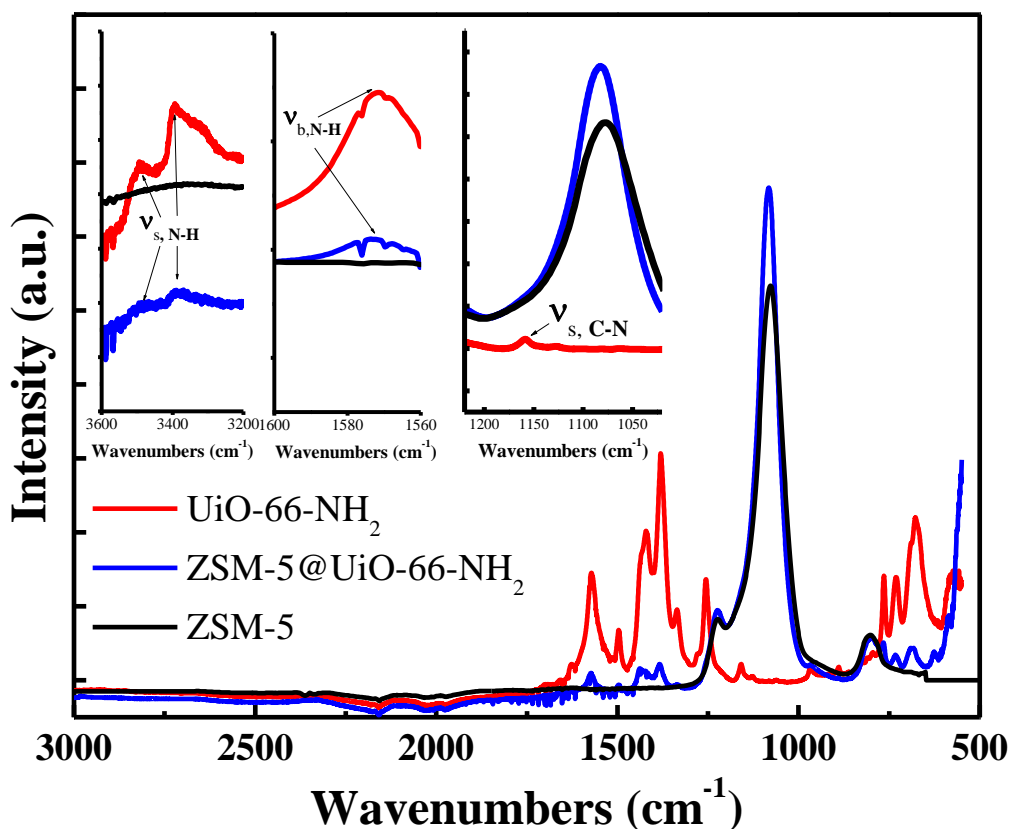


Figure 3-5. FTIR spectra of UiO-66-NH₂, ZSM-5 and ZSM-5@UiO-66-NH₂, respectively.

The surface area calculation implies that the UiO-66-NH₂ content in the ZSM-5@UiO-66-NH₂ composite was very low. This result can also be obtained by comparing the relative intensity of XRD and FT-IR peaks in the composite that belong to UiO-66-NH₂ and ZSM-5. This will lead to unequivalent acid and basic site numbers in the composite and affect the catalytic performance.

The catalytic activity of the bifunctional ZSM-5@UiO-66-NH₂ composite was studied in the reaction shown in Scheme 2-2. The first reaction step requires acid sites which can be supplied by the ZSM-5 core, while the second step involves basic sites coming from the amine groups on the organic linkers of the UiO-66-NH₂. The reaction results of as-synthesized ZSM-5@UiO-66-NH₂ and acid-exchanged ZSM-5@UiO-66-NH₂ are shown in Figure 3-6 in terms of molar fractions of each component versus reaction time. For as-synthesized ZSM-5@UiO-66-NH₂ composite, the yield for benzylidene malononitrile was 20% after 24 h of reaction, which is comparable to the reaction result of HCl-ED-ZSM-5@UiO-66 described in 2.3.

Figure 3-6 (B) shows catalytic reaction result of the acid-exchanged ZSM-5@UiO-66-NH₂. After acid exchange, the acid activity of ZSM-5 core was resumed to the level of pure ZSM-5. This dramatic improvement in acid activity that was not presented in the ZSM-5@UiO-66 case (in Chapter 2) indicates that the ethylene diamine impairs the acid activity in ZSM-5 greatly and irreversibly. The presynthetic modification in the synthesis of ZSM-5@UiO-66-NH₂ circumvent the amine grafting after synthesis and can preserve the acidity in ZSM-5.

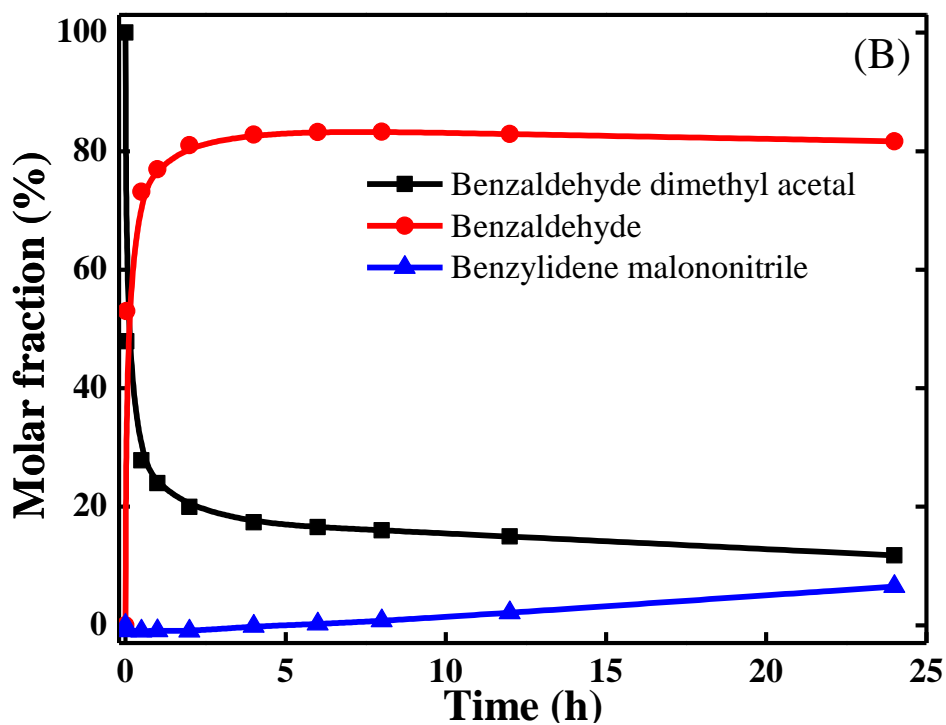
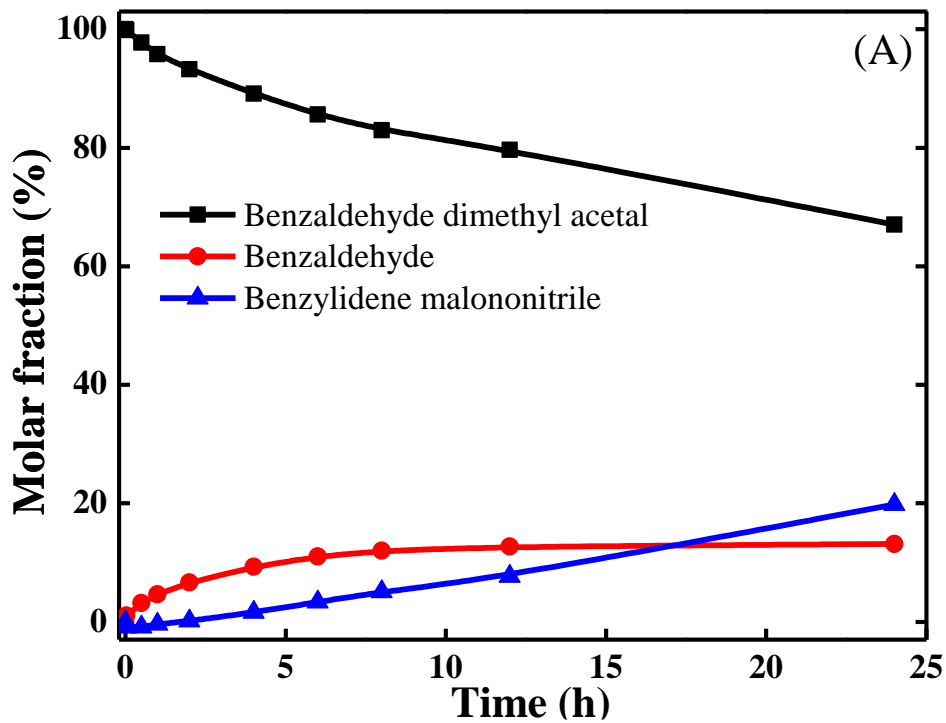


Figure 3-6. Catalytic reaction results of as-synthesized ZSM-5@UiO-66-NH₂ and acid-exchanged ZSM-5@UiO-66-NH₂. Molar fraction of benzaldehyde dimethyl acetal, benzaldehyde and benzylidene malononitrile versus reaction time.

3.4 Conclusions

The ZSM-5@UiO-66-NH₂ core-shell composite was successfully synthesized by solvothermal growth of UiO-66-NH₂ shell on the surface of ZSM-5 particles that were pre-synthesized via hydrothermal crystallization. The morphologies of ZSM-5, UiO-66, and ZSM-5@UiO-66-NH₂ composite were observed by SEM and TEM, clearly showing the formation of core-shell zeolite@MOF composite. The crystallinity of the samples was confirmed by XRD and the element composition was confirmed by EDX. Textural properties of the samples were extracted from N₂ adsorption-desorption isotherms, clearly showing the pore systems in the combined nanoporous materials. The existence of amine group in the UiO-66-NH₂ framework and the composite was confirmed by EDX and FT-IR measurements.

The presynthetic modification of BDC linkers with amine groups endows the composite with basic catalytic activity. The as-synthesized composite and acid exchanged composite were tested in cascade catalytic reactions. The as-synthesized composite showed catalytic activity for both steps of the cascade reaction. The acid-exchanged composite showed improved performance for the first-step reaction, however, the basic activity wasn't comparable to the acid activity. This is because of the low UiO-66-NH₂ content in the core-shell composite, derived from the surface area calculations and peak intensity comparison in XRD and FT-IR measurements. The bifunctionality can be optimized by increasing MOF content in the core-shell composite.

Chapter 4: Synthesis of ZSM-5@MIL-101 Core-Shell Particles as Bifunctional Catalysts

4.1 Introduction

The synthesis method of ZSM-5@UiO-66 described in Chapter 2 can be readily applied to other zeolite@MOF composites. In this chapter the method was expanded to MIL-101, another thermally stable MOF capable of postsynthetic modification with ethylene diamine in the metal cluster.[58, 100] Commercial ZSM-5 (Figure 4-1 (A)) was used as the core. The synthesis solution of MIL-101 contains hydrofluoric acid or tetramethylammonium hydroxide (TMAOH) as structure directing agent.[58, 133] Either of the substrates will impair the ZSM-5 particles present in the synthesis solution. Hydrofluoric acid can dissolve ZSM-5 at room temperature. TMAOH is used as structure directing agent in the ZSM-5 synthesis, which could possibly cause etching or recrystallization of ZSM-5 particles.

4.2 Experimental

4.2.1 Materials

Tetramethylammonium hydroxide (TMAOH, 25 wt% water solution), $\text{Cr}(\text{NO}_3)_3 \cdot 9\text{H}_2\text{O}$ (98.5%) and benzenedicarboxylate (BDC, 98%) were purchased from Alfa Aesar. Malononitrile (99%) and ethylene diamine (ED, 99.5%) were purchased from Sigma-Aldrich. Anhydrous toluene (99.5%) was purchased from BDH. Hydrochloric acid (36.5%-38.0%) was purchased from JT Baker. Acetonitrile (99.9%) was purchased from Fisher. Benzaldehyde dimethyl acetal (98%) was purchased from

SAFC. All chemicals were used as received without further treatment. Deionized (DI) water was used in all purpose.

4.2.2 Synthesis of MIL-101 and ZSM-5@MIL-101

There are generally two synthetic systems for MIL-101. One is using acidic solution, mainly hydrofluoric acid. The other one contains TMAOH in the solution, which is considered milder and adopted here. 0.1823 g TMAOH was dissolved in 14.8177 g DI water. Then 0.1108 g BDC and 0.2668 g $\text{Cr}(\text{NO}_3)_3 \cdot 9\text{H}_2\text{O}$ were added into the mixture. The solution was transferred to a Teflon-lined steel autoclave and allowed to react at 453 K for 48 h. The product was collected by centrifugation and washed with DI water and ethanol for 3 times each. After washing, the sample was dried in a dynamic vacuum oven at 343 K.

The synthesis of ZSM-5@MIL-101 core-shell structured composite was conducted using the same procedure as that of MIL-101 particles except that 0.15 g commercial ZSM-5 particles were added to the synthesis solution and stirred for 1 h to get a stable colloid in the beginning of the synthesis.

4.2.3 Incorporation of amine ($-\text{NH}_2$) groups into ZSM-5@MIL-101 composite

The incorporation of amine groups in the composite was performed in a 150 mL flask equipped with a reflux condenser and heated in a temperature controlled oil bath under atmospheric pressure and magnetic stirring (1" stirring bar and 500 rpm stirring speed) conditions. 150 μL ethylene diamine was added to 90 mL anhydrous toluene in the flask. 1.5g ZSM-5@MIL-101 particles were added to the solution

sequentially. The mixture was refluxed at 385 K for 12 h. The particles were collected by centrifugation and washed with ethanol for 3 times. The particles were then dried in conventional oven at 343 K. The sample was denoted as ED-ZSM-5@MIL-101 after this step.

4.2.4 Acid Exchange Activation

The ED-ZSM-5@MIL-101 was soaked in HCl ethanol solution in order to extract free ethylene diamine trapped in zeolite and MOF micropores. The acid exchange was performed in a 50 mL flask equipped with a reflux condenser and heated in a temperature controlled oil bath under atmospheric pressure and magnetic stirring. 0.6 g ED-ZSM-5@MIL-101 was added to 100 mL 0.15 mol L⁻¹ HCl ethanol solution. The mixture was refluxed at 363 K 3 times for a total of 6 h. The acid exchanged particles were washed with water and ethanol repeatedly. The sample was then dried at 423K in vacuum oven. The sample was denoted as HCl-ED-ZSM-5@MIL-101 after this step.

4.2.5 Product characterizations

The crystalline phase of catalyst samples was determined by X-Ray powder diffraction (XRD) using Bruker D8 Advance Lynx Powder Diffractometer. The integration time was 0.3 hours and the step size was 0.032 degrees/second. The morphology of the samples was obtained by a scanning electron microscope (SEM, Hitachi SU-70). N₂ adsorption-desorption measurements were carried out at 77 K on an Autosorb-iQ analyzer (Quantachrome Instruments), respectively. Prior to the N₂ and Ar measurements, samples were outgas at 423 K overnight.

4.2.6 Catalytic reaction test over ZSM-5@MIL-101 composite

The liquid phase catalytic conversion of benzylidene malononitrile from malononitrile and benzaldehyde dimethyl acetal (Scheme 2-2) was performed in a three-necked flask equipped with a reflux condenser and heated in a temperature controlled oil bath under atmospheric pressure and magnetic stirring (0.5" stirring bar and 500 rpm stirring speed) conditions. In a typical experiment, 20 mL acetonitrile (99.9%, Fisher), 0.0866 g malononitrile (1.31 mmol, 99%, Sigma-Aldrich), 7.5 μ L DI water, and 0.05 g catalyst were added into the flask in sequence. After bubbled the mixture with flowing helium for 0.5 h, the flask was immersed in the oil bath preheated at 353 K. The reaction mixture was maintained for 0.5 h at the required reaction temperature and stirring conditions and then 0.2045 mL of benzaldehyde dimethyl acetal (1.36 mmol) was added. This moment of the addition was taken as the initial reaction time. Liquid samples were withdrawn at regular intervals and analyzed by the gas chromatograph (Agilent 7890A) equipped with a methyl-siloxane capillary column (HP-1, 50.0 m x 320 μ m x 0.52 μ m) connected to a flame ionization detector (FID).

4.3 Results and Discussion

The morphology of ZSM-5, MIL-101, and ZSM-5@MIL-101 composite particles were observed with SEM. Figure 4-1 (A) shows the representative SEM image of ZSM-5 particles. The commercial ZSM-5 particles have a broad size distribution with an average size of 450 nm. Figure 4-1 (B) shows the representative SEM image of MIL-101 particles. The MIL-101 particles don't have a certain shape and aggregate

into large particles. The as-synthesized ZSM-5@MIL-101 core-shell composite is shown in Figure 4-1 (C), showing a mixture of particles with different sizes. The average particle size was increased to 550nm, showing the growth of MIL-101 shell onto the ZSM-5 core. The morphology of the core-shell structured composite differs with the ZSM-5@UiO-66 because of MIL-101 in this synthesis method doesn't have a well-defined crystal shape.

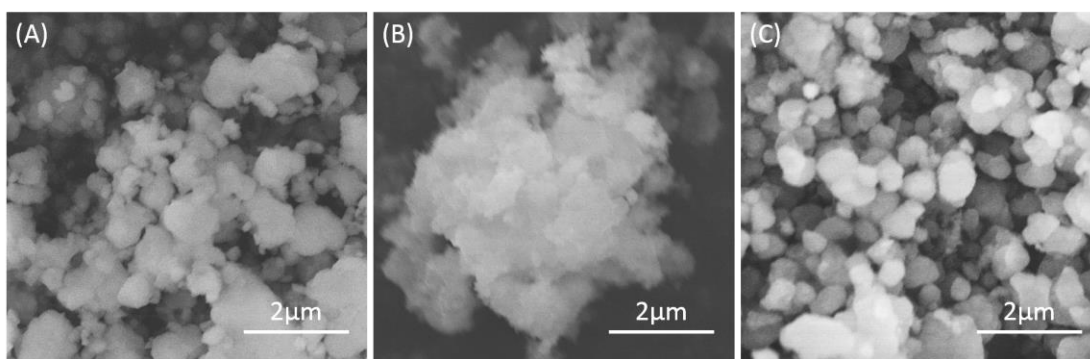


Figure 4-1. SEM images of (A) commercial ZSM-5 zeolite, (B) MIL-101 MOF, and (C) ZSM-5@MIL-101.

Powder X-ray diffraction was applied to confirm the composition and crystallinity of the particles. Figure 4-2 shows the XRD patterns of the as-synthesized ZSM-5, MIL-101 and ZSM-5@MIL-101 particles, respectively. Both ZSM-5 (a) and MIL-101 (b) are crystallized, resembling the characteristic of a crystalline ZSM-5 and MIL-101 reported in literature. The ZSM-5@MIL-101 (c) composite consists of diffraction peaks from both MIL-101 and ZSM-5, suggesting the presence of both phases in the composite materials. In addition, the absence of new diffraction peaks or broadening of characteristic peaks of ZSM-5 or MIL-101 indicate no other structure forms and deterioration of the crystalline phases in the synthesis conditions.

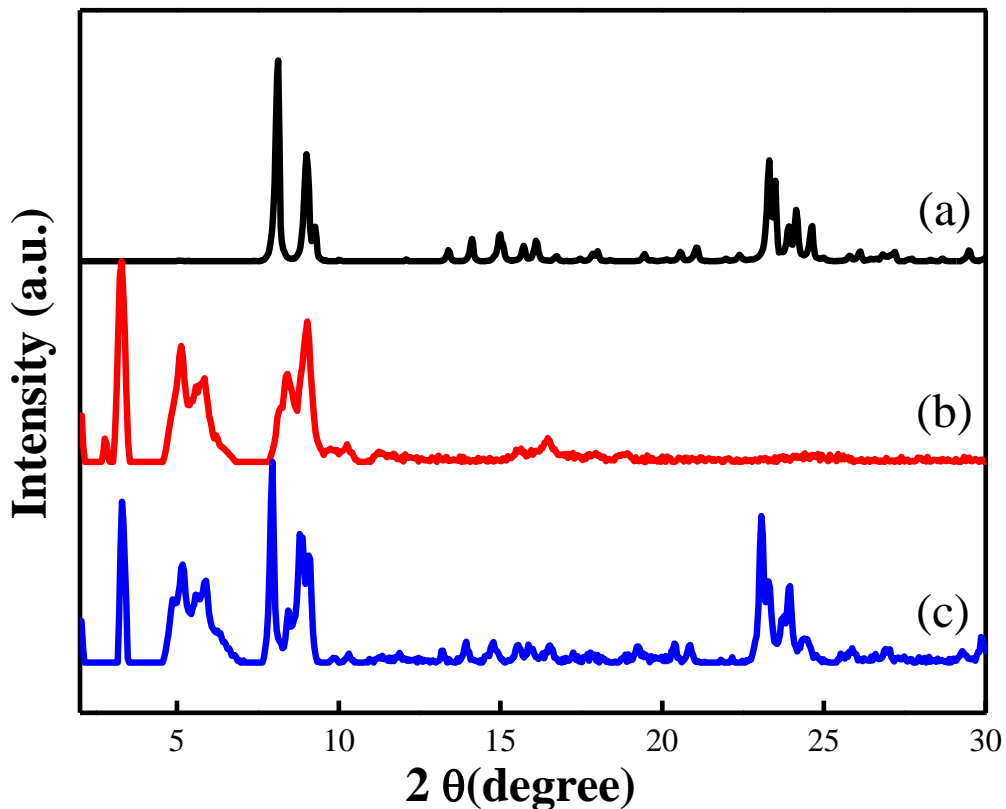


Figure 4-2. XRD patterns of (a) ZSM-5, (b) MIL-101 and (c) ZSM-5@MIL-101, respectively.

N_2 adsorption-desorption isotherms (Figure 4-3) were used to characterize the textural properties of the samples. The surface areas of MIL-101, ZSM-5, ZSM-5@MIL-101 and ED-ZSM-5@MIL-101 calculated by the multipoint BET method were $1580 \text{ m}^2/\text{g}$, $459 \text{ m}^2/\text{g}$, $422 \text{ m}^2/\text{g}$ and $351 \text{ m}^2/\text{g}$, respectively. The total pore volumes of aforementioned samples calculated at $P/P_0=0.95$ were 0.91 mL/g , 0.27 mL/g , 0.33 mL/g and 0.23 mL/g , respectively. The surface area and total pore volume of core-shell composite dropped dramatically from its parenting materials, indicating intergrowth of these two materials or corruption of ZSM-5 micropores by TMAOH in the synthesis solution. The surface area and total pore volume decreased after adding ethylene diamine.

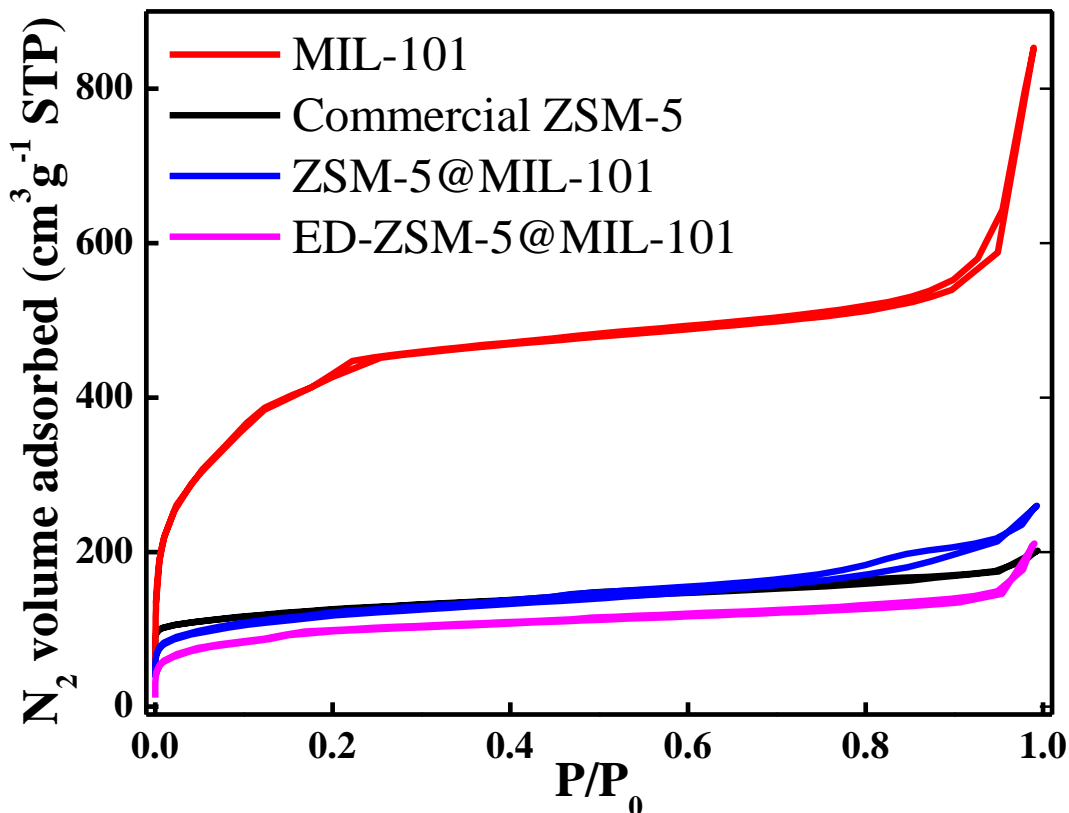


Figure 4-3. N₂ adsorption-desorption isotherms of MIL-101, ZSM-5, ZSM-5@MIL-101, and ED-ZSM-5@MIL-101, respectively.

The catalytic activity of the ZSM-5@MIL-101 was studied in the cascade reactions shown in Scheme 2-2. The first reaction step requires acid sites which can be supplied by the ZSM-5 core, while the second step involves basic sites which come from the amine groups in the MIL-101 shell. The composite after adding ethylene diamine was treated with 0.15M HCl ethanol solution and evacuated at 473 K. The reaction results are shown in Figure 4-4 with the molar fraction of each component versus reaction time. The reactant benzaldehyde dimethyl acetal was consumed completely at the beginning of the reaction. The TMAOH in the synthesis solution may cause desilication to the ZSM-5 core, resulting in rise of framework Al content and acidity.

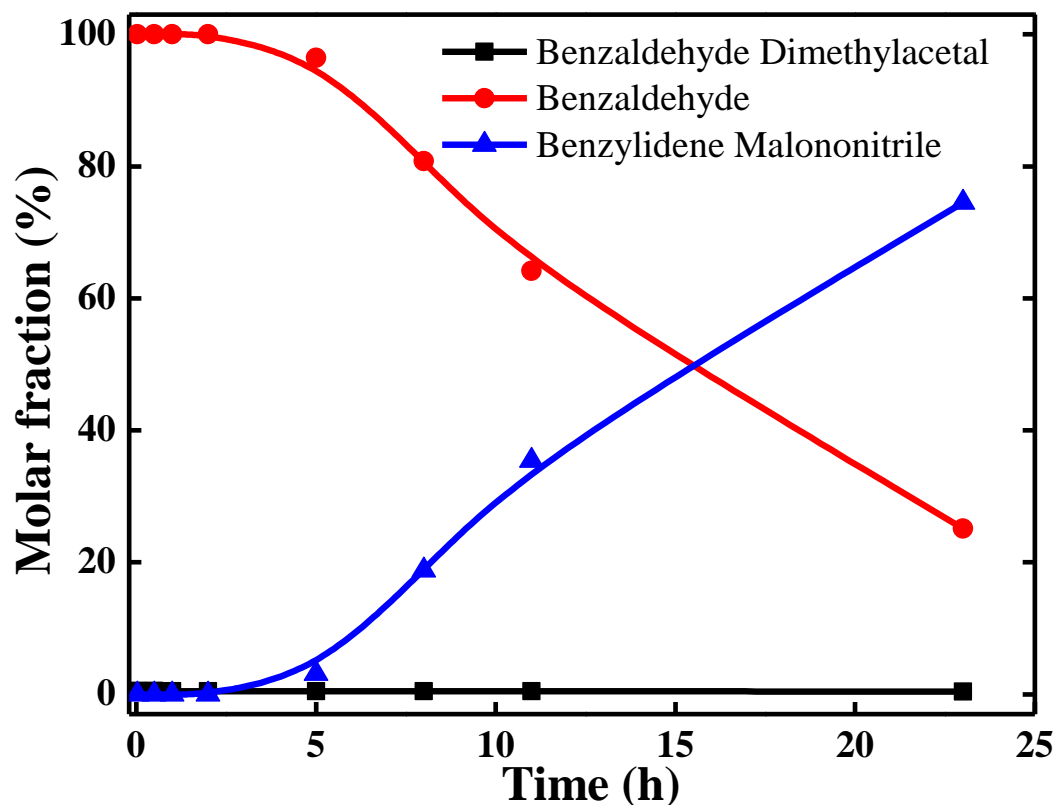


Figure 4-4. Catalytic reaction results of ZSM-5@MIL-101. Molar fraction of benzaldehyde dimethyl acetal, benzaldehyde and benzylidene malononitrile versus reaction time.

4.4 Conclusions

The core-shell composite ZSM-5@MIL-101 was synthesized using the same procedure as that of ZSM-5@UiO-66. The morphologies of ZSM-5, MIL-101, and ZSM-5@MIL-101 composite were observed by SEM. The crystallinity of the samples was confirmed by XRD. Textural properties of the samples were extracted from N₂ adsorption-desorption isotherms, showing a decrease of surface area and pore volume of the composite from its parenting materials. Post-synthetic modification with ethylene diamine in the MIL-101 framework incorporated amine groups into the composite. The acidity in ZSM-5 generated by aluminum in the tetrahedral site of the zeolite framework and basicity in MIL-101 originated from the amine groups enabled

ZSM-5@MIL-101 composite acid-base bifunctionality for catalytic cascade reactions.

The reaction results showed strong acidity compared to its basicity.

Chapter 5: Conclusions and Future Work

5.1 Conclusions

In conclusion, zeolite@MOF core-shell composites were synthesized by solvothermal growth of UiO-66, MIL-101 and UiO-66-NH₂ on the surface of ZSM-5 particles that were pre-synthesized via hydrothermal crystallization. Postsynthetic modification of the UiO-66 and MIL-101 framework incorporated amine groups in the metal clusters. Presynthetic modification was used to incorporate amine groups in UiO-66-NH₂ on the organic linkers. The acidity in ZSM-5 generated by aluminum in the tetrahedral site of the zeolite framework and basicity in MOFs originated from the amine groups enabled ZSM-5@MOF composites acid-base bifunctionality for catalytic cascade reactions.

The synthesis of benzylidene malonitrile from malonitrile and benzaldehyde dimethyl acetal, a process involving the hydrolysis of the acetal catalyzed by the Brønsted acid sites in zeolite, followed by a Knoevenagel condensation reaction catalyzed by the basic sites in MOF confirmed the bifunctional activity of the zeolite@MOF composites. The present work is the first example of synthesizing zeolite@MOF core-shell composites and exploring their applications as bifunctional catalysts in one-pot cascade reactions. This study is an important platform towards zeolite@MOF nanoporous composite systems that integrate the advantages of thermal, mechanical and structural stability of inorganic zeolites and functional and structural flexibility of MOFs for a variety of applications in the future.

5.2 Future Work

5.2.1 Mechanism investigation on growth of MOFs on zeolite surface

The future works of this thesis as extensions contains several parts. The first part should be the insight on the growth mechanism for formation of MOF on the zeolite surface. In this thesis, a hypothesis was made that the similarity of lattice parameters between MOF and zeolite and the heteroatoms in zeolite framework (Al) could facilitate the growth of MOF around zeolite. In order to prove the hypothesis and to generate more universal synthesis methods for zeolite@MOF composites, the validity of the two factors should be investigated in detail.

In case of applications that require shape selectivity of both MOF and zeolite, full coverage of MOF on zeolite is desired. The surface modification of zeolite with analogs of MOF building blocks (functional groups with amine or carboxylic acid) is a promising approach to achieve this goal.

5.2.2 Optimization the functionalization process of zeolite@MOF composites

The functionalization of zeolite@MOF composites can be achieved by pre-/post- synthetic modification, which has been illustrated in this thesis. The postsynthetic modification, however, impaired the acidity in ZSM-5. To solve this problem, alternative systematic routes should be explored for functionalizing the composites. The combination of presynthetic and postsynthetic modification, or introduction of postsynthetic deprotection could endow the composites bifunctionality without losing the intrinsic acidity of ZSM-5.

The effect of geometry of the core-shell composites on the catalytic reaction can be studied by changing the core size and shell thickness. The zeolite core size can be controlled by hydrothermal synthesis conditions (temperature, duration) of ZSM-5. The shell thickness can be changed in various ways. Usually it's hard to increase the thickness by simply extending the reaction time or changing the concentration. The layer-by-layer synthesis method or multiple growth cycles can be used to increase the MOF thickness.

5.2.3 Shape selectivity of zeolite@MOF composites in other applications

The zeolite@MOF core-shell composites are promising materials in many potential applications. Their bifunctionality has been demonstrated by the probe cascade reactions. It can be readily expanded to other acid-base catalyzed cascade reactions. Other functional groups can be introduced into the composites for extra applications. Another application being considered is using seamless MOF shell as the molecular sieve to screen the molecules going to the catalytic sites in zeolite core. Although zeolite itself has shape selective features, the external active sites will make negative contribution especially in mesoporous zeolites. Flimsy MOFs can be introduced to the core-shell structure which would decompose easily under certain conditions. This can be used in drug or chemical delivery systems.

References

1. McNaught, A.D. and A. Wilkinson, *IUPAC Compendium of chemical terminology*, 2000, International Union of Pure and Applied Chemistry.
2. Morris, R.E. and P.S. Wheatley, *Gas Storage in Nanoporous Materials*. Angewandte Chemie International Edition, 2008. **47**(27): p. 4966-4981.
3. Lu, G.Q., X.S. Zhao, and T.K. Wei, *Nanoporous materials: science and engineering*. Vol. 4. 2004: Imperial College Press.
4. Minachev Kh, M. and I. Isakov Ya, *Catalytic Properties of Zeolites? A General Review*, in *Molecular Sieves*. 1973, American Chemical Society. p. 451-460.
5. Kulprathipanja, S. and J. Wiley, *Zeolites in industrial separation and catalysis*. 2010: Wiley Online Library.
6. Corma, A., H. García, and F.X. Llabrés i Xamena, *Engineering Metal Organic Frameworks for Heterogeneous Catalysis*. Chemical Reviews, 2010. **110**(8): p. 4606-4655.
7. Li, J.-R., J. Sculley, and H.-C. Zhou, *Metal–Organic Frameworks for Separations*. Chemical Reviews, 2011. **112**(2): p. 869-932.
8. Jacobs, P., et al., *Introduction to zeolite science and practice*. 2001: Elsevier Science.
9. Cronstedt, A.F., *RÖN och BESKRIFNING Om en oberkant barg art, som kallas Zeolites*. Kongl Vetenskaps Akademiens Handlingar Stockholm, 1765. **17**: p. 120.
10. Flanigen, E.M., *Zeolites and molecular sieves an historical perspective*. Studies in Surface Science and Catalysis, 1991. **58**: p. 13-34.
11. Cundy, C.S. and P.A. Cox, *The hydrothermal synthesis of zeolites: history and development from the earliest days to the present time*. Chemical Reviews, 2003. **103**(3): p. 663-702.
12. Snyder, M.A. and M. Tsapatsis, *Hierarchical Nanomanufacturing: From Shaped Zeolite Nanoparticles to High-Performance Separation Membranes*. Angewandte Chemie International Edition, 2007. **46**(40): p. 7560-7573.
13. Perez-Ramirez, J., et al., *Hierarchical zeolites: enhanced utilisation of microporous crystals in catalysis by advances in materials design*. Chemical Society Reviews, 2008. **37**(11): p. 2530-2542.
14. Choi, M., et al., *Stable single-unit-cell nanosheets of zeolite MFI as active and long-lived catalysts*. Nature, 2009. **461**(7261): p. 246-249.
15. Baerlocher, C., L.B. McCusker, and D.H. Olson, *Atlas of zeolite framework types*. 2007: Elsevier.
16. Gillett, S.L. *Toward a Silicate-Based Molecular Nanotechnology I. Background and Review*. in *The Fifth Foresight Conference on Molecular Nanotechnology, Palo Alto California*. 1997.
17. Claridge, R.P., et al., *Faujasite catalysis of aromatic nitrations with dinitrogen pentoxide. The effect of aluminium content on catalytic activity and regioselectivity. The nitration of pyrazole*. Journal of the Chemical Society, Perkin Transactions 2, 2001(2): p. 197-200.

18. Corma, A., et al., *Modified faujasite zeolites as catalysts in organic reactions: Esterification of carboxylic acids in the presence of HY zeolites*. Journal of Catalysis, 1989. **120**(1): p. 78-87.
19. Christensen, C.H., et al., *Catalytic Benzene Alkylation over Mesoporous Zeolite Single Crystals: Improving Activity and Selectivity with a New Family of Porous Materials*. Journal of the American Chemical Society, 2003. **125**(44): p. 13370-13371.
20. Wang, D., J.H. Lunsford, and M.P. Rosynek, *Characterization of a Mo/ZSM-5 Catalyst for the Conversion of Methane to Benzene*. Journal of Catalysis, 1997. **169**(1): p. 347-358.
21. Gottardi, G. and E. Galli, *Natural zeolites*. 1985: Springer-Verlag Berlin.
22. Ibrahim, S.A., *Synthesis and Characterization of Zeolites from Sodium Aluminosilicate Solution*, 2007, Universiti Sains Malaysia.
23. Dyer, A., *An introduction to zeolite molecular sieves*. 1988. Medium: X; Size: Pages: (149 p).
24. Meier, W.M. and D.H. Olson, *Atlas of zeolite structure types*. Vol. 26. 1987: Butterworths London etc.
25. Zhang, L., et al., *Organic template-free synthesis of ZSM-5/ZSM-11 co-crystalline zeolite*. Microporous and Mesoporous Materials, 2012. **147**(1): p. 117-126.
26. Barrer, R.M., *Hydrothermal chemistry of zeolites*. 1982.
27. Li, G., E. Kikuchi, and M. Matsukata, *ZSM-5 zeolite membranes prepared from a clear template-free solution*. Microporous and Mesoporous Materials, 2003. **60**(1-3): p. 225-235.
28. Song, J., et al., *Organic Template Free Synthesis of Aluminosilicate Zeolite ECR-1*. Chemistry of Materials, 2006. **18**(12): p. 2775-2777.
29. Cundy, C.S., *Microwave techniques in the synthesis and modification of zeolite catalysts. A review*. Collection of Czechoslovak chemical communications, 1998. **63**(11): p. 1699-1723.
30. Arafat, A., et al., *Microwave preparation of zeolite Y and ZSM-5*. Zeolites, 1993. **13**(3): p. 162-165.
31. Stach, H., et al., *Adsorption equilibria of hydrocarbons on highly dealuminated zeolites*. Zeolites, 1986. **6**(2): p. 74-90.
32. Corma, A., et al., *Determination of the Pore Topology of Zeolite IM-5 by Means of Catalytic Test Reactions and Hydrocarbon Adsorption Measurements*. Journal of Catalysis, 2000. **189**(2): p. 382-394.
33. Haag, W.O., R.M. Lago, and P.B. Weisz, *Transport and reactivity of hydrocarbon molecules in a shape-selective zeolite*. Faraday Discussions of the Chemical Society, 1981. **72**(0): p. 317-330.
34. Yan, T.Y., *Separation of p-xylene and ethylbenzene from C8 aromatics using medium-pore zeolites*. Industrial & Engineering Chemistry Research, 1989. **28**(5): p. 572-576.
35. Santacesaria, E., et al., *Separation of xylenes on Y zeolites. 1. Determination of the adsorption equilibrium parameters, selectivities, and mass transfer coefficients through finite bath experiments*. Industrial & Engineering Chemistry Process Design and Development, 1982. **21**(3): p. 440-445.

36. Kazansky, V.B., *The Catalytic Site from a Chemical Point of View*, in *Studies in Surface Science and Catalysis*, M.S.H.G.K. J.C. Jansen and J. Weitkamp, Editors. 1994, Elsevier. p. 251-272.
37. Furukawa, H., et al., *The Chemistry and Applications of Metal-Organic Frameworks*. Science, 2013. **341**(6149): p. 974.
38. Stock, N. and S. Biswas, *Synthesis of Metal-Organic Frameworks (MOFs): Routes to Various MOF Topologies, Morphologies, and Composites*. Chemical Reviews, 2011. **112**(2): p. 933-969.
39. Hoskins, B.F. and R. Robson, *Infinite polymeric frameworks consisting of three dimensionally linked rod-like segments*. Journal of the American Chemical Society, 1989. **111**(15): p. 5962-5964.
40. Gable, R.W., B.F. Hoskins, and R. Robson, *A new type of interpenetration involving enmeshed independent square grid sheets. The structure of diaquabis-(4,4[prime or minute]-bipyridine)zinc hexafluorosilicate*. Journal of the Chemical Society, Chemical Communications, 1990(23): p. 1677-1678.
41. Gable, R.W., B.F. Hoskins, and R. Robson, *Synthesis and structure of [NMe₄][CuPt(CN)₄]: an infinite three-dimensional framework related to PtS which generates intersecting hexagonal channels of large cross section*. Journal of the Chemical Society, Chemical Communications, 1990(10): p. 762-763.
42. Aharoni, S.M. and S.F. Edwards, *Rigid polymer networks*. Vol. 118. 1994: Springer-Verlag.
43. Burch, R.R., *Oxidation-reduction reactions for preparation of [Ti(OC₆H₄O)₂]_n and related metalloquinone polymers: hybrid inorganic-organic metal oxides*. Chemistry of Materials, 1990. **2**(6): p. 633-635.
44. Chapman, O.L., *Diamondoid polymeric compositions*, 1991, Google Patents.
45. Webster, O.W., et al., *Hypercrosslinked rigid-rod polymers*. Makromolekulare Chemie. Macromolecular Symposia, 1992. **54-55**(1): p. 477-482.
46. Yaghi, O.M., G. Li, and H. Li, *Selective binding and removal of guests in a microporous metal-organic framework*. Nature, 1995. **378**(6558): p. 703-706.
47. Yaghi, O.M. and H. Li, *Hydrothermal Synthesis of a Metal-Organic Framework Containing Large Rectangular Channels*. Journal of the American Chemical Society, 1995. **117**(41): p. 10401-10402.
48. Yaghi, O.M., et al., *Selective Guest Binding by Tailored Channels in a 3-D Porous Zinc(II)-Benzenetricarboxylate Network*. Journal of the American Chemical Society, 1997. **119**(12): p. 2861-2868.
49. Li, H., et al., *Establishing Microporosity in Open Metal-Organic Frameworks: Gas Sorption Isotherms for Zn(BDC) (BDC = 1,4-Benzenedicarboxylate)*. Journal of the American Chemical Society, 1998. **120**(33): p. 8571-8572.
50. Furukawa, H., et al., *The Chemistry and Applications of Metal-Organic Frameworks*. Science, 2013. **341**(6149).
51. Tranchemontagne, D.J., et al., *Secondary building units, nets and bonding in the chemistry of metal-organic frameworks*. Chemical Society Reviews, 2009. **38**(5): p. 1257-1283.
52. Li, H., et al., *Design and synthesis of an exceptionally stable and highly porous metal-organic framework*. Nature, 1999. **402**(6759): p. 276-279.

53. Chui, S.S.-Y., et al., *A Chemically Functionalizable Nanoporous Material [Cu₃(TMA)₂(H₂O)₃]_n*. *Science*, 1999. **283**(5405): p. 1148-1150.
54. Tian, Y.-Q., et al., *[Co₅(im)₁₀ · 2 MB] ∞: A Metal-Organic Open-Framework with Zeolite-Like Topology*. *Angewandte Chemie*, 2002. **114**(8): p. 1442-1444.
55. Phan, A., et al., *Synthesis, Structure, and Carbon Dioxide Capture Properties of Zeolitic Imidazolate Frameworks*. *Accounts of Chemical Research*, 2009. **43**(1): p. 58-67.
56. Huang, X., J. Zhang, and X. Chen, *[Zn(bim)₂] · (H₂O)_{1.67}: A metal-organic open-framework with sodalite topology*. *Chinese Science Bulletin*, 2003. **48**(15): p. 1531-1534.
57. Venna, S.R. and M.A. Carreon, *Highly Permeable Zeolite Imidazolate Framework-8 Membranes for CO₂/CH₄ Separation*. *Journal of the American Chemical Society*, 2009. **132**(1): p. 76-78.
58. Férey, G., et al., *A Chromium Terephthalate-Based Solid with Unusually Large Pore Volumes and Surface Area*. *Science*, 2005. **309**(5743): p. 2040-2042.
59. Férey, G., et al., *A Hybrid Solid with Giant Pores Prepared by a Combination of Targeted Chemistry, Simulation, and Powder Diffraction*. *Angewandte Chemie*, 2004. **116**(46): p. 6456-6461.
60. Cavka, J.H., et al., *A New Zirconium Inorganic Building Brick Forming Metal Organic Frameworks with Exceptional Stability*. *Journal of the American Chemical Society*, 2008. **130**(42): p. 13850-13851.
61. Pan, Y. and Z. Lai, *Sharp separation of C₂/C₃ hydrocarbon mixtures by zeolitic imidazolate framework-8 (ZIF-8) membranes synthesized in aqueous solutions*. *Chemical Communications*, 2011. **47**(37): p. 10275-10277.
62. Rosi, N.L., et al., *Hydrogen Storage in Microporous Metal-Organic Frameworks*. *Science*, 2003. **300**(5622): p. 1127-1129.
63. Cravillon, J., et al., *Rapid Room-Temperature Synthesis and Characterization of Nanocrystals of a Prototypical Zeolitic Imidazolate Framework*. *Chemistry of Materials*, 2009. **21**(8): p. 1410-1412.
64. Zhuang, J.-L., et al., *Rapid Room-Temperature Synthesis of Metal–Organic Framework HKUST-1 Crystals in Bulk and as Oriented and Patterned Thin Films*. *Advanced Functional Materials*, 2011. **21**(8): p. 1442-1447.
65. Mueller, U., et al., *Method for electrochemical production of a crystalline porous metal organic skeleton material*, 2005, Google Patents.
66. Jhung, S.H., J. Lee, and J. Chang, *Microwave synthesis of a nanoporous hybrid material, chromium trimesate*. *BULLETIN-KOREAN CHEMICAL SOCIETY*, 2005. **26**(6): p. 880.
67. Pichon, A., A. Lazuen-Garay, and S.L. James, *Solvent-free synthesis of a microporous metal-organic framework*. *CrystEngComm*, 2006. **8**(3): p. 211-214.
68. Qiu, L.-G., et al., *Facile synthesis of nanocrystals of a microporous metal-organic framework by an ultrasonic method and selective sensing of organoamines*. *Chemical Communications*, 2008(31): p. 3642-3644.
69. Richter, I., M. Schubert, and U. Mueller, *Porous metal organic framework based on pyrroles and pyridinones*, 2007, Google Patents.

70. Schlesinger, M., et al., *Evaluation of synthetic methods for microporous metal–organic frameworks exemplified by the competitive formation of [Cu₂(btc)₃(H₂O)₃] and [Cu₂(btc)(OH)(H₂O)]*. *Microporous and Mesoporous Materials*, 2010. **132**(1–2): p. 121-127.
71. Klinowski, J., et al., *Microwave-Assisted Synthesis of Metal-Organic Frameworks*. *Dalton Transactions*, 2011. **40**(2): p. 321-330.
72. Horcajada, P., et al., *Porous metal-organic-framework nanoscale carriers as a potential platform for drug delivery and imaging*. *Nature materials*, 2010. **9**(2): p. 172-178.
73. Fernández-Bertran, J.F., *Mechanochemistry: an overview*. *Pure and applied chemistry*, 1999. **71**(4): p. 581-586.
74. Son, W.-J., et al., *Sonochemical synthesis of MOF-5*. *Chemical Communications*, 2008(47): p. 6336-6338.
75. Deng, H., et al., *Multiple Functional Groups of Varying Ratios in Metal-Organic Frameworks*. *Science*, 2010. **327**(5967): p. 846-850.
76. Wang, Z. and S.M. Cohen, *Postsynthetic modification of metal-organic frameworks*. *Chemical Society Reviews*, 2009. **38**(5): p. 1315-1329.
77. Cohen, S.M., *Modifying MOFs: new chemistry, new materials*. *Chemical Science*, 2010. **1**(1): p. 32-36.
78. Tanabe, K.K. and S.M. Cohen, *Postsynthetic modification of metal-organic frameworks-a progress report*. *Chemical Society Reviews*, 2011. **40**(2): p. 498-519.
79. Cohen, S.M., *Postsynthetic methods for the functionalization of metal–organic frameworks*. *Chemical reviews*, 2011. **112**(2): p. 970-1000.
80. Yamada, T. and H. Kitagawa, *Protection and Deprotection Approach for the Introduction of Functional Groups into Metal–Organic Frameworks*. *Journal of the American Chemical Society*, 2009. **131**(18): p. 6312-6313.
81. Deshpande, R.K., J.L. Minnaar, and S.G. Telfer, *Thermolabile Groups in Metal–Organic Frameworks: Suppression of Network Interpenetration, Post-Synthetic Cavity Expansion, and Protection of Reactive Functional Groups*. *Angewandte Chemie International Edition*, 2010. **49**(27): p. 4598-4602.
82. Chen, B., et al., *A Microporous Metal–Organic Framework for Gas-Chromatographic Separation of Alkanes*. *Angewandte Chemie*, 2006. **118**(9): p. 1418-1421.
83. Hamon, L., et al., *Co-adsorption and Separation of CO₂–CH₄ Mixtures in the Highly Flexible MIL-53(Cr) MOF*. *Journal of the American Chemical Society*, 2009. **131**(47): p. 17490-17499.
84. Bae, T.-H., et al., *A High-Performance Gas-Separation Membrane Containing Submicrometer-Sized Metal–Organic Framework Crystals*. *Angewandte Chemie International Edition*, 2010. **49**(51): p. 9863-9866.
85. Farha, O.K., et al., *De novo synthesis of a metal–organic framework material featuring ultrahigh surface area and gas storage capacities*. *Nature chemistry*, 2010. **2**(11): p. 944-948.
86. Lee, J., et al., *Metal–organic framework materials as catalysts*. *Chemical Society Reviews*, 2009. **38**(5): p. 1450-1459.

87. Shultz, A.M., et al., *A Catalytically Active, Permanently Microporous MOF with Metalloporphyrin Struts*. Journal of the American Chemical Society, 2009. **131**(12): p. 4204-4205.
88. Noro, S.-i., et al., *A New, Methane Adsorbent, Porous Coordination Polymer $[[\text{CuSiF}_6(4,4' \text{-bipyridine})_2]_n]$* . Angewandte Chemie International Edition, 2000. **39**(12): p. 2081-2084.
89. Ma, S., et al., *Metal-Organic Framework from an Anthracene Derivative Containing Nanoscopic Cages Exhibiting High Methane Uptake*. Journal of the American Chemical Society, 2007. **130**(3): p. 1012-1016.
90. Zhao, X., et al., *Hysteretic Adsorption and Desorption of Hydrogen by Nanoporous Metal-Organic Frameworks*. Science, 2004. **306**(5698): p. 1012-1015.
91. Li, Y. and R.T. Yang, *Significantly Enhanced Hydrogen Storage in Metal-Organic Frameworks via Spillover*. Journal of the American Chemical Society, 2005. **128**(3): p. 726-727.
92. Ordoñez, M.J.C., et al., *Molecular sieving realized with ZIF-8/Matrimid® mixed-matrix membranes*. Journal of Membrane Science, 2010. **361**(1-2): p. 28-37.
93. Tanaka, K., et al., *Highly efficient chromatographic resolution of sulfoxides using a new homochiral MOF-silica composite*. Chemical Communications, 2012. **48**(68): p. 8577-8579.
94. Efraty, A. and I. Feinberg, *Catalytic hydrogenation and isomerization of 1-hexene with $[\text{RhCl}(\text{CO})(1,4\text{-}(\text{CN})_2\text{C}_6\text{H}_4)]_n$ in the dark and under irradiation*. Inorganic Chemistry, 1982. **21**(8): p. 3115-3118.
95. Tannenbaum, R., *Three-Dimensional Coordination Polymers of Ruthenium(2+) with 1,4-Diisocyanobenzene Ligands and Their Catalytic Activity*. Chemistry of Materials, 1994. **6**(4): p. 550-555.
96. Fujita, M., et al., *Preparation, Clathration Ability, and Catalysis of a Two-Dimensional Square Network Material Composed of Cadmium(II) and 4,4'-Bipyridine*. Journal of the American Chemical Society, 1994. **116**(3): p. 1151-1152.
97. Gomez-Lor, B., et al., *$\text{In}_2(\text{OH})_3(\text{BDC})1.5$ (BDC = 1,4-Benzendicarboxylate): An In(III) Supramolecular 3D Framework with Catalytic Activity*. Inorganic Chemistry, 2002. **41**(9): p. 2429-2432.
98. Kato, C.N., et al., *Microporous dinuclear copper(II) trans-1,4-cyclohexanedicarboxylate: heterogeneous oxidation catalysis with hydrogen peroxide and X-ray powder structure of peroxo copper(II) intermediate*. Journal of Catalysis, 2005. **230**(1): p. 226-236.
99. Yu, Z.-T., et al., *Construction of a microporous inorganic-organic hybrid compound with uranyl units*. Chemical Communications, 2004(16): p. 1814-1815.
100. Hwang, Y.K., et al., *Amine Grafting on Coordinatively Unsaturated Metal Centers of MOFs: Consequences for Catalysis and Metal Encapsulation*. Angewandte Chemie-international Edition, 2008. **47**(22): p. 4144-4148.
101. Hasegawa, S., et al., *Three-Dimensional Porous Coordination Polymer Functionalized with Amide Groups Based on Tridentate Ligand: Selective*

- Sorption and Catalysis*. Journal of the American Chemical Society, 2007. **129**(9): p. 2607-2614.
102. Seo, J.S., et al., *A homochiral metal–organic porous material for enantioselective separation and catalysis*. Nature, 2000. **404**(6781): p. 982-986.
 103. Uemura, T., N. Yanai, and S. Kitagawa, *Polymerization reactions in porous coordination polymers*. Chemical Society Reviews, 2009. **38**(5): p. 1228-1236.
 104. Banerjee, M., et al., *Postsynthetic Modification Switches an Achiral Framework to Catalytically Active Homochiral Metal–Organic Porous Materials*. Journal of the American Chemical Society, 2009. **131**(22): p. 7524-7525.
 105. Esken, D., et al., *Au@ZIFs: Stabilization and Encapsulation of Cavity-Size Matching Gold Clusters inside Functionalized Zeolite Imidazolate Frameworks, ZIFs*. Chemistry of Materials, 2010. **22**(23): p. 6393-6401.
 106. Aguado, S., et al., *Tuning the activity by controlling the wettability of MOF eggshell catalysts: A quantitative structure–activity study*. Journal of Catalysis, 2011. **284**(2): p. 207-214.
 107. Sorribas, S., et al., *Ordered mesoporous silica-(ZIF-8) core-shell spheres*. Chemical Communications, 2012. **48**(75): p. 9388-9390.
 108. Yang, S.J., et al., *Preparation and Enhanced Hydrostability and Hydrogen Storage Capacity of CNT@MOF-5 Hybrid Composite*. Chemistry of Materials, 2009. **21**(9): p. 1893-1897.
 109. Zhan, W.-w., et al., *Semiconductor@Metal–Organic Framework Core–Shell Heterostructures: A Case of ZnO@ZIF-8 Nanorods with Selective Photoelectrochemical Response*. Journal of the American Chemical Society, 2013. **135**(5): p. 1926-1933.
 110. Zlotea, C., et al., *Pd Nanoparticles Embedded into a Metal-Organic Framework: Synthesis, Structural Characteristics, and Hydrogen Sorption Properties*. Journal of the American Chemical Society, 2010. **132**(9): p. 2991-2997.
 111. Dhakshinamoorthy, A. and H. Garcia, *Catalysis by metal nanoparticles embedded on metal-organic frameworks*. Chemical Society Reviews, 2012. **41**(15): p. 5262-5284.
 112. Houk, R.J.T., et al., *Silver Cluster Formation, Dynamics, and Chemistry in Metal–Organic Frameworks*. Nano Letters, 2009. **9**(10): p. 3413-3418.
 113. Lu, G., et al., *Imparting functionality to a metal–organic framework material by controlled nanoparticle encapsulation*. Nature chemistry, 2012. **4**(4): p. 310-316.
 114. Lohe, M.R., et al., *Heating and separation using nanomagnet-functionalized metal-organic frameworks*. Chemical Communications, 2011. **47**(11): p. 3075-3077.
 115. Xing, L., et al., *Coordination Polymer Coated Mesoporous Silica Nanoparticles for pH-Responsive Drug Release*. Advanced Materials, 2012. **24**(48): p. 6433-6437.
 116. Jo, C., H.J. Lee, and M. Oh, *One-Pot Synthesis of Silica@Coordination Polymer Core–Shell Microspheres with Controlled Shell Thickness*. Advanced Materials, 2011. **23**(15): p. 1716-1719.

117. Lee, H.J., W. Cho, and M. Oh, *Advanced fabrication of metal-organic frameworks: template-directed formation of polystyrene@ZIF-8 core-shell and hollow ZIF-8 microspheres*. *Chemical Communications*, 2012. **48**(2): p. 221-223.
118. Nozik, A.J., et al., *Semiconductor Quantum Dots and Quantum Dot Arrays and Applications of Multiple Exciton Generation to Third-Generation Photovoltaic Solar Cells*. *Chemical Reviews*, 2010. **110**(11): p. 6873-6890.
119. Zhu, Q.-L. and Q. Xu, *Metal-organic framework composites*. *Chemical Society Reviews*, 2014: p. Accepted.
120. Ramos-Fernandez, E.V., et al., *MOFs meet monoliths: Hierarchical structuring metal organic framework catalysts*. *Applied Catalysis A-general*, 2011. **391**(1-2): p. 261-267.
121. Lai, Z., et al., *Microstructural Optimization of a Zeolite Membrane for Organic Vapor Separation*. *Science*, 2003. **300**(5618): p. 456-460.
122. Chen, N.Y. and W.J. Reagan, *Evidence of autocatalysis in methanol to hydrocarbon reactions over zeolite catalysts*. *Journal of Catalysis*, 1979. **59**(1): p. 123-129.
123. Martínez, C. and A. Corma, *Inorganic molecular sieves: Preparation, modification and industrial application in catalytic processes*. *Coordination Chemistry Reviews*, 2011. **255**(13-14): p. 1558-1580.
124. Xu, R., et al., *From Zeolites to Porous MOF Materials-the 40th Anniversary of International Zeolite Conference: Proceedings of the 15th International Zeolite Conference, Beijing, PR China, 12-17th August 2007*. Vol. 170. 2007: Elsevier.
125. Argauer, R.J. and G.R. Landolt, *Crystalline zeolite zsm-5 and method of preparing the same*, 1972, US Patent 3,702,886.
126. Olson, D., et al., *Crystal structure and structure-related properties of ZSM-5*. *J. Phys. Chem.*, 1981. **85**(15): p. 2238-2243.
127. Quann, R.J., et al., *Chemistry of olefin oligomerization over ZSM-5 catalyst*. *Industrial & Engineering Chemistry Research*, 1988. **27**(4): p. 565-570.
128. Wu, E.L., et al., *ZSM-5-type materials. Factors affecting crystal symmetry*. *J. Phys. Chem.*, 1979. **83**(21): p. 2777-2781.
129. Liu, S., et al., *Fast Syntheses of MOFs Using Nanosized Zeolite Crystal Seeds In Situ Generated from Microsized Zeolites*. *Cryst. Growth Des.*, 2013. **13**(7): p. 2697-2702.
130. Valenzano, L., et al., *Disclosing the Complex Structure of UiO-66 Metal Organic Framework: A Synergic Combination of Experiment and Theory*. *Chemistry of Materials*, 2011. **23**(7): p. 1700-1718.
131. Flanigen Edith, M., H. Khatami, and A. Szymanski Herman, *Infrared Structural Studies of Zeolite Frameworks*, in *Molecular Sieve Zeolites-I*. 1974, American Chemical Society. p. 201-229.
132. Giorgini, M.G., et al., *Vibrational spectra and assignments of ethylene-diamine and its deuterated derivatives*. *Journal of Raman Spectroscopy*, 1983. **14**(1): p. 16-21.
133. Yang, J., et al., *Synthesis of metal-organic framework MIL-101 in TMAOH-Cr(NO₃)₃-H₂BDC-H₂O and its hydrogen-storage behavior*. *Microporous and Mesoporous Materials*, 2010. **130**(1-3): p. 174-179.